In vitro fate mapping of stem cell development at the single cell level

THÈSE N^{O} 9030 (2018)

PRÉSENTÉE LE 14 DÉCEMBRE 2018
À LA FACULTÉ DES SCIENCES DE LA VIE
UNITÉ DU PROF. LUTOLF
PROGRAMME DOCTORAL EN BIOTECHNOLOGIE ET GÉNIE BIOLOGIQUE

ÉCOLE POLYTECHNIQUE FÉDÉRALE DE LAUSANNE

POUR L'OBTENTION DU GRADE DE DOCTEUR ÈS SCIENCES

PAR

Vincent TRACHSEL

acceptée sur proposition du jury:

Prof. F. Naef, président du jury
Prof. M. Lütolf, directeur de thèse
Dr A. Wilson, rapporteuse
Dr M. Ehrbar, rapporteur
Prof. Ph. Renaud, rapporteur

ÉCOLE POLYTECHNIQUE
FÉDÉRALE DE LAUSANNE

Suisse
2018

“Education is the most powerful weapon which you can use to change the world”

- Nelson Mandela

to Mélanie …

Acknowledgements

This PhD thesis would not have been accomplished without the unconditional support and help of many people to whom I want to express my deep gratitude.

First of all, I would like to thank my supervisor Prof. Matthias Lutolf not only for having given me the opportunity to work on a such exciting project but also for the trust during these years and for the freedom to pursue my project. His constant support was indeed instrumental in me becoming an independent scientist.

I'd like to thank my committee members Prof. Philippe Renaud, Dr. Anne Wilson, Dr. Martin Ehrbar and Prof. Felix Naef for their valuable feedback and constructive criticism on my thesis.

I would like to thank the members of LSCB – I have learned so much with you and in so many different aspects, so many thanks to you all. I've definitely evolved as a person and as a scientist than what I was when I started the PhD partially because of you. In particular, I would like to thank Gena for the valuable help you have provided over these years, and for having taught me what "scientific rigor" is, it will definitely be a valuable asset for me in the future. Mukul thanks for being always such a motivated and positive person. It was a real pleasure to work with you. Thanks to Gena and Mukul for reading through different parts of this thesis and providing valuable feedback. I would also like to thank Aline for introducing me to the fascinating world of hematopoietic stem cells. Thanks to Yoji for always being there to share a coffee over interesting discussions. I am also grateful to Saba, JiSoo and the "Pope" for sharing with me my lunches and for all the laughs we had. Thanks to my collaborators outside the lab: Nicola, Marcela, Vasco and Olaia. I want to thank also my previous supervisor Justin Cooper-White and his lab (especially Clementine and Benoit) for the wonderful time back in Australia and also to motivate me to start a PhD.

During the PhD, I was lucky to have access to wonderful facilities. Therefore, I would like to thank the center of Micro nanotechnology (CMI), and more in particular thanks to Joffrey Pernollet, Julien Dorsaz and Georges-André Racine. Also thanks to the Flow Cytometry Core facility for the numerous

sorts you have done for me. Thanks to Miguel Garcia, Loïc Tauzin, Valérie Glutz and André Mozes for the support. In addition, I would like to say thanks to the Bioimaging and Optics facility, especially to Olivier Burri and Thierry Laroche for their valuable inputs during my experiments on different microscopes.

"Only when it is dark enough, can you see the stars" once said Martin Luther King. There were many instances during the PhD when I was in the dark; luckily, I was surrounded by amazing "stars" who helped me to get through it. I would like to take this opportunity to thank "these stars". The brightest star shinning in my sky is you Melanie. I have no word to express my gratitude and my love for you. Thanks for your unconditional love, to have always been there, to have helped me to feel good and to always push me forward. The second star is my son Lucien. I am so grateful to be your dad; your smile makes me feel so happy and forget my worries. In my sky, there are also "groups of stars" that forms some constellations. Definitely the most wonderful constellations are the "Trachsel family" and the "Antille Family". A special thank goes to my brother Fabrice and his wife Aline who shared with me so many evenings around a beer or a cup of tea. Finally, I'd like to thank the "Spiclette" and "Good or Cute" constellations, Alizée, Cédric, Elise, Matthieu, François, David, Corina, Léo, Soso, Julie, Ramsès and the two Christian. It was great to share this time with you at EPFL. Many thanks to you all for your support and to be part of my life.

Neuchâtel le 14.09.2018 Vincent Trachsel

Abstract

Hematopoietic stem cells (HSCs) are responsible for the continuous production of all blood cells. This unique ability has made it possible to successfully use HSCs in the clinical setting to remedy various blood disorders. However, despite six decades of research, the full potential of HSCs to treat patients with hematological malignancies is still restricted by the low number of functional stem cells that can be isolated from different sources. *In vitro* HSC expansion has been widely considered a potential solution but has proven to be extremely difficult due to the rapid loss of functional potential of cells in the culture outside of their natural microenvironmental niche. In order to achieve robust HSC expansion *in vitro*, it is crucial to better understand the mechanisms that regulate HSC fate choices. Moreover, the absence of reliable markers for identifying functional HSCs on a culture dish necessitates the use of expensive and time-consuming *in vivo* assays. The discovery of predictive phenotypic markers for HSC potential could address this problem. Many platforms for analyzing HSC fate at the single-cell level have been reported, but they generally suffer from poor cell viability, limited throughput, unreliable phenotyping by immunocytochemistry, and the difficulty of performing long-term cell cultures. Additionally, these platforms are usually fabricated from polydimethylsiloxane (PDMS), a polymer known to have several disadvantages for cell-based applications.

This thesis addresses these shortcomings through the development of a robust microchip system for the high-resolution, live-cell analysis of hundreds to thousands of single stem cells and their daughter cells. The platform combines key advantages of microfluidic technology (for cell lineage analysis) and hydrogel microwell array technology (for gentle cell capture and long-term culture). The platform is fabricated from two different layers of hydrogel to create a closed array of grooves, where cells' movements are restricted and grow along one axis. This design enables an unambiguous tracking of a single cell and all of its progeny over several generations. These two layers are produced from different biocompatible hydrogels: poly (2-hydroxyethyl methylacrylate) / trimethylolpropane trimethacrylate (pHEMA-TMPTMA), a copolymer acting as a topographically structured cellular substrate that can be closed with a polyethylene glycol (PEG) hydrogel lid. These two parts are combined together and covalently bonded to each other after the seeding of live cells into the grooves of the bottom part. To assess the potential of the platform for single stem-cell analyses, HSCs were cultured and their behavior (including cell fate, proliferation kinetics, and functionality) were thoroughly characterized.

To analyze imaging data obtained from single-cell time-lapse experiments performed on the platform, an algorithm was developed to automatically identify and track single HSCs and their daughter cells, efficiently extracting various parameters, such as single-cell proliferation kinetics, cell fate choices, and lineage relationships.

Mitochondria have recently been identified as key modulators of HSC function; however, their specific role in fate regulation has remained obscure. Therefore, the single-cell analysis platform was applied to measure the distribution of mitochondrial mass in dividing HSCs and their progeny to assess a potential correlation with HSC fate choices. This analysis led to the conclusion that mitochondria are unequally distributed during single HSC divisions that are kinetically asynchronous. This could suggest the existence of a mechanism that segregates mitochondria preferentially to one of the daughter cells during an asymmetric HSC division.

Later in the thesis, a strategy is described to analyze the fate of daughter cells from HSCs that are activated and fate-instructed within the *in vivo* niche in the bone marrow of mice. This study led to the identification of a set of genes that are asymmetrically expressed between HSC daughter cells, both at the gene and the protein level. Furthermore, by combining two asymmetrically expressed markers, new phenotypes were identified that allow discrimination of a differentiated from a self-renewing daughter HSC.

Finally, the microchip platform was applied to study interactions between a single CD8+ T-lymphocyte and antigen-presenting cells (APCs), enabling an analysis of cell progeny derived from single T-cells after activation. We successfully showed two types of interaction between a T-cell and the APC, namely, immunological synapse and kinapse. Furthermore, we observed that the protein expression is more asymmetric on daughter cells of the second generations than the first ones.

Taken together, this thesis presents a novel system of single-cell analysis to study cell lineage relationships of rare and difficult-to-culture mammalian cell types, such as HSCs and T-lymphocytes. Reliable tracking combined with immunostaining enables the discovery of novel markers and mechanisms that can be used to identify distinct cell lineages and behaviors *in vitro*, opening up exciting perspectives for basic stem-cell biology and its clinical translation.

Keywords

single cell, cell tracking, lineage tracking, hematopoietic stem cells (HSCs), asymmetric cell division, T cells, stem cell fate, lineage analysis, asynchronous divisions, fatty acid oxidation (FAO), mitochondria, peroxisomes, daughter cells, hydrogel

Résumé

Les cellules souches hématopoïétiques (HSCs) permettent la production de toutes les cellules sanguines, et ce, pendant la vie entière des individus. Cette capacité de régénération peut être utilisé en clinique pour traiter les troubles et maladies sanguines. Cependant malgré 60 ans de recherches, nous ne sommes toujours pas encore arrivés à utiliser toutes les vertus des HSCs pour guérir les maladies, et ceci est directement lié au nombre limité de HSCs que nous pouvons extraire de différentes sources. Pour permettre d'utiliser les HSCs de façon optimale, il faudrait pouvoir les multiplier *in vitro* en laboratoire, mais cette pratique s'est montrée plus difficile que prévu. En effet, les HSCs perdent leur pouvoir thérapeutique lorsqu'elles sont cultivées *in vitro*. La raison principale de ce phénomène est liée au fait que nous ne sommes pas capables de reproduire l'environnement naturel des HSCs (la niche dans la moelle osseuse) qui leur est nécessaire pour effectuer leur travail. Pour pouvoir multiplier les HSCs *in vitro*, il faudrait d'abord comprendre comment la niche interagît avec les HSCs. De plus, lorsque les HSCs sont cultivées *in vitro*, elles perdent leurs marqueurs de cellules souches. Nous ne sommes donc plus capables d'identifier quelle cellule garde un pouvoir thérapeutique et laquelle se différencie en cellules sanguines matures. Ainsi, la seule méthode pour pouvoir dire quelle cellule est encore souche est de faire une transplantation dans un animal malade et de voir si la cellule est capable de régénérer le sang de l'animal, ce qui est une méthode très couteuse et longue. La solution pour trouver des marqueurs de cellules souches *in vitro* serait d'isoler les cellules souches une à une et d'étudier leur descendance. De nombreuses plateformes d'analyse des HSCs au niveau de la cellule unique ont été créées, mais elles sont inutilisables dans le cadre des HSCs car ces plateformes se caractérisent par une viabilité cellulaire faible, d'un faible rendement, d'un phénotypage non fiable par immunocytochimie et de la difficulté à mener une culture cellulaire à long terme. En outre, ces plateformes sont généralement fabriquées à partir de polydiméthylsiloxane (PDMS), un polymère connu pour avoir des effets négatifs sur les cellules.

Cette thèse aborde et résout ces problèmes par le développement d'une nouvelle plateforme qui permet l'analyse de centaines de descendances de HSCs. Cette plateforme regroupe les avantages des plateformes microfluidiques où les cellules peuvent être encapsulées pour permettre l'observation des descendances, avec les avantages des plateformes à « puits microscopiques » qui permettent l'étude de cellules fragiles. La plateforme est fabriquée à partir de deux couches différentes d'hydrogels qui ensemble permettent de créer une matrice de sillon fermée. Les cellules dans les sillons sont obligées de grandir et bouger selon un axe unique. Ce design permet donc de suivre les cellules de façon non ambiguë. Les deux couches d'hydrogels sont produites à partir de deux matériaux différents : poly (2-hydroxyethyl méthacrylate) / triméthylolpropane triméthacrylate copolymère (pHEMA-TMPTMA) et de polyéthylène glycol (PEG). Ces deux couches sont combinées après avoir préalablement déposé les cellules dans les sillons de la couche inférieure. Durant la fermeture de la plateforme les couches inférieures et supérieures sont collées de façon covalente par une réaction de type « chimie click » (par addition de Michael entre un thiol et un vinylsulfone). Les cultures de HSCs sur plateforme ont été caractérisées par différents paramètres cellulaires comme le destin cellulaire, la prolifération, la fonctionnalité cellulaire.

Pour permettre une étude des descendances des cellules de façon rigoureuse et à haut débit, nous avons aussi développé un programme qui permet de créer des arbres généalogiques.

Nous avons ensuite utilisé la plateforme pour observer la distribution des mitochondries dans les différentes descendances afin de mieux comprendre sa corrélation avec les choix du devenir des HSCs. Cette analyse a abouti à la conclusion que les mitochondries sont inégalement distribuées lors d'une division asymétrique des HSCs. Nous proposons ainsi l'existence d'un mécanisme de distribution spécifique qui sépare les mitochondries dans une cellule plutôt que dans une autre.

Dans la partie suivante de la thèse, nous avons décrit une stratégie pour analyser le sort des cellules filles des HSCs ayant reçu une instruction de niche. Cette étude a conduit à l'identification d'un ensemble de gènes exprimés de manière asymétrique au niveau protéinique entre les cellules filles. En combinant deux marqueurs exprimés de manière asymétrique, nous avons trouvé des phénotypes pour définir quelle cellule fille s’est différenciée et quelle cellule fille est restée « souche ».

Enfin, dans la dernière partie de la thèse, nous avons développé une nouvelle méthodologie qui permet non seulement l’étude de la synapse immunologique entre un lymphocyte T CD8 + naïf et une cellule présentatrice d’antigène (APC), mais aussi l’analyse de la descendance dérivée de la cellule T après son activation.

En résumé, cette thèse présente une nouvelle plateforme pour analyser les descendances des HSCs et des lymphocytes T. Un suivi fiable associé à une immunofluorescence a permis de découvrir des marqueurs et des mécanismes pouvant être utilisés pour identifier des différences de cellules dans la descendance de HSCs *in vitro*. De plus, nous avons également montré que la plateforme peut être utilisée pour aborder des questions fondamentales dans le domaine de l'immunologie.

Mots-clés

Cellule unique, analyse de la descendance, suivis de la descendance, cellule souche hématopoïétique (HSCs), division asymétrique, cellule T, destin de cellule, division asynchrone, oxydation des acides gras, mitochondries, peroxysomes, cellules sœurs, hydrogel

Contents

Acknowledgements .... **v**

Abstract .... **vii**

Keywords .... **viii**

Résumé .... **ix**

Mots-clés .... **x**

Motivation and objectives **15**

Motivation 15

Objectives and overview 15

Chapter 1 Introduction **17**

1.1 Hematopoietic stem cells 17

1.1.1 The bone marrow niche 18

1.1.2 HSCs in the clinic 19

1.1.3 HSC expansion *in vitro* 20

1.1.4 Markers defining HSCs 21

1.2 Micro-device for analysis at the single cell level 21

1.2.1 Cell tracking using conventional culture method 22

1.2.2 Single cell tracking using microwell arrays – “Passive platforms” 22

1.2.3 Single cell analysis using flow-based platform - “Active platforms” 23

1.2.4 Lineage tracking platform for HSCs 25

Chapter 2 Hydrogel-based groove array for lineage tracking of rare and fragile single cells **27**

2.1 Introduction 27

2.2 Materials and methods 29

2.2.1 pHEMA-TMPTMA groove platform fabrication 29

2.2.2 Preparation of acrylate-modified glass slide 29

2.2.3 Preparation of groove array, based on pHEMA-TMPTMA hydrogel polymer (bottom part of the platform) 29

2.2.4 pHEMA-TMPTMA surface characterization 29

2.2.5 Derivatization of the hydrogel surface with functional groups or proteins 29

2.2.6 Derivatization with thiols 30

2.2.7 Surface immobilization of proteins (proof-of-concept experiment) 30

- 2.2.8 Confocal imaging 30
- 2.2.9 Preparation of PEG hydrogel-based lid (top part of the platform) 30
- 2.2.10 Platform closure 32
- 2.2.11 HSCs extraction 32
- 2.2.12 Cell culture and time-lapse image acquisition 32
- 2.2.13 Immunofluorescent staining and confocal imaging 32

2.3 Results and discussion 33
- 2.3.1 Platform concept 33
- 2.3.2 Platform fabrication 34
- 2.3.3 Cell culture and multi-lineage tracking 36
- 2.3.4 Temporal and phenotypic information mapping 39

2.4 Conclusions 40
- 2.4.1 Acknowledgements 40

Supplementary Information for chapter 2 41

Chapter 3 Automated algorithm for the lineage tracking of single hematopoietic stem cells 43

3.1 Introduction 43

3.2 Materials and Methods 45
- 3.2.1 Isolation of LT-HSCs 45
- 3.2.2 Time-lapse microscopy 45
- 3.2.3 Automated cell tracking and reconstruction of the lineage tree 45
- 3.2.4 Statistical analysis 46

3.3 Results and discussion 46
- 3.3.1 Development of an automated lineage tracking algorithm for HSC analysis 46
- 3.3.2 Cell segmentation 46
- 3.3.3 Detection of the differentiation into megakaryocytes 49
- 3.3.4 Cell linking 49
- 3.3.5 HSCs’ analysis in the presence of drugs 54

3.4 Conclusions 55

3.5 Acknowledgements 56

Supplementary Information for chapter 3 57

Chapter 4 Monitoring of mitochondrial mass of HSCs in culture 59

4.1 Introduction 59

4.2 Materials and Methods 60
- 4.2.1 Isolation of LT-HSCs 60
- 4.2.2 Single HSC trapping and lineage tracking 60
- 4.2.3 Mitochondrial mass measurement 60
- 4.2.4 Colony Formation 61

4.2.5 Statistical Analysis 61

4.3 Results and Discussion 61

4.3.1 Characterization of HSCs cultured on a micro-groove platform for lineage tracking 61

4.3.2 Mitochondrial mass measurement in LT-HSCs and their lineages 62

4.3.3 Mitochondria are asymmetrically distributed in sister cells after divisions 62

4.3.4 Mitochondrial mass distribution asymmetry in different cell generations 65

4.3.5 Mitochondrial mass distribution asymmetry, correlated to mitochondrial mass of the mother cell . 67

4.3.6 Initial mitochondrial mass marks LT-HSCs fate 67

4.4 Conclusion 69

4.5 Acknowledgement 69

Chapter 5 Analysis of asymmetric markers in the first generation of cells derived from murine HSCs 71

5.1 Introduction 71

5.2 Materials and methods 72

5.2.1 *In vivo* activation of HSCs 72

5.2.2 Antibodies 72

5.2.3 Cell cycle analysis 72

5.2.4 Micro-groove array platform fabrication 72

5.2.5 PEG microwell array fabrication 72

5.2.6 Single cell proliferation analysis by time-lapse microscopy 73

5.2.7 Flow cytometry and cell sorting 73

5.2.8 HSC culture 73

5.2.9 Single cell proliferation analysis 73

5.2.10 Micromanipulation of paired daughter cells for single cell analysis 73

5.2.11 Selection of candidate genes 73

5.2.12 Single cell qRT-PCR 74

5.2.13 Immunostaining and images analysis in the multi groove platform 75

5.2.14 Glut1 staining for FACS analysis 75

5.2.15 Transplantation 75

5.2.16 CFU assay 75

5.2.17 Statistics 75

5.3 Results 76

5.3.1 *In vivo* activation of HSCs by IFNa increases asynchronous cell divisions 76

5.3.2 Identification of the asymmetric gene set using PDC gene expression analysis 78

5.3.3 Analysis of the protein expression of Glut1, JAM3 and HK2 by immunofluorescent staining 81

5.3.4 Characterization of Glut1 and JAM3 as markers for ACD in mHSCs 82

5.4 Discussion 84

Supplementary information for chapter 5 86

Chapter 6 Fate analysis of CD8+ T cell at the single cell level ... 89
6.1 Introduction ... 89
6.2 Material and method ... 90
6.2.1 CD8+ T cells extraction ... 90
6.2.2 EG7 cell culture ... 91
6.2.3 EG7 irradiation dose titration ... 91
6.2.4 Activation of OT-I CD8+ T cells and analysis ... 91
6.2.5 Time-lapse imaging ... 91
6.2.6 Image analysis ... 91
6.3 Result and discussion ... 92
6.3.1 CD8+ T cell activation with EG7 ... 92
6.3.2 EG7 and OT1 culture on the micro groove platform ... 93
6.3.3 Analysis of asymmetry between daughter cells ... 95
6.4 Conclusion ... 98
6.5 Acknowledgements ... 99
Supplementary Information for Chapter 6 ... 100
Chapter 7 General discussion and outlook ... 101
7.1 Technological development (Chapters 2 and 3) ... 101
7.1.1 Suggestion for the enhancement of the current platform ... 102
7.2 Biological experiments (Chapters 4 to 6) ... 102
7.2.1 Chapter 4 “Monitoring of mitochondrial mass of HSCs in culture” ... 103
7.2.2 Chapter 5 “Analysis of asymmetric markers in the first generation of cells derived from murine HSCs” ... 103
7.2.3 Chapter 6 “Fate analysis of CD8+ T cell at the single cell level” ... 104
7.3 Future biological application ... 104
7.3.1 Mouse and human HSCs ... 104
7.3.2 Suggestion of studies with other stem or tumor cells ... 105
References ... 107
Curriculum Vitae ... 123

Motivation and objectives

Motivation

During the past century, scientists discovered the remarkable ability of stem cells to give rise to all specialized cell types of a tissue, while at the same time producing more of themselves in a process termed self-renewal. This dual ability allows stem cells to maintain and repair tissues throughout the life of an organism and has made stem cells the prime cell type for clinical applications. In particular, hematopoietic stem cells (HSCs) were the first stem cell type to enter the clinics and are still very widely used for the treatment of leukemia and other blood disorders. In mice, even a single HSC is capable to reconstitute the entire blood system[1]. In mammals, adult HSCs are located in the bone marrow in a complex tissue environment called niche. Within the niche, the stem cells are exposed to external cues that dictate their fate, ensuring long-term self-renewal and blood production. Removal of stem cells from their niche (e.g. such as in cell culture) results in rapid differentiation. Numerous attempts to recreate HSC niche-like conditions *in vitro*, e.g. by testing cocktails of cytokines and growth factors[2] or by mimicking the extracellular matrix (ECM) conditions found in the niche, have been tested but a robust HSC expansion without loss of therapeutic potential has been difficult to identify[3,4]. Clearly, a better understanding of the fundamental mechanisms that regulate HSC self-renewal at single cell level are key in order to fully exploit their clinical potential.

Objectives and overview

The overall goal of this thesis is the development of a technology for the precise analysis of the progeny of single HSCs. This platform should combine advantages of microfluidics devices, where cells can be encapsulated to allow lineage tracking, and the easy cell handling, high-throughput analysis and gentle cell deposition provided by microwell array technologies. Since HSCs are extremely rare cells (~1000 cells per mouse), this platform should also allow easy handling of these cells without significant cell loss. Finally, the platform should be user-friendly so that any laboratory can implement it without any expertise in the use of micro-devices.

Chapter 1 of this thesis present an overview of the biology of the hematopoietic system. I also highlight the importance of studying HSCs at the single cell level and existing approaches enabling the observation of cell lineages using micro-systems.

Chapter 2 describes the development of an innovative high-throughput platform for single HSC lineage tracking.

Manual single-cell tracking and lineage analysis is tedious and time-consuming. To allow fast and efficient analysis of lineages obtained using the platform described in chapter 2, an automated lineage-tracking algorithm was created (**Chapter 3**). The algorithm automatically finds cells on images and associates them through frames, thus allowing the building of lineage trees.

Chapter 4 reports the characterization of HSC culture on the microchip platform and also shows the monitoring of mitochondrial mass of HSC during culture.

Chapter 5 presents an innovative methodology to discern differences in gene and protein expression between paired daughter cells after the first division. This analysis enabled the identification of novel markers that could be used to determine functional stem cells from committed progenitors during culture.

Chapter 6 presents a new application of the platform in the area of T cell biology. The experiment consists of a co-culture of T cell and antigen-presenting cells, that enables the observation of the entire process from antigen presentation to a T cell, to its proliferation. The analysis suggests that the first initial divisions of T cells are asymmetric and give rise to two distinct lineages.

Chapter 7 summarizes the studies performed in this thesis and discusses their relevance and outlines future perspectives.

Chapter 1 Introduction

1.1 Hematopoietic stem cells

Blood is a unique tissue that is responsible for multiple functions, such as carrying oxygen from the lungs to all other organs, helping them recover from bleeding, remodeling bones by removing dead cells and fighting infections from pathogens. All these functions are maintained by different specialized cells that need to be continuously replenished, due to their short life span. This homeostatic process of generation of blood cells is called “hematopoiesis”[5]. While many of these specialized cells circulate in the bloodstream, they originate from blood-forming environment, notably the bone marrow in adult mammals. Marrow is home to the most primitive cells of the blood tissue – the hematopoietic stem cells (HSCs) that are the ultimate and only source of all blood cells[5,6]. Although responsible for the regeneration of billions of new hematopoietic cells each day, HSCs are rare, with a proportion in the marrow of about 1 in 10,000 cells or in the bloodstream of 1 in 100,000[7]. To support the production of all blood cell lineages, HSCs first give rise to more proliferative cells, the short-term HSCs (ST-HSCs) and multipotent progenitor cells (MPPs). These multipotent progenitors generate large numbers of cells that progressively differentiate by first giving rise to lineage restricted progenitors that themselves further divide and progressively differentiate to form all the specialized cells of the hematopoietic system (Figure 1.1) [8,9].

The pool of HSCs decreases every time a cell is committed to differentiating, which would rapidly lead to HSC exhaustion. This phenomenon is counteracted by the capability of HSCs to self-renew (i.e., to produce more of themselves). It is noteworthy that this capacity is exclusive to HSCs and is lacking in progenitor cells, thereby making HSCs the only cells capable of long-term reconstitution of the blood tissue. The balance between differentiation and self-renewal determines the overall number of HSCs. This number of HSCs is finely controlled by a specialized environment called “the hematopoietic stem cells niche”.

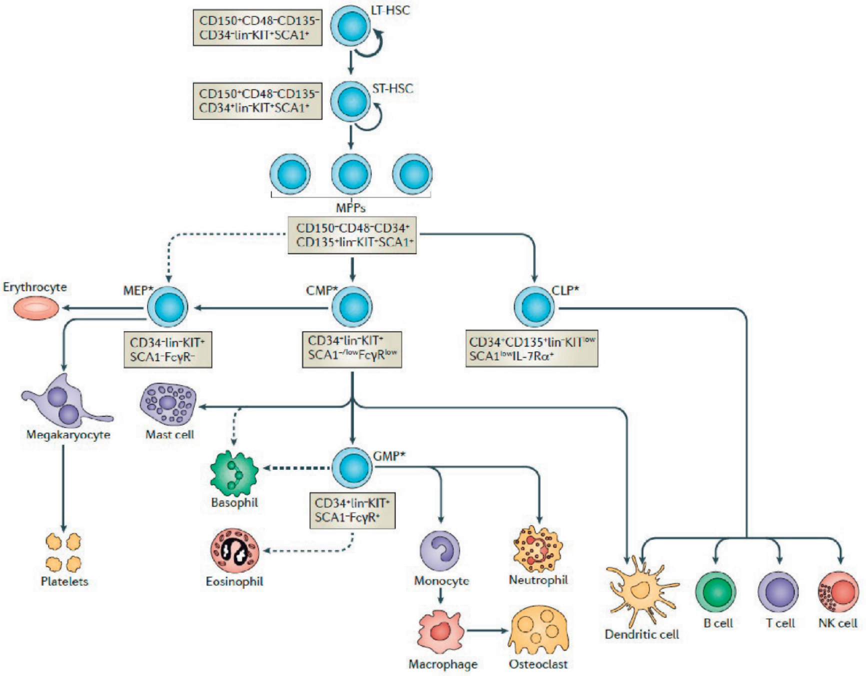
LT-HSC
$CD150^+CD48^-CD135^-$ $CD34^-lin^-KIT^+SCA1^+$
ST-HSC
$CD150^+CD48^-CD135^-$ $CD34^+lin^-KIT^+SCA1^+$
MPPs
$CD150^-CD48^-CD34^+$ $CD135^+lin^-KIT^+SCA1^+$
Erythrocyte
MEP*
CMP*
CLP*
$CD34^-lin^-KIT^+$ $SCA1^-Fc\gamma R^-$
$CD34^+lin^-KIT^+$ $SCA1^{-/low}Fc\gamma R^{low}$
$CD34^+CD135^+lin^-KIT^{low}$ $SCA1^{low}IL\text{-}7R\alpha^+$
Megakaryocyte
Mast cell
GMP*
Basophil
$CD34^+lin^-KIT^+$ $SCA1^-Fc\gamma R^+$
Platelets
Eosinophil
Monocyte
Neutrophil
Dendritic cell
B cell
T cell
NK cell
Macrophage
Osteoclast

Figure 1.1: The hematopoietic hierarchy. At the top of the hierarchy lies the most primitive population of the hematopoietic system: The LT-HSCs (Long-term HSCs). These cells can self-renew and differentiate. This dual ability permits at the same time to ensure lifelong blood production and protect HSCs from exhaustion. In contrast to LT-HSCs, ST-HSCs (Short-term HSCs) exhibit more limited self-renewal potential. ST-HSCs give rise to MPPs (Multipotent progenitors) that are cycling regularly. The MPPs give rise to the oligopotent progenitors (megakaryocyte-erythrocyte progenitor: MEP, common myeloid progenitor: CMP, lymphoid progenitor: CLP), and progenitors differentiate progressively into all the specialized cells of the blood tissue. Image from [10].

1.1.1 The bone marrow niche

The concept of the niche was proposed by Schofield in 1978[10] and can be defined as a specialized environment that promotes the maintenance of stem cells and regulates stem cell function[11,12]. The hematopoietic stem cell niche is composed of a multitude of different cells that nurture HSCs and provide cues that dictate HSC fate, namely quiescence, self-renewal, migration, apoptosis and differentiation (Figure 1.2D).

Observation of the localization of HSCs in tissue section (Figure 1.2A) revealed the existence of a “perivascular niche”, due to the presence of HSCs adjacent to sinusoidal blood vessels in the bone marrow and spleen[13], and of an “endosteal niche”, due to the presence of HSCs at the interface of the bone and the marrow (Figure 1.2B)[14]. Different studies have shown the crucial role of niche-cells like mesenchymal stem cells (MSCs), endothelial cells, neural cells and osteoblasts in mediating HSCs’ fate. In the endosteal niche in particular, osteoblasts were shown to be important for the maintenance of HSCs and their survival by expressing different factors like angiopoietin, Wnt, Notch, thrombopoietin and osteopontin[15–21]. Using transgenic mice, Calvi et al. demonstrated that an increase in osteoblast numbers induced HSC expansion, whereas osteoblast ablation resulted in a decrease of long-term HSCs’ self-renewal capacity and thereby reduced the HSC pool[22,23]. Other studies have revealed a subset of osteoblasts expressing the N-cadherin form N-cadherin/β-catenin complex with HSCs, perhaps mediating the attachment or adhesion of HSCs within the niche[24]. In the perivascular niche, CXCL12-abundant reticular cells (CAR) and MSCs were also shown to regulate HSCs' fate. Ablation of these cells resulted in a severe decrease in HSC numbers[25,26].

In addition to cell-cell interactions and soluble signals, the niche also provides "physical factors" such as oxygen tension[27,28]. Parmar et al. stained HSCs with a chemical marker for hypoxia and demonstrated that HSCs are in an hypoxic environment and are themselves hypoxic[29]. Spencer et al. performed measurements on the oxygen tension in the bone marrow niche and found that the oxygen tension is indeed low in the bone marrow[30]. In line with these results, other groups have shown that hypoxia inducible factor (HIF1α) – a regulator of oxygen homeostasis – is up-regulated in HSCs[31]. HIF1α was shown to promote HSCs' quiescence and maintenance[32]. Interestingly, HIF1α indirectly prevents pyruvate from entering the tricarboxylic acid cycle (TCA), thus blocking mitochondrial respiration[32] , making glycolysis the main energy source for HSCs[32,33].

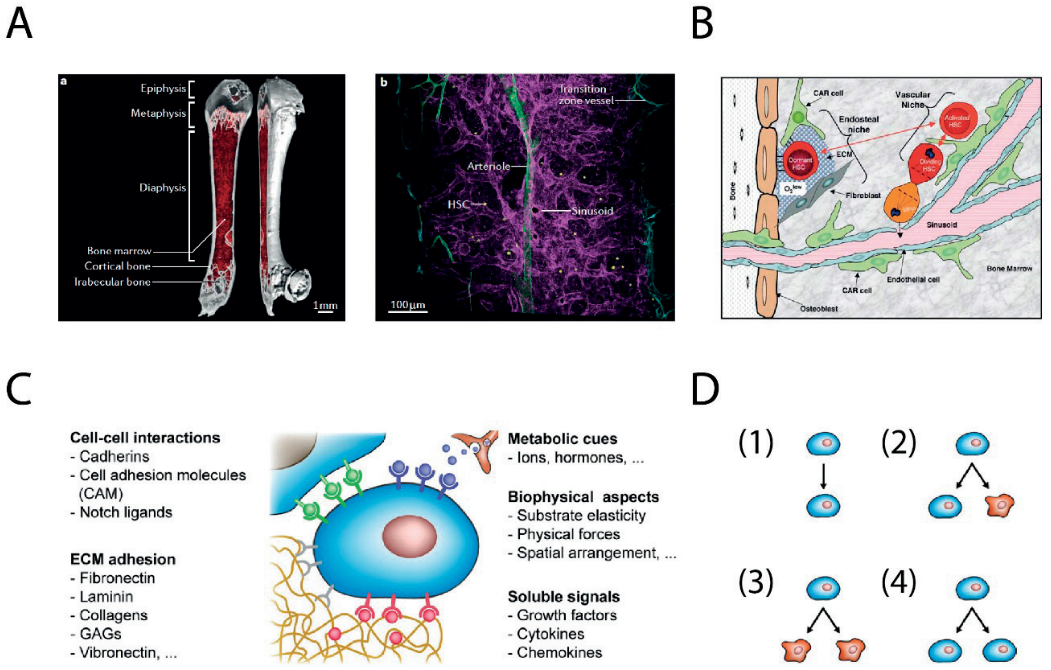
A
a
Epiphysis
Metaphysis
Diaphysis
Bone marrow
Cortical bone
Trabecular bone
1mm
b
Transition zone vessel
Arteriole
HSC
Sinusoid
100µm
B
CAR cell
Vascular Niche
Endosteal niche
Activated HSC
ECM
Dormant HSC
Dividing HSC
O_2^{low}
Bone
Fibroblast
MPP
Sinusoid
Bone Marrow
Endothelial cell
CAR cell
Osteoblast
C
Cell-cell interactions
- Cadherins
- Cell adhesion molecules (CAM)
- Notch ligands
ECM adhesion
- Fibronectin
- Laminin
- Collagens
- GAGs
- Vibronectin, ...
Metabolic cues
- Ions, hormones, ...
Biophysical aspects
- Substrate elasticity
- Physical forces
- Spatial arrangement, ...
Soluble signals
- Growth factors
- Cytokines
- Chemokines
D
(1)
(2)
(3)
(4)

Figure 1.2: The bone marrow, the HSC niche, and HSCs' fate. (A) On the left, a cross-section of a mouse femur showing parts of the bone and the marrow. On the right, an image of the vasculature (sinusoid in purple, arterioles in green, and transition vessels in blue) and HSCs (stained in yellow). Adapted from[11]. (B) Scheme of the two HSC niches – the endosteal niche and the vascular niche. The HSCs in the endosteal niche reside in a very hypoxic environment and are mostly in a quiescent state. The extracellular matrix (ECM) and the CXCL12-abundant reticular cells (CAR) seem to keep HSCs in a state of dormancy. In the vascular niche, activated HSCs are mostly located near the sinusoid, where HSC progenies are able to enter the bloodstream. Adapted from[14]. (C)-(D) Scheme of extrinsic cues in the niche that dictate HSCs' fate choices. Fate choices can be (1) quiescence or migration, (2) asymmetric division, (3) symmetric commitment, (4) symmetric self-renewal. Adapted from[233].

1.1.2 HSCs in the clinic

The regenerative potential of HSCs in humans was demonstrated in 1956, when the first bone marrow transplant was successfully performed to rescue a patient suffering from leukemia[34]. Marrow transplantation is still the procedure of choice today to treat blood-related diseases[7]. Clinical estimations reported that 40,000 transplantations were performed in Europe in 2014[35]. However, bone marrow transplantation efficiency is currently limited due to the high doses of HSCs required to achieve the rapid and sustained engraftment that is critical for patient survival and recovery[36]. The rate of mortality is therefore still high and ranges between 7% for patients with acute leukemia in remission and 27% for patients with refractory acute leukemia (100 days post transplantation)[34]. Moreover, 8–10% of the patients who survive for 2 years without disease relapse fail to survive due to hematopoietic failure[34].

Currently, the widespread application of HSCs to treat patients is severely restricted by the low number of cells that can be isolated from umbilical cord blood[7]. HSC expansion *in vitro* is therefore considered a potential solution that held great promise in clinics, but it has proven to be difficult to implement[37].

1.1.3 HSC expansion *in vitro*

As previously mentioned, methods that would be beneficial for the treatment of blood disorders require pre-amplification of HSCs *in vitro* while retaining HSCs' healing potential. Attempts to expand these cells have never resulted in a significant expansion of HSCs, unlike other types of stem cells, such as neurons stem cells, intestinal stem cells and embryonic stem cells, where expansion is routinely performed[7]. When HSCs are cultured *in vitro*, they rapidly differentiate as early as the first initial divisions and lose their stem properties[38]. The reasons lie in the fact that *in vitro* cultures are not able to recapitulate the bone marrow niche. Lack of critical cues from the niche pushes HSCs to a "default" fate of differentiation toward committed progenitors[7]. Despite considerable effort to understand the fundamental mechanisms underlying HSCs' fate choices, we are currently still unable to expand HSCs *ex vivo*. Fundamental biological mechanisms need to be understood in order to fully control HSC expansion through *in vitro* culture. Although HSC expansion is not yet possible over the long term, extensive efforts have been made to culture mouse HSCs. During the past decades, several proteins and chemicals have been identified for their actions supporting *ex vivo* expansion of hematopoietic progenitors. Stem cell factor (SCF) is one of the most important factors mediating HSCs' self-renewal[39]. Thrombopoietin (TPO) was described to be essential for HSCs and its genetic elimination leads to reduction of HSCs[40,41]. Serum-free culture supplemented by SCF and TPO has been shown to support survival and proliferation of HSCs. In contrast, other cytokines including IL3, IL6, IL11 and Flt3 ligand in combination with either SCF and/or TPO have been reported to mediate rapid HSC proliferation associated with a loss of long-term reconstitution potential[42]. *In vitro* treatment with Wnt3a has also been shown to promote HSCs' expansion[43]. However, conditional expression of β-catenin, an intracellular transducer of Wnt signaling, revealed impaired multilineage differentiation and transient increase in HSC numbers followed by exhaustion of the HSC pool[44,45].

Moreover, different pathways regulate important aspects of HSC maintenance. The TGF-b/smad signaling was shown to be a crucial pathway for maintenance of HSC quiescence[46]. Another important actor that prevents HSC differentiation and helps in HSC expansion *in vitro* is the Notch signaling pathways[47]. Suzuki et al. demonstrated that supplementation of Delta 1 (Notch ligand) with SCF, TPO, Flt3, IL3, IL6 in a serum-free medium resulted in a six-fold increase in the cell numbers. Intriguingly, Chiba et al. have reported that only small quantities/concentrations of Notch ligand support cord blood expansion and that high quantities/concentrations of Notch ligand induce apoptosis', if this satisfies your intended meaning.[47,48].

As previously explained, HSCs reside in a hypoxic niche, which imposes dramatic changes in their metabolic status in comparison to progenitor cells[49]. It was recently demonstrated that modulation of the metabolism via exposure to certain drugs could modulate HSC fate. Vannini et al. demonstrated that lowering the mitochondrial potential by drug-induced uncoupling of mitochondrial electron transport chain drives self-renewal *in vitro*[50]. Importantly, the authors also showed that low mitochondrial potential marks functional HSCs *in vitro*. Ito et al. performed another notable study controlling HSCs' fate. They artificially induced a metabolic switch through the activation of mitochondrial fatty acid oxidation (FAO), which resulted in an increase of asymmetric divisions (HSCs' maintenance)[51]. In contrast, when FAO was inhibited a loss of HSCs' self-renewal capacity was observed.

1.1.4 Markers defining HSCs

A variety of markers have been discovered to reliably identify functional HSCs when extracted from the murine bone marrow. The gold standard to assess whether a population is enriched in HSCs is to test the capacity of cells to reconstitute the blood tissue of a lethally irradiated mouse. The first markers in the field were based on the cellular size and density in combination with Hoechst staining[52]. Since then, major efforts have been undertaken to find a cell surface marker that can be used for HSC isolation by flow cytometry. For the mouse model, a set of markers allows the identification of all specialized hematopoietic cell lineages (defined as Lin). Within the Lin- (negative selection of Lin), HSCs were initially shown to reside in the positive fraction of cKit (cKit+) and Sca (Sca+), a population known as LKS (Lin-cKit+Sca+)[53]. LKS and CD34 negative population was shown to enrich for functional HSCs but was later shown to be a highly heterogenous populations, as demonstrated by long-term blood reconstitution assay[1]. Different markers have been identified in subsequent years to improve HSC enrichment, especially since the introduction of the SLAM family markers (CD150 and CD48), which highly improved the purity of HSCs[54,55].

A commonly used combination of these markers to purify functional HSCs is LKS CD34-CD150+CD48- [14]. Other combinations allow identification of early progenitors in the hematopoietic hierarchy by upregulation of both CD34 and CD48 (ST-HSCs) or by a down-regulation of CD150 (MPPs) [14]. Importantly, Zhang et al. demonstrated that these markers used to sort fresh HSCs or progenitor cells are expressed differently during culture *in vitro*[37], and become unreliable.

1.2 Micro-device for analysis at the single cell level

Living tissues are formed by different cell types, and the assumption was that each cell type has a distinct function, lineage and fate[56]. Single cell studies have revealed that this assumption is incorrect. While a population of a cell type might be identical morphologically or have similar phenotype, this population is made up of individual cells that differ dramatically[57]. Therefore, analysis of an entire cell population results in averaged measurements, and hides cell-cell variations within the population[57]. Cell-cell variations might have important consequences in the functioning and health of a tissue. A relevant example was demonstrated by Sato et al., who used HeLa cells – a presumably homogeneous cancer cell line – and revealed that only a small subset of cells can self-renew and are responsible for the replenishment of the entire colony[58]. It is understood that single cell analysis allows precise measurement of cell populations by considering that each cell is unique; however, analysis at the single cell level is often a challenge. Until recently, single cell studies have been limited by the cost and throughput required to examine large numbers of cells. These issues are even more challenging when the starting population of cells to be analyzed is rare (e.g., HSCs, circulating tumor cells)[57,59]. These limitations and roadblocks inspired scientists to fabricate new tools to enable observation at the single cell level, in high throughput and at low cost. In the following sections, I present methods that enable single analysis.

1.2.1 Cell tracking using conventional culture method

The isolation of single cells from an entire cell population should be performed in such a way that cells preserve their biological integrity[56]. The most straightforward and probably easiest method involves only gravity, of letting cells in suspension fall onto a flat substrate. Once cells have reached the bottom of the plate, single cells are tracked using time-lapse microscope. This method enables lineage tracking[60], immunofluorescence staining analysis (only with adherent cells) [61], and protein expression analysis when cells are genetically modified and express a reporter gene[62]. Recently, Alber et al. combined this approach with genetically modified cells to measure synthesis and degradation rates of endogenous protein in embryonic stem cells (ESCs)[63].

The main disadvantages of this method were: (1) cell movement in all directions, resulting in a mix-up of all lineages, (2) the requirement of using adherent cells, (3) cells had to be imaged quite frequently (2-4 min) to not lose single cell tracking[64], (4) formation of cell aggregates that prevent single cell analysis, (5) single cell analysis could only be performed reliably as long as cells were isolated from one another and could be treated as non-interacting single cells[65], (6) low throughput.

The limitations of the above culture system have spurred the development of numerous cell culture platforms using state-of-the-art microfabrication technologies. The term microfabrication involves the implementation of miniaturized structures at the micron scale using techniques such as photolithography, soft lithography, laser ablation, embossing and micromachining[66].

1.2.2 Single cell tracking using microwell arrays – “Passive platforms”

One of the most common platforms for single cell analysis is the microwell array[67,68]. Microwell arrays are topographically structured surfaces of “opened” micron-sized chambers (i.e., microwell) (Figure 1.3A). Microwells can be made in different materials including bulk polymer[69,70], polymer hydrogels[68] and even glass[71]. Microwells vary in size and height depending on the application, allowing single cell isolation by sedimentation (gravity). After cell seeding each microwell will contain the lineage derived from one single cell.

Advantages of microwell arrays are countless, due to their ease of fabrication combined with their high versatility in terms of modification. Possible modifications include: biomolecules anchoring on the microwell surface, stiffness of the material, shape of the microwells and proteolytic degradation of the substrate[63,68,72].

In the context of stem cells, microwell array tethered with biomolecule can be used to mimic some components of the *in vivo* niche. The so-called “artificial niche” in the microwell arrays is combined with single cell imaging to asses change of behavior of stem cells [68,73]. To ultimately prove that the “artificial niche” has a positive effect on the stem cells (i.e., it protects stem cells from loss of stemness), the functionality of cells must be tested via transplantation into a sick host [68,73].

It is important to note that adherent cells can migrate away from their initial captured microwell. To support adherent cells’ culture onto microwell array the substrate should prevent cell adhesion in order to avoid cells overcoming the topographical barrier[74]. Typical non-adhesive substrates include agarose and poly(ethylene glycol) (PEG) hydrogels[68,75].

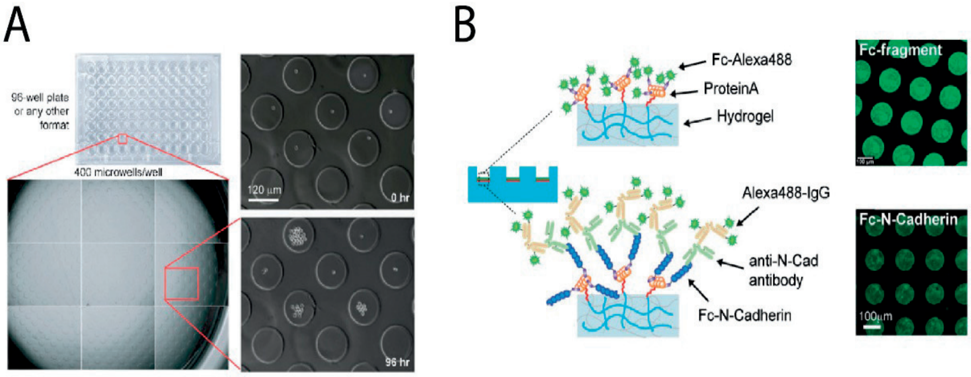

Figure 1.3: Microwell technology. (A) PEG microwell arrays allow single cell studies in high throughput. Each well of the 96-well plate contained 400 microwells made in PEG hydrogel. (B) Example of a strategy to anchor biologically active biomolecules on the PEG microwell surface. This technique allows the presentation of "niche-like" candidates to cells and consequently to study the specific role of biomolecules in HSCs' fate decisions. Image from[149].

To minimize cell handling and increase the single cell capture efficiency in one microwell, Lindström et al. developed a method where each cell can be placed at an exact position[76]. To this end, they combined a microwell platform placed on a motorized stage with a conventional flow cytometer. The motorized stage permitted precise movement of the microwell platform so that each cell that was ejected from the cytometer arrived in a different microwell[76]. This technique is especially interesting when dealing with a small number of cells. Despite clear advantages over conventional mammalian cell culture substrates, microwell arrays have some limitations: (1) Microwell arrays are "passive" platforms, medium cannot be changed easily because any perturbation would flush cells away, (2) The movements of cells in microwells make it difficult to track individual cells, (3) Post-culture assay (i.e., immunocytochemistry) is not possible for the same reasons as in (1).

1.2.3 Single cell analysis using flow-based platform - "Active platforms"

Alternative approaches have addressed the microwell limitations by using microfluidic platforms. Microfluidics is a generic term describing platforms that contain a pattern of micro channels. The ensemble of micro channels forms the "microfluidic network" that is connected to the macro-environment by holes. For single cell analysis, the microfluidic network is used to direct cells in suspension into individual cavities where they are cultured individually.

Park and others enabled single analysis on a microfluidic platform by merging the microwell array platform with a channel network placed on top of the microwells[77,78]. In this platform, the flow pushes cells in the top channel horizontally and by gravitational force cells are gently directed vertically until they reach the microwells at the bottom. However, trapping efficacy is quite low in such platforms. By adding a valve at both entrance and exit of the top channel, Jan et al. were able to interrupt the flow, which allowed cells to sediment more freely in the microwells, yielding better capture efficiency[77]. Based on the same concept, Lecault et al. designed a platform to enable long-term culture of HSCs. The perfusion of the device at different times with a medium containing SCF (i.e stem cell factor) made it possible to observe when the stimulation by stem cell factor was first required for HSCs to exit their quiescent state[79]. It is noteworthy that the platform of Lecault, is the only one allowing HSC culture over the long term in the presence of flow.

Other groups focused on the efficiency and throughput of single cell trapping in microfluidic devices. Dino Di Carlo, Tan and Takeuchi, pioneers in the field, created two different trapping devices using flow streamlines to direct single cells into a small unit usually called a “hydrodynamic trap”. Arrays of hydrodynamic traps can be generated, facilitating high-throughput single cell analysis [80–86]. However, many of these devices do not allow observation of cell progenies due to lack of space in the hydrodynamic traps. Consequently, other groups combined hydrodynamic traps with microwells placed next to the hydrodynamic traps. This modification permitted observation of the entire cell lineage, migration and differentiation[87–89]. Another solution to observe cell lineages is to isolate daughter cells after division in downstream hydrodynamic traps[82,90].

Other platforms using hydrodynamic traps have been shown to enable on-chip or off-chip RT-qPCR for single cell gene analysis[82,91,92]. Other approaches to single cell capture use external forces to retain cells in desired positions produced by dielectrophoresis force (DEP) optical tweezers, magnetic and acoustic waves [93–97]or pico-liter droplets[98].

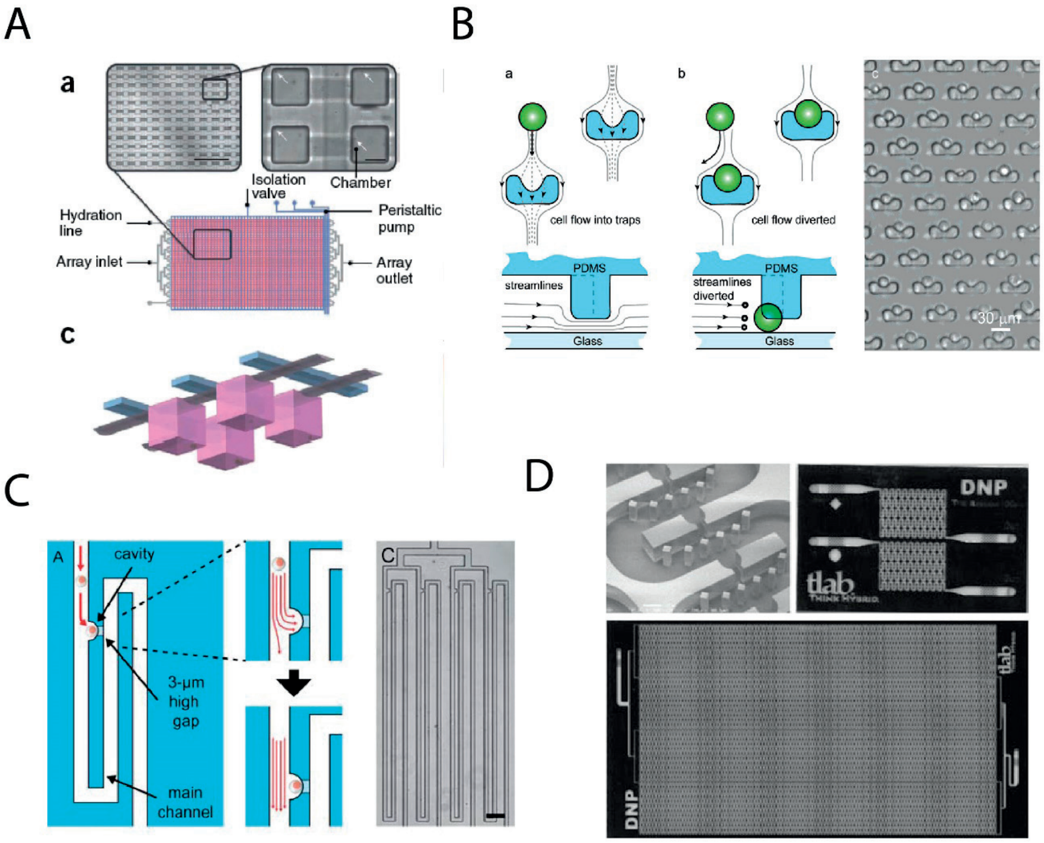
A
a
Isolation valve
Chamber
Hydration line
Peristaltic pump
Array inlet
Array outlet
c
B
a
cell flow into traps
PDMS
streamlines
Glass
b
cell flow diverted
PDMS
streamlines diverted
Glass
30 µm
C
A
cavity
3-µm high gap
main channel
C
D
DNP
tlab
DNP
tlab

Figure 1.4: Microfluidics-based devices for single cell trapping. (A) Microwells (or chambers in the image, in pink) are connected to a network of channels (in blue). The channel network is placed on top of the microwells, therefore cells can sediment from the channel into the microwells. Each microwell will contain one colony derived from one single cell. The depth of the microwell prevents cells escaping or being flushed away during perfusion. Image adapted from80. (B) Hydrodynamic trap array. Flow streamlines direct cells into the traps. It follows a change of flow-resistance through the hydrodynamic traps that prevents additional cells being captured in the same traps. (C-D) Platforms with alternative designs of hydrodynamic traps91. (D) Hydrodynamic traps array allowing ultra-high throughput of single cell analysis87.

1.2.4 Lineage tracking platform for HSCs

Single cell lineage tracking provides useful biological data, such as proliferation kinetics and single cell lineage tree construction. Lineage trees are necessary to unambiguously decode differential responses of a single cell in distinct states[64,99]. This is particularly interesting to implement in the frame of stem cells, in order to study the different cell types that can arise from the initial mother cell[100]. Analyzing stem cell progenies is an old approach that was already performed in 1905 by Conklin et al.[101]. However, modern techniques revolutionized the field by allowing direct observation of gene or protein expression in the progeny via fluorescent reporter gene or protein quantification via immunofluorescence staining. Lineage tracking can be achieved *in vitro* and *in vivo*, but here the focus is only on *in vitro* techniques.

The most straightforward approach that enables lineage tracking *in vitro* is to seed cells on a conventional culture plate and to acquire images at regular time intervals. However, it has to be considered that cells are usually motile, which has the following consequences: (1) Tracking can become ambiguous, especially if the frequency of acquisition is not high enough to resolve cell movement precisely, (2) Progenies from two distinct single cells can be mixed, (3) Cells can exit the field of view.

Issues (1) and (2) can be resolved by imaging cells every 2-4 min and by seeding cells at a low concentration, so that one FOV contains only one progeny[60]. Problem (3) can be fixed only by using another culture approach (like a microwell array platform as indicated previously). For this reason, this approach has the disadvantage of having a very low throughput while creating an enormous number of images. Nevertheless, pioneers in the field have used this approach to analyze lineage[60,102,103] of mesodermal cells giving rise to endothelial cells and blood colonies. Through this experiment the authors demonstrated that a progeny of blood cells can have as ancestors hemogenic endothelial cells[60]. To cope with the large amount of data generated in such experiments, they created a computer-based algorithm that automatically builds lineage trees. The limitation of such a system is that the tracking algorithm requires fluorescent images to detect cells and it is combined with a high rate of image acquisition. This leads to phototoxicity and cell death in the long term.

Establishment of novel tools to study lineages without the requirement of frequently imaging cells and without fluorescent reporters to track cells would be highly beneficial. This problem was addressed by Rowat et al., who used an elegant strategy to capture single cells and observe their progenies using a microfluidic platform. Briefly, single mother cells are directed into a long, rectangular trapping channel and captured at the extremity of this channel by a hydrodynamic trap[89]. Because the trapping channel is long and narrow, daughter cells are forced to grow in a line, which allows unambiguous progeny tracking (Figure 1.5A). An equivalent method consists of isolating cell progeny after each division in downstream trapping units[82,104] . Another strategy was proposed by Moffitt et al., who proposed seeding bacteria onto a platform containing long tracks, followed by encapsulation of the cells with an agarose lid (Figure 1.5B)[105]. Similar to Rowat's platform, cells were forced to grow in line, which allowed reliable tracking.

Despite the number of microfluidics platforms that allow single cell trapping, only an extremely small number of them support long-term culture, probably due to the fact that cells suffer from shear stress and die. The most successful idea was probably the hydrodynamics traps, but this device fails to support fragile cells such as HSCs, probably due to the deleterious damage resulting from shear stress[106,107].

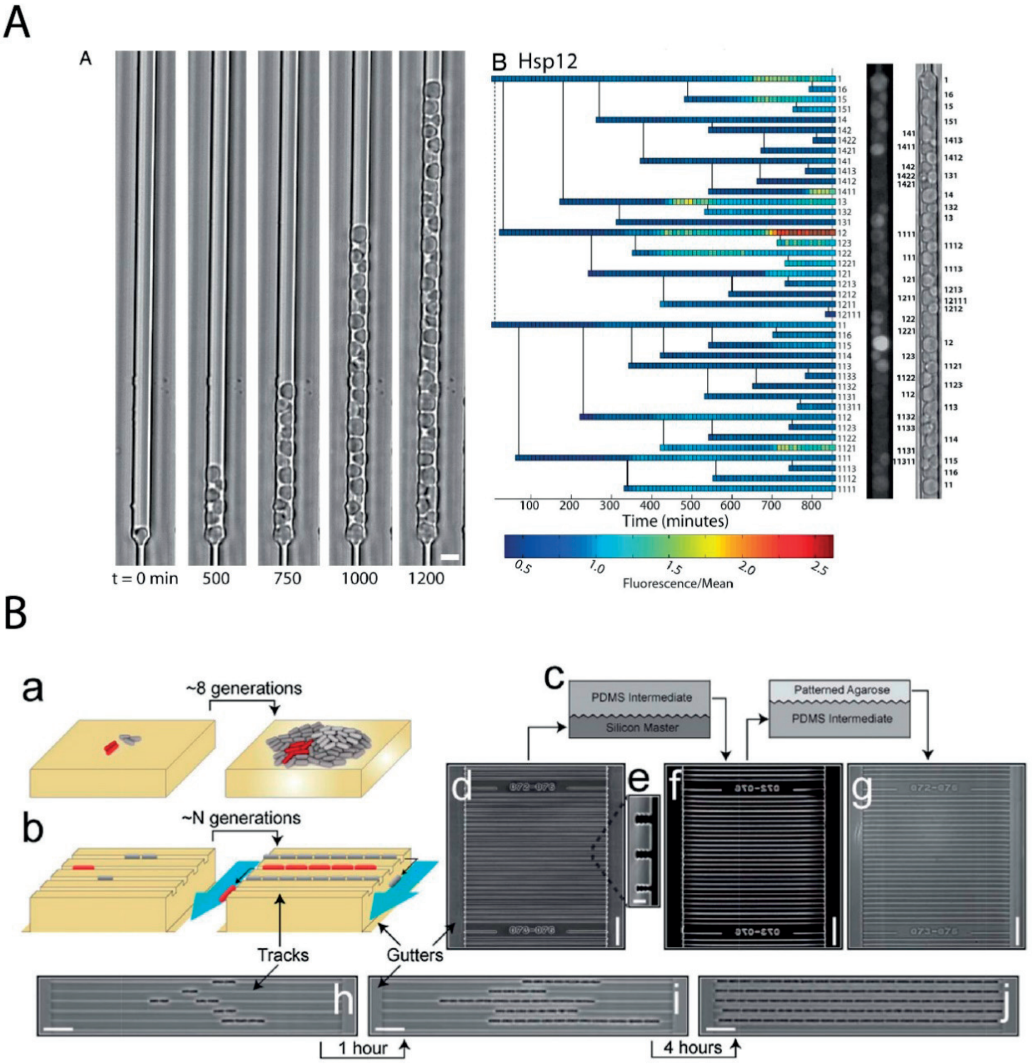
A
A
t = 0 min
500
750
1000
1200
B Hsp12
1
16
15
151
14
142
1422
1421
141
1413
1412
1411
13
132
131
12
123
122
1221
121
1213
1212
1211
12111
11
116
115
114
113
1133
1132
1131
11311
112
1123
1122
1121
111
1113
1112
1111
100
200
300
400
500
600
700
800
Time (minutes)
0.5
1.0
1.5
2.0
2.5
Fluorescence/Mean
B
a
~8 generations
b
~N generations
Tracks
Gutters
c
PDMS Intermediate
Silicon Master
Patterned Agarose
PDMS Intermediate
d
e
f
g
h
i
j
1 hour
4 hours

Figure 1.5**:** Single cell trapping device that allow progeny tracking. (A) (Left) Individual yeast cells are captured by an hydrodynamic traps and cultured in a long channel. The width and height of the channel are calculated so that cells are constrained and must grow in line, ensuring unambiguous lineage tracking. (Right) Measurements of protein expression on individual yeast. Images from[89] (B) Lineage tracking of yeast in an agarose hydrogel and polydimethylsiloxane (PDMS) platform. Here bacteria are captured by sedimentation and encapsulated in grooves. Similarly to (A) unambiguous tracking is enabled by constraining cell so that they must grow in line. Image from [105]

Chapter 2 Hydrogel-based groove array for lineage tracking of rare and fragile single cells

Abstract

Single cell isolation, followed by tracking of the progeny over a long period of time, has proved to be challenging. Key difficulties of this task involve the necessity of continuous and frequent visualization of cellular dynamics for several days in a row, the need of a platform that would allow unambiguous tracking of cell lineages, and the requirement of a reliable methodology of single cell isolation which would not affect the survival or fate of the cell. Here, we introduce a novel gravity-based single cell, multi-lineage tracking platform, designed for working with rare and fragile cells (<1-10k). To achieve single cell capture and its lineage tracking, we have developed a new type of closed rectangular chamber, produced from two distinct hydrogel materials: poly(2-hydroxyethyl methacrylate)-trimethylolpropane trimethacrylate copolymer (pHEMA-TMPTMA) and self-assembling poly(ethylene glycol) (PEG). This chamber encapsulates an array of grooves, in which single cells are cultured. Single cells are restricted to growing in a line inside the same, unique grooves of the platform, to which they were seeded at the beginning of the experiment. Such a design enables unambiguous tracking of a single cell and its progeny. The gravity-based cell seeding method allows protection of the cells from the deleterious mechanical stress of a flow-based trapping system and also to achieve highly efficient single cell capture. The permeable nature of porous hydrogel material facilitates access of the cells to the nutrients of the culture medium, opening up the possibility of long-running experiments, including tracking of multiple generations of single cell progeny. To evaluate the potential of this platform, we applied it to investigation of the proliferation kinetics and peroxisomal protein expression levels within the independent lineages of single, non-adherent primitive hematopoietic stem cells (HSCs).

2.1 Introduction

Precise analysis of the key processes controlling the fate of a single stem cell and its lineage is an essential step towards understanding the fundamental processes taking place in stem cells. This knowledge is valuable for their successful application in regenerative medicine. However, single stem cell isolation and progeny tracking has proved to be challenging, especially when the initial material is rare[57].

A common strategy for progeny tracking involves the isolation of mother cells in individual chambers. After the mother cell division, its daughter cells are then constrained in a long chamber and grow in a line[89,88,105] or, alternatively, are captured in the downstream trapping units[82,104]. Such devices allow unambiguous tracking of the cell progeny. However, in the majority of microfluidic devices hydrodynamic traps are implemented to capture single cells to a chamber, where the flow continuously pushes them, thus minimizing cell escape[81]. While this approach is effective for single cell isolation, such devices have some practical disadvantages, especially in work involving experiments with rare and sensitive cells. Firstly, cell loss during transportation from macro- to micro-environments is considerable[108]; secondly, the flow tends to induce mechanical shear stress, which is deleterious for stem cell survival and might bias its fate in the long term. To reduce shear stress, the flow rate could be decreased, but this usually leads to the formation of bubbles in the microfluidic network due to water evaporation through the PDMS pores[109]. A remarkable microfluidic device, developed by Lecault et al.[110], partially solves these problems by supporting HSC expansion via gravity-based isolation of cells into deep squared chambers containing microwells, where at the bottom of the microwell shear stress is minimized. Thus, at the end of the experiment each microwell contains a colony of cells derived from a single cell. This device is similar to the platform, based on array of microwells, that also uses gravity to trap cells inside the small cavities, where they divide[111]. Significantly, in the case of experiments with rare and fragile cell types, microwell array-based platforms provide several practical advantages, such as minimizing the number of cells lost during the transfer from the macro- to micro-environment; passive nutrient delivery to the cells (i.e., without creation of an active flow), which greatly improves cell viability; and the possibility of high-throughput analysis[112,76]. However, in the last two examples microcolonies are not spatially organized. This disadvantage imposes a requirement of very frequent (if not continuous) imaging to allow efficient cell progeny tracking. For the same reason, microwell array-based approaches would not allow fixation and further workup of the cells, which is necessary for analysis of protein expression by immunofluorescent staining.

The primary goal of this work was to improve existing approaches to the tracking of single cells and their progeny by combining the advantages of passive (i.e., without use of fluidics) devices, such as microwell arrays, with the benefits of closed platform such as a microfluidic device, where cells are spatially organized, allowing unambiguous tracking of the cell progeny. Importantly, such an approach would make possible the correlation of the experimental data obtained by tracking of single live cells with the data on protein expression levels in the same cells that can be gained by fixation and immunofluorescent staining. We have strived, therefore, to develop a microgroove-based platform, which can be closed after the cell seeding step to protect the cells from escaping from the initial groove or from interchanging their relative positions as well as to preclude the loss of the fixed cells after fixation. Crucially, such closure should not lead to any impairment of cell viability.

However, platform closure in the presence of cells is a difficult task, due to the fact that such a procedure could potentially be harmful to live cells. PDMS bonding, for example, is achieved by activating surfaces via oxygen plasma treatment, a lethal procedure for cells[113]. Alternative polymers, that offer other bonding approaches, were recently developed. In particular, robust strategies of covalent chemical bonding of layers via “click” chemistry provide numerous advantages[114,115]. These chemical reactions are efficient, selective and can be easily implemented in the context of different substrates. Efficient bonding of two polymers in particular can be achieved in a one-step fashion, when one polymer exhibits excess of thiol groups on its surface and the other excess of the complementary thiol-reactive groups[116]. Thus, we have chosen to implement thiol-vinylsulfone Michael reaction as the method of platform closure in the presence of cells. This reaction is particularly interesting, because it occurs near physiological pH and temperature[117,118].

To validate the potential of our platform design, we have used it to track the division kinetics of single hematopoietic stem cells (HSCs) and correlated this information to the levels of peroxisomal protein PMP70 expression in the same cells.

Additionally, our platform design allows the cell-contacting surface of the polymer to be readily coated with bioactive molecules. We have demonstrated the proof of this concept by modifying the surface with fluorescent FITC-BSA protein.

2.2 Materials and methods

2.2.1 pHEMA-TMPTMA groove platform fabrication

Azobisisobutyronitrile (AIBN), 2-Hydroxyethyl methacrylate (HEMA), Trimethylolpropane trimethacrylate (TMPTMA), Pentaerythritol tetraacrylate (PETA), Acetic acid, (3-Mercaptopropyl)trimethoxysilane (MPS), acetic acid (AA), Tributylphosphine were all purchased from Sigma Aldrich Switzerland and were used as received, if not specified. Tetrahydrofuran (THF) (Sigma) was dried under molecular sieves before use.

2.2.2 Preparation of acrylate-modified glass slide

12mm glass slides were subjected to liquid phase salinization in order to derivatize their surfaces with acrylate functional groups (Supplementary Figure S2.1A). Slides were placed into the holding rack and immersed in a close tank, containing a solution of 4% MPS and 3% of aqueous acetic acid (1:10 AA:H2O volume ratio) in ethanol. Glass slides were incubated overnight at 80°C in oven in the N_2 atmosphere. They were further rinsed thoroughly with ethanol and dried in N_2 flow at 80°C for 15min or overnight at RT, then immediately immersed in a solution of 0.05% tributylphosphine and 2.5% PETA in THF and allowed to react at room temperature under argon atmosphere for 30min. Derivatized glass slides were washed in THF and dried at RT. Derivatized slides were used for further steps within 2 days.

2.2.3 Preparation of groove array, based on pHEMA-TMPTMA hydrogel polymer (bottom part of the platform)

pHEMA-TMPTMA was polymerized on 0.13mm thick glass slide (Corning Glass), derivatized with acrylate groups to ensure optimal adhesion between the glass surface and polymer (Figure 2.1A, Supplementary Figure S2.1A). Bulk pHEMA-TMPTMA hydrogel was prepared by radical polymerization at 70°C in oven with N2 flow, using a reaction mixture, consisting of HEMA, TMPTMA, ddH20 and AIBN in the following volume ratios: 88.5:10:1:0.5. The solution was mixed and purged with N_2 for 5minutes and directly poured onto PDMS stamps. Standard soft lithography processes were implemented to create PDMS stamps. They were directly cast on silicon wafer, reproducing the desired pattern of rectangular pillars. The acrylate-derivatized glass slides were placed onto a 5-10uL drop of polymerization mixture (Figure 2.1B). Polymerization was performed for 24h. Upon completion of polymerization, PDMS stamp was peeled off from the cross-linked hydrogel, the resulting platforms were washed with THF in order to remove residual monomers and dried in a chemical hood overnight prior to the next steps.

2.2.4 pHEMA-TMPTMA surface characterization

Surface topography of pHEMA was measured on the WYKO NT 1100 optical profilometer (Veeco, Plainview, NY) and scanning electron microscope (SEM) Zeiss LEO 1550 for more precise structural observation.

2.2.5 Derivatization of the hydrogel surface with functional groups or proteins

The free hydroxyl groups of pHEMA-TMPTMA hydrogel were derivatized with tricholotriazine (TCT), introducing electrophilic dichlorotriazine moieties to the polymer surface and making it reactive to various nucleophiles (Supplementary Figure S2.1B). Briefly, platforms were immersed in a solution, containing 2% TCT and 4% DIPEA in THF, placed into a desiccator and allowed to react for 30min under stirring under argon atmosphere at RT. Upon reaction completion, the platforms were washed 3 times with THF and then ddH20.

A two-step reaction was further used to covalently bind nucleophile-bearing molecules to the activated pHEMA-TMPTMA hydrogel surface (Supplementary Figure S2.1B). The triazine ring-bound chlorines can be substituted in a stepwise manner, based on the strength of the corresponding nucleophile and temperature of the reaction[119].

2.2.6 Derivatization with thiols

The activated platforms were immersed in a buffered solution (PBS, pH 7), containing 3% dithiothreitol (DTT), under argon atmosphere. After 3 days of incubation, the platforms were washed 3 times with PBS (pH 5.5) and immersed in acidic PBS buffer (pH 5.5) at 4°C to protect thiols from oxidation until use. To prove the presence of covalently-bound thiols on the resulting hydrogel surface, DTT-derivatized platforms were incubated with the solution of thiol-reactive fluorophore Cell Tracker Violet (Thermofisher). Unspecific binding of the fluorescent dye was controlled by comparison to the results, obtained by incubation of the non-DTT-derivatized pHEMA-TMPTMA hydrogel with Cell Tracker Violet solution under same conditions (Figure 2.3).

2.2.7 Surface immobilization of proteins (proof-of-concept experiment)

A solution of 1% (w/w) FITC-labelled BSA (Sigma Aldrich, Switzerland) (pH 7.4) was reacted overnight with TCT-derivatized pHEMA-TMPTMA surface to demonstrate the possibility of covalent binding of the protein molecules to the activated hydrogel surface. Unspecific binding of the protein was controlled by comparison to the results, obtained by incubation of the non-TCT-derivatized pHEMA-TMPTMA hydrogel with FITC-labelled BSA solution under same conditions (Figure 2.3).

2.2.8 Confocal imaging

Z-stack images at 60x of grooves were acquired using confocal microscope (slices thickness=0.3um, Nikon Ti-Z, crest spinning disc) and 3D reconstructions were performed using imageJ.

2.2.9 Preparation of PEG hydrogel-based lid (top part of the platform)

To create a lid, which is permeable for cell culture nutrients, and which can be used in the combination with the bottom part (thiol-bearing pHEMA-TMPTMA hydrogel) to close the platform, preventing the live cells from escaping from the grooves, electrophilic thiol-reacting PEG hydrogel was prepared according to Lutolf and al[120]. PEG polymer was produced through reaction of 10kDa 4-arm-PEG-TH and 20kDa 4-arm-PEG-VS precursors, mixed to the final concentration of 2.5% total PEG in a triethanolamine buffer 0.03M (pH 7.7)[121]. Polymerization of PEG was achieved by spreading 10uL of precursor mixture onto the 9mm glass slides, which were previously immerged in a solution of polyvinyl alcohol (PVA) and then dried at RT. To ensure the presence of free vinylsulfone groups within the resulting hydrogel, the molar ratio between PEG-thiol (PEG-TH) and PEG-vinylsulfone (PEG-VS) precursors was adjusted to 40% excess of PEG-VS. This allowed to achieve the closure of the platform through the covalent binding of the surfaces, based on the Michael addition of thiols of the bottom part to the vinylsulfone groups of the top part (Figure 2.1C).

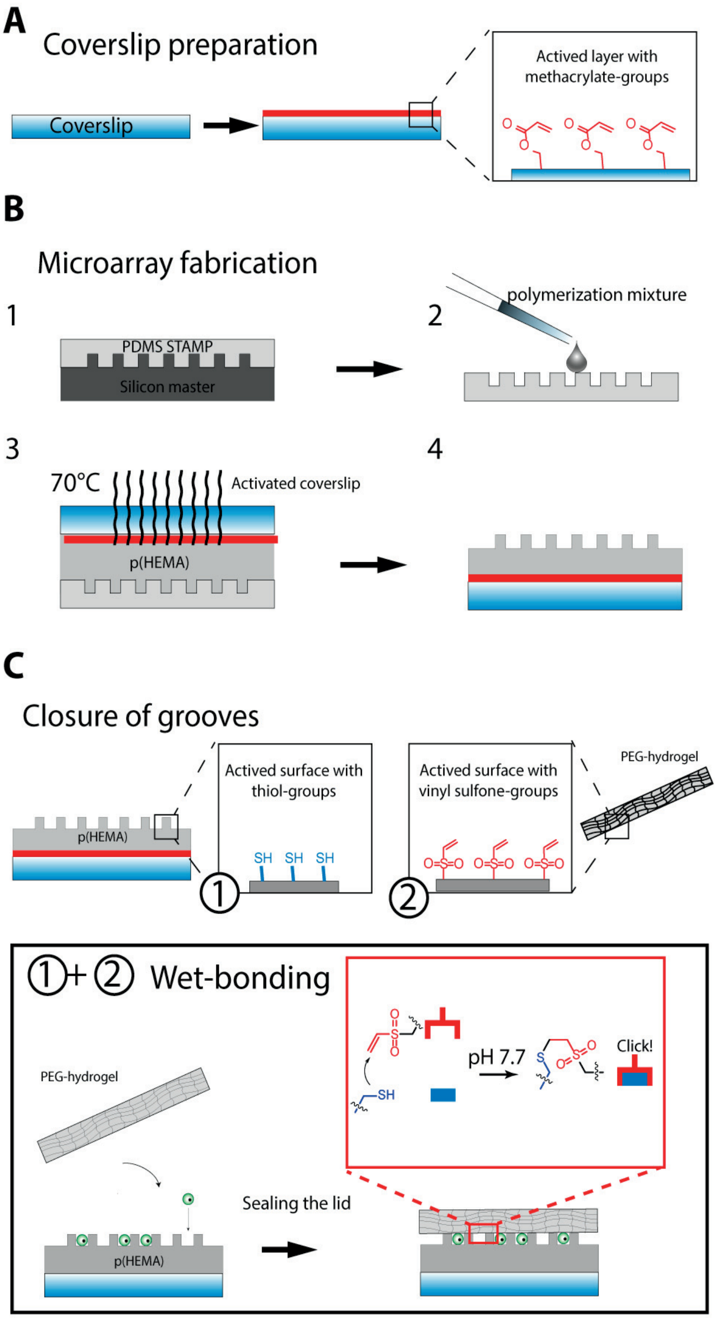
A
Coverslip preparation
Coverslip
Actived layer with methacrylate-groups
B
Microarray fabrication
1
PDMS STAMP
Silicon master
2
polymerization mixture
3
70°C
Activated coverslip
p(HEMA)
4
C
Closure of grooves
p(HEMA)
Actived surface with thiol-groups
SH SH SH
①
Actived surface with vinyl sulfone-groups
②
PEG-hydrogel
①+② Wet-bonding
PEG-hydrogel
p(HEMA)
Sealing the lid
pH 7.7
Click!
SH

Figure 2.1: General strategy and fabrication steps, used for the platform manufacture. (A) Optimal adhesion between glass slide and pHEMA-TMPTMA polymer is obtained by activating the glass substrate with acrylate groups via a two-step reaction (see also Fig. SI, A). (B) Fabrication of the bottom part of the platform. (1) PDMS stamp is cast on a silicon wafer. (2-3) Polymerization mixture is applied to the stamp and the curing is performed at 70°C. (4) PDMS is removed from fully cross-linked pHEMA-TMPTMA. (C) Closure of the groove and cell encapsulation is performed via “click” chemistry between thiol moieties on the bottom part (1) and vinylsulfone moieties present on the top part of the platform (PEG-lid) (2).

2.2.10 Platform closure

The platform closure was performed by carefully placing a glass slide, containing the PEG lid, onto pHEMA-TMPTMA hydrogel-based bottom part, containing the groove array with the previously seeded live cells. The platform was further immersed in a PBS buffered solution (pH 8) at RT and centrifuged at 5g for 15min to allow the Michael addition to occur. After that the glass substrate was carefully removed from the lid and the resulting closed platform with encapsulated live cells was washed 3 times with the standard culture medium.

2.2.11 HSCs extraction

Hematopoietic stem and progenitor cells were isolated from crushed bone marrow of 8-16 weeks C57Bl/6 mice. Erythroid cells were eliminated by incubation with red blood cell lysis buffer (Biolegend). Lineage depletion (CD3, B220, Ter-119, CD11, Gr-1) was performed using the Hematopoietic Progenitor Cell Enrichment set (BD Biosciences). Cells were stained with SAV-PO (Life Technologies), Kit-PE-CY7 (2B8, BioLegend), Sca1-PE (D7, BioLegend), CD150-BV784 (TC15-12F12.2, BioLegend), CD48-PB (GM48-1, BioLegend), CD34-eF660 (RAM34), eBioscience). LT-HSCs were sorted as Lin− C-kit+ Sca1+ (LKS) CD150+ CD48− CD34−, ST-HSCs as LKS CD150+ CD34+ and MPP as LKS CD150-CD34+.

2.2.12 Cell culture and time-lapse image acquisition

After extraction, cells were seeded onto the platform and time-lapse microscopy was performed. Cells were imaged every 30min or 1h. HSCs were cultured in serum free medium (StemlineII, Sigma-Aldrich, St. Louis, USA) supplemented with 100ng/ml stem cell factor (SCF) and 2ng/ml Flt-3 ligand (R&D Systems, Minneapolis, USA). PPAR-δ agonist (GW501516, Sigma Aldrich) was supplemented at a concentration of 20nM, if needed.

2.2.13 Immunofluorescent staining and confocal imaging

At the end of culture, cells were fixed in 2% PFA and permeablized with 0.1% TritonX. Cells were stained with anti-PMP70 antibody (Abcam). Z-stack images were acquired at a magnification of 60x using a Visitron CSU-W1 confocal spinning disk microscope.

2.3 Results and discussion

2.3.1 Platform concept

To study single cell progeny, we developed a hybrid hydrogel-based platform to create a closed array of grooves that enables precise tracking and analysis of the lineage of single cells, including rare, non-adherent stem cells. Our strategy primarily focused on the gentle handling of cells during their trapping and culture, but also on the practical ease of manipulation of a small number of sensitive cells. The concept of the device is based on the microfluidic platform presented by Rowat in 2009. Briefly, single mother cells are directed into a long, rectangular trapping channel, in which daughter cells are forced to grow in a line[89]. To be able to close the device to achieve encapsulation of single cells inside the individual grooves, we selected PEG-based hydrogel as a highly permeable top layer (lid) and pHEMA-TMPTMA-based hydrogel as a bottom layer to serve as the basis for a rigid groove structure. In our device design, nutrients can passively diffuse through hydrogel pores and reach the cells trapped in the grooves. This allows us to avoid the recurrent problems of PDMS- and flow-based devices[57,109], mentioned earlier.

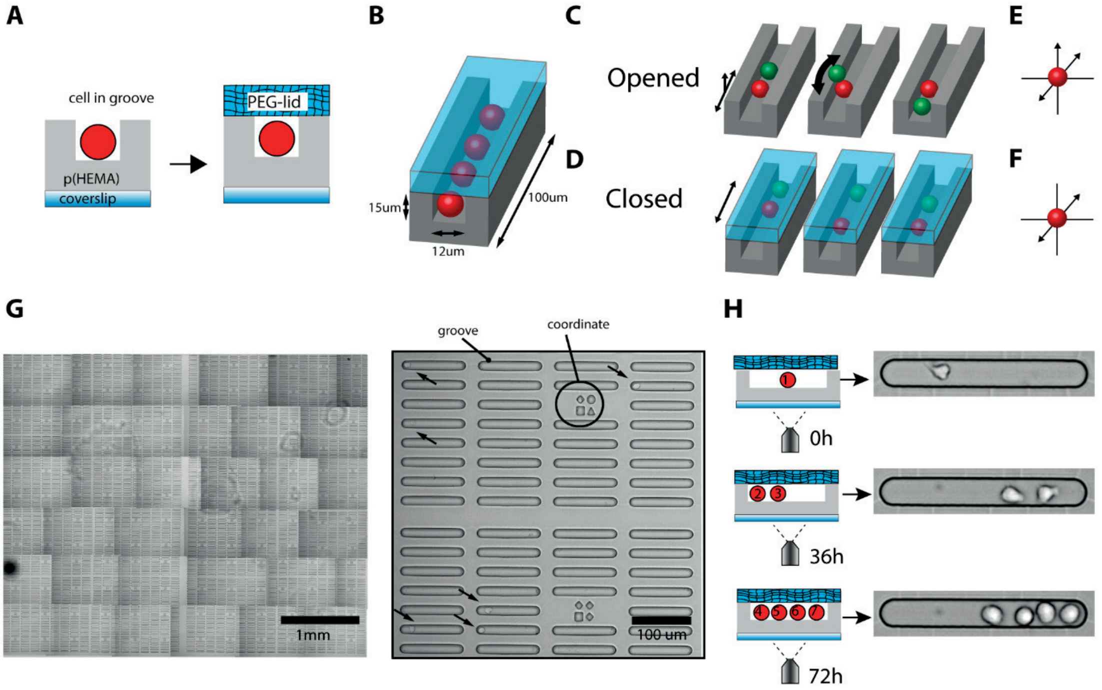

Figure 2.2: Overview of single cell trapping and tracking method principles used in the platform. (A) The device is closed after gravitational cell sedimentation through “click” reaction. (B) Groove dimensions are designed for particular cell types, here the dimensions used are 12x15x100um (width x height x length). (C-E) A cell in the open platform can freely move and therefore interchange its position with other cells, which leads to ambiguous tracking. (D-F) In a closed platform, cells are encapsulated and restricted to moving and growing along one axis. (G) Micro-groove array (left) with a high magnification image of a representative area (right). Black arrows indicate single cells seeded onto the platform. The positions of particular grooves can be unambiguously identified through the presence of coordinate landmarks, introduced during the soft lithography stage. (H) Temporal information (proliferation kinetics) can be assessed by time-lapse microscopy.

2.3.2 Platform fabrication

We have designed a device based on rectangular microgrooves array, to facilitate the lineage tracking of a rare cell population and allow convenient analysis (Figure 2.2G and Figure 2.3A). The platform fabrication relies on separate production of a bottom and a top part. These parts are produced from two chemically different hydrogel materials: the bottom part from 2-hydroxyethyl methylacrylate/trimethylolpropane trimethacrylate copolymer (pHEMA-TMPTMA) and the top part (lid) from self-assembling poly(ethylene glycol) (PEG) (Figure 2.1B-C). These two parts are combined together after the live cells are seeded into the grooves of the bottom part. During the closure of the platform the top and bottom parts are covalently bonded to each other through the use of click-chemistry (thiol-vinylsulfone Michael reaction). pHEMA-TMPTMA hydrogel is much stiffer and provides a robust mechanical structure for the cell-encapsulating groove compartment of the bottom part. In contrast, the PEG lid is soft and permeable for cell culture nutrients, thus allowing them to reach live cells during the course of the experiment. This combination of mechanical durability and easy supply of nutrients opens up the possibility of carrying over lineage tracking experiments for multiple generations of a single cell progeny.

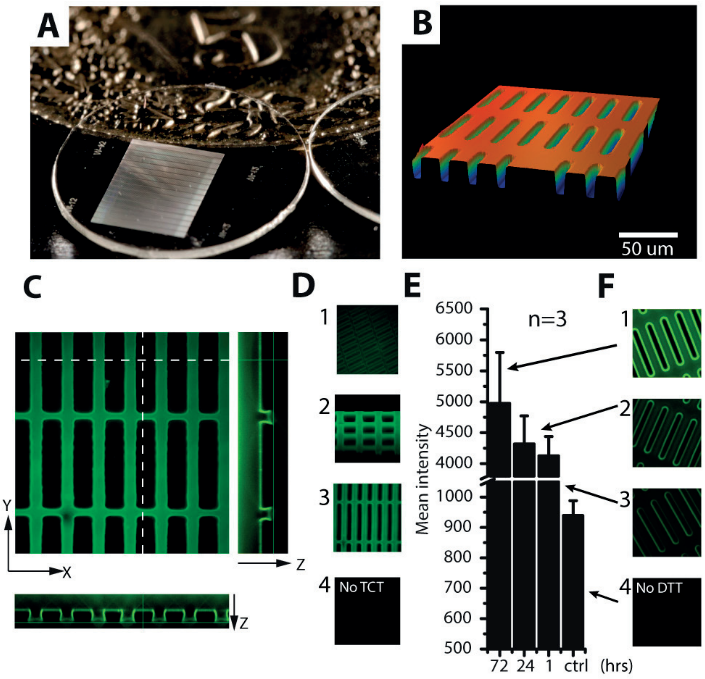

Figure 2.3: pHEMA-TMPTMA surface characterization and derivatization. (A) A photograph of the bottom part of the platform made of a glass coverslip with a layer of pHEMA-TMPTMA polymer, containing 4300 micro-grooves. A small coin is shown in the photograph for scale. (B) 3D shape reconstruction of the platform grooves, obtained by optical profilometry. (C-D) 3D reconstruction of confocal images of the platform grooves, after BSA-FITC was allowed to react with dichlorotriazine moieties on the TCT-derivatized pHEMA-TMPTMA surface. (E-F) TCT-derivatized pHEMA-TMPTMA polymer was allowed to react with DTT for 72h (1), 24h (2), 1h (3), or not reacted.

Groove dimensions were optimized to suit the tracking of single hematopoietic stem or progenitor cell. The width of the groove (12um) was chosen in order to prevent the possibility of two daughter cells interchanging their relative positions (Figure 2.2B-E). This condition is mandatory for the subsequent unambiguous tracking of a single cell lineage tree.

PDMS was chosen as an inert mold for bottom part production during pHEMA-TMPTMA polymerization. A potential problem with the usage of PDMS material could be mild adhesion of the PDMS mold to the pHEMA-TMPTMA upon the completion of polymerization. Such an eventuality could hypothetically introduce mechanical defects into the groove features, when the PDMS is peeled from the polymerized pHEMA-TMPTMA. To check whether such a problem had occurred, the quality of surface topography of the pHEMA-TMPTMA polymer, obtained after the PDMS mold was peeled off, was characterized with an optical profilometer and SEM imaging. As illustrated in Figure 2.3B, the groove features do not show any significant defects. Closer inspection of the SEM images (Supplementary Figure S2.2) shows that even submicron structural features of the PDMS mold, which appeared as the consequence of the previous production step, are preserved on the surface of the groove wall, proving that the structural quality of the resulting pHEMA-TMPTMA grooves can be reliably reproduced.

On its own, pHEMA-TMPTMA hydrogel does not possess the ability to covalently bind biologically active molecules, while such surface modifications could be used to customize the properties of the material to achieve optimal culture conditions for a variety of cell types. It is also necessary to be able to derivatize the polymer surface with the free thiol groups to facilitate the possibility of subsequent closure of the platform. These requirements can be met through activation of the surface of pHEMA-TMPTMA polymer with sufficiently reactive electrophilic moieties, to which various nucleophiles could be covalently anchored. To achieve that, we utilized a two-step chemical modification of pHEMA-TMPTMA surface. First, the pHEMA-TMPTMA polymer was treated with TCT to derivatize the hydroxyl groups of polymer surface with the reactive dichlorotriazine moieties (Supplementary Figure S2.1B). This renders the polymer surface reactive towards various nucleophiles. Dichlorotriazine moieties can be subsequently substituted with DTT to introduce thiols or with amine- or thiol-containing biological molecules (e.g., proteins). Successful activation of pHEMA-TMPTMA with TCT was proven by immobilization of fluorescent FITC-BSA protein on the polymer surface (Figure 2.3C-D). Similarly, to prove the successful derivatization of the surface with thiols, surface immobilization of the thiol-reactive fluorophore Cell Tracker Violet was demonstrated (Figure 2.3E-F). In both cases the intensity of the fluorescence signal detected for the modified polymer surface was much higher in comparison to the underivatized polymer.

Our platform is aimed at permitting a precise, image-based analysis of the progeny of a single cell at high magnification. Since the high magnification light microscope objectives have a relatively narrow working distance range, the distance between the cells and objective must be as small as possible. This can be achieved by minimizing the thickness of the polymer at the bottom of the grooves within pHEMA-TMPTMA hydrogel. This problem was successfully solved by spreading 5 to 10ul of pre-polymerized mixture on a circular PDMS mold approximately 8mm in diameter. It was noticed that during polymerization part of the material was lost due to evaporation; however, this did not introduce significant practical problems for further imaging experiments, performed with 60x magnification objective (Figure 2.5B). Another complication was caused by the fact that, when pHEMA-TMPTMA polymer was produced on a non-modified glass cover slip surface, it tended to crack and delaminate from the cover slip during the cell culture experiments within 24 hours. This precluded the possibility of long-term cell tracking experiments. We hypothesize that mechanical stress, resulting from the swelling of the hydrogel immersed in water, and low natural affinity of pHEMA-

TMPTMA to the glass are the reasons for this phenomenon. A similar problem was observed for another HEMA-based polymer in a previously published study[122]. Therefore, we chemically modified the glass surface, derivatizing it with free acrylate moieties, to which the pHEMA-TMPTMA can be cross-linked during the polymerization (Supplementary Figure 2.1A). First, a silane coupling agent (MPS) was used to modify the glass cover slip surface with free thiols, and the pentaerythritol acrylate (PETA) was used to react with the resulting thiol groups, introducing free acrylate groups to the surface of the glass cover slip (Supplementary Figure S2.1A). When the polymerization of pHEMA-TMPTMA was performed on such an activated glass surface, no delamination occurred during the cell culture experiments. A few microscopic cracks within the polymer can still be observed (as seen in Figure 2.4B), which can be explained by the residual mechanical tension in the material during the swelling; however, these minor cracks do not create any practical problems for further live cell experiments.

The covalent bonding of the top and bottom parts of the platform (platform closure) was performed through the Michael reaction between thiol groups introduced to pHEMA-TMPTMA surface and vinylsulfone groups present on the PEG lid (Figure 2.1C). The rate of this reaction increases with pH, but to optimize the cell viability during the platform closure the buffer pH was set to 7.7[117]. We have observed that sufficient adhesion between top and bottom parts of the platform occurred after 15min in these conditions. Prior to platform closure, the mixture of PEG precursors is allowed to crosslink on a glass substrate to provide the support for convenient manual manipulation of the lid. However, removing the polymerized PEG lid from the glass surface without damaging it in these conditions proved to be difficult. Therefore, a pre-coating of the glass cover slip surface with a sacrificial layer of polyvinyl alcohol (PVA) was implemented, in accordance with Nelson[123]. As PVA rapidly dissolves in water-based medium after immersion, this approach allows easy detachment of the glass from the PEG lid. In the optimized procedure of the platform closure, a glass cover slip with an attached PEG lid is carefully placed on top of the bottom layer with the subsequent removal of the cover slip by a horizontal sliding motion. This method avoids damage to the platform structure or the entrapped cells. The adhesion force between the PEG and pHEMA-TMPTMA must be sufficient to sustain external mechanical forces during the cell culture experiments and post-culture assays, involving multiple changes of the media. Therefore, we tested the strength of adhesion by mimicking mechanical stress through pipetting of the culture medium up and down in the proximity of the closed platform lid. These tests showed that in the majority of cases the lid stayed in place. Differences in adhesion strength are likely caused by human technique errors during the lid deposition step.

2.3.3 Cell culture and multi-lineage tracking

The applicability of the platform for practical biological assays was tested on murine hematopoietic stem cell (LT-HSCs, ST-HSCs) and progenitor populations (MPP). These cells are widely recognized to be fragile and extremely sensitive to external stress[57,124], presenting significant technical challenges for the platforms which are used to study them. To our knowledge, no experimental data involving the multi-lineage tracking of a single cell progeny was reported for the most primitive hematopoietic stem cell population (LT-HSCs). Thus, we strived to implement our closable microgroove-based approach for the culture of HSCs.

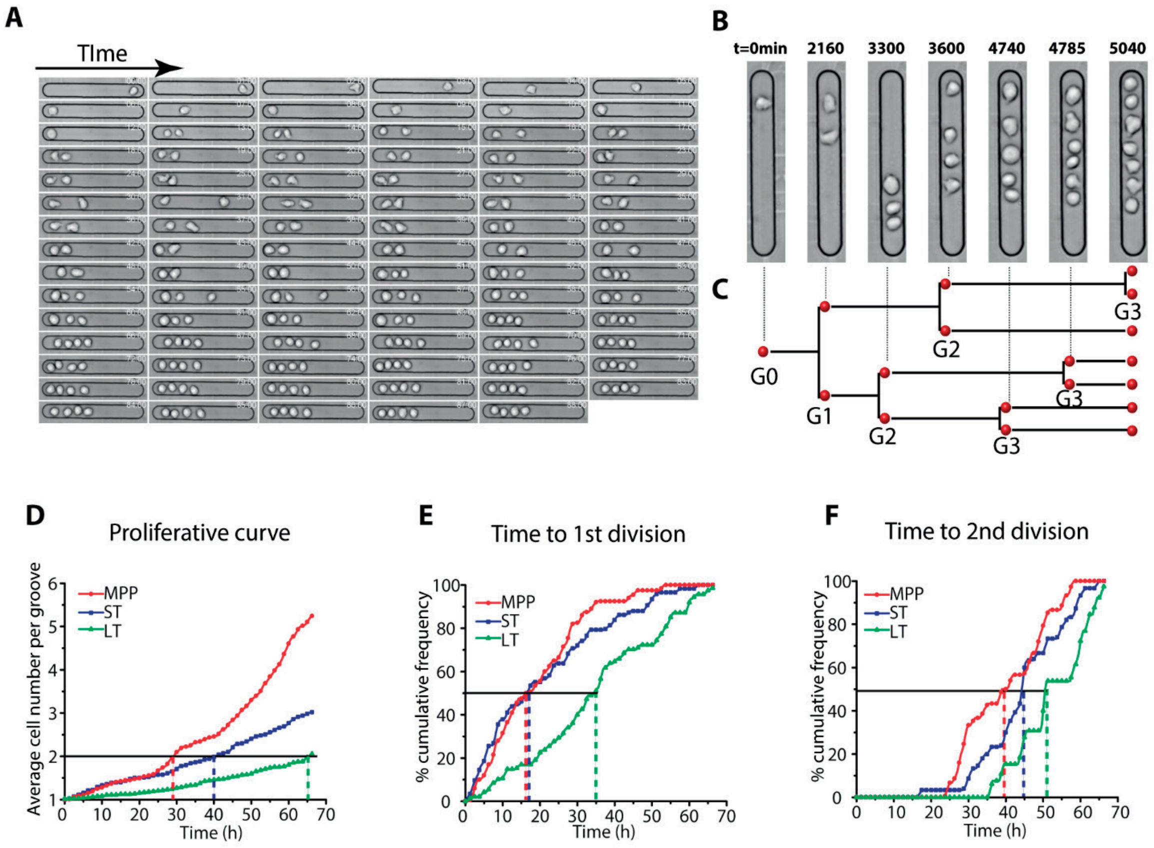

Figure 2.4: Multi-lineage tracking of single hematopoietic stem cells and proliferation kinetics analysis of HSC populations. (A) Representative images obtained during time-lapse microscopy of single LT-HSCs. (B-C) Single cell dividing up to the 3rd generation with corresponding lineage tree. (D) Average proliferation rates, measured for live single cells of 3 different populations of HSCs: ST-, LT-HSCs and MPP. As expected, the most primitive cells (LT and ST) exhibit slower kinetics, compared to MPP. Percentage of dead cells: MPP=0%, ST-HSCs=9.5%, LT-HSCs=25.3%, (red, MPP; blue, ST-HSCs; green, LT-HSCs). (E) Cumulative histogram of time spent until first division for indicated population (red, MPP; blue, ST-HSCs; green, LT-HSCs). (F) Cumulative histogram of time between the first and second divisions (red, MPP; blue, ST-HSCs; green, LT-HSCs). Number of live single cells for LT-HSCs n=74, ST-HSCs n=67, MPP n=45.

The number of cells seeded into the platform at the beginning of a typical biological experiment was significantly smaller than the number of corresponding grooves in the platform. This allowed achieving the situation where, following the seeding step, most of the grooves initially contained just a single cell inside (Figure 2.2G). We checked whether the encapsulation of HSCs impairs their survival. We also analyzed the viability of HSCs following 3 days of culture in our platform. The cells demonstrated good viability (>75% with LT-HSCs, >90% with ST-HSCs and MPP) in these conditions. More detailed analysis showed that most cell death events happened at the beginning of the experiment, shortly after the cells were seeded into the grooves. This suggests that these cells were damaged during the multiple manipulations prior to seeding. Overall, the viability analysis suggests that the culture inside the platform does not induce significant cell death in HSCs. Multi-lineage cell tracking and the cell division analysis were performed following bright field time-lapse microscopy, when the images were acquired every 30min or 1h. Efficient tracking of the kinetics of cell division within a groove was achieved in all experimental conditions (Figure 2.4A-B). In particular, we did not observe

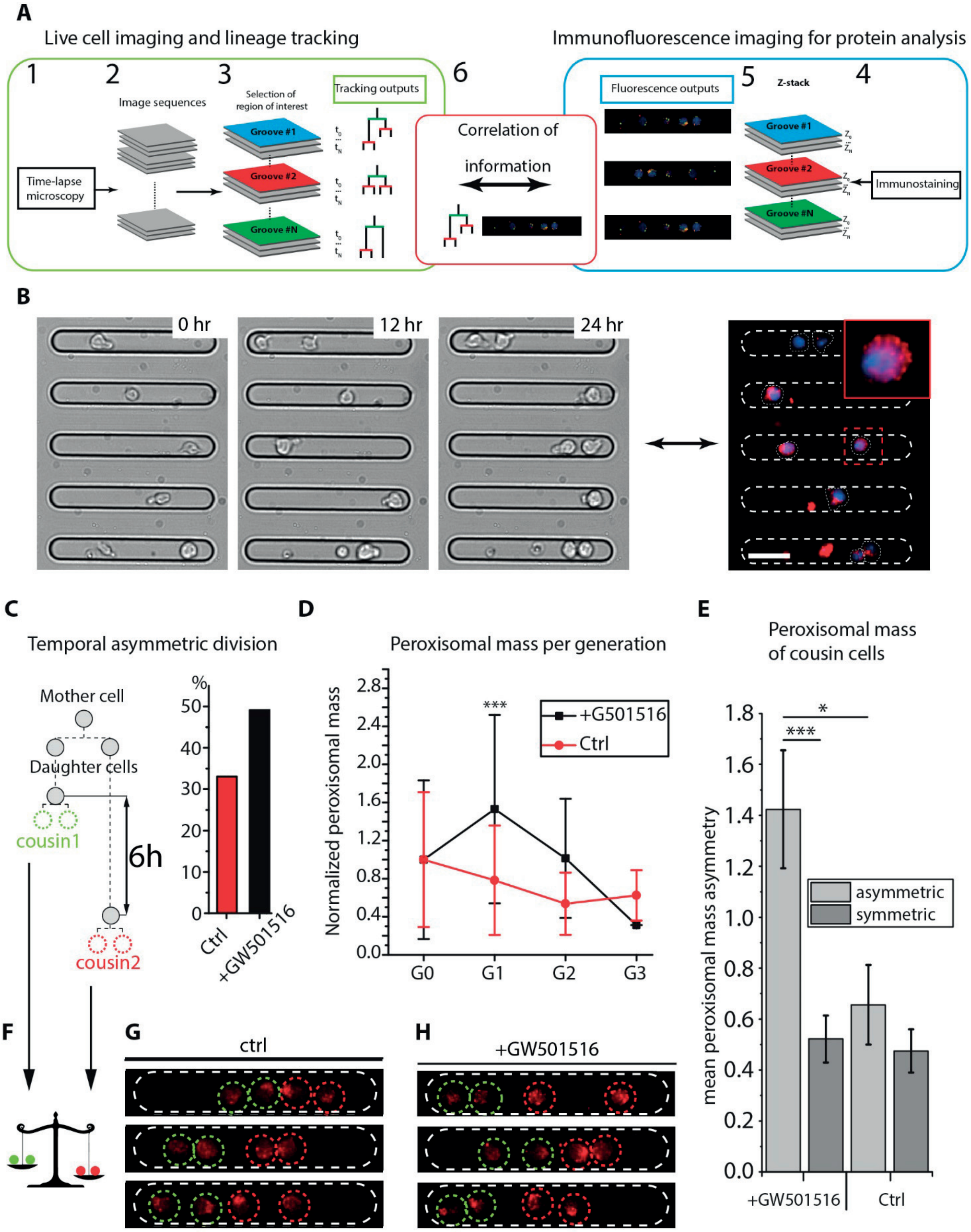

Figure 2.5 Temporal and phenotypic information mapping. (A) (1) Single cells inside the grooves are tracked by bright field microscopy imaging at low magnification (10x). (2-3) Corresponding lineage trees are extracted from time-lapse images. (4) The cells are fixed and processed for immunofluorescent staining. (5) Confocal fluorescent imaging of fixed cells is performed at high magnification (60x). (6) Finally, temporal and phenotypic information is correlated. (B) HSCs are cultured for 24h, then fixed, stained with PMP70 (red) and Hoechst (blue), and Z-stacks of confocal fluorescent images are acquired (60x magnification). Cells remained at their initial positions after culture and staining, enabling correlation of phenotypic and temporal information mapping. Scale bar = 25 μm. (C) HSCs were cultured either in the presence of PPAR-δ agonist (GW501516), or not. An increase of temporally asymmetric divisions (33% to 48% in untreated and treated populations, respectively) was observed. (D) PMP70 protein expression (representing peroxisomal mass) was quantified in several HSC generations (G0, G1, G2, G3: zero, first, second and third order generation, respectively). (E) Quantification of PMP70 signal intensity (representing peroxisomal mass) for cousin cells was correlated to temporally asymmetric and symmetric divisions. (C,E,F) For each pair of cousin cells (depicted in green or red on schemes), index of symmetry of peroxisomal mass distribution was calculated as a ratio as follows: $(A)symmetry = \frac{mean(cousin1)-mean(cousin2)}{mean\ (cousin2)}$, with $mean(cousin1) > mean(cousin2)$. (G-H) PMP70 staining of cells. Images show the sum of pixels along z-axis. Error bars represent SD, n=232 cells (GW501516 treated cells), n=248 cells (control). Statistical analysis was performed by one-way ANOVA and Bonferroni post-Hoc test. ***p< 0.001

the phenomenon of “cell escaping”, where a cell, initially seeded into one groove is moved to another, or when the cells “jump” on top of one another, interchanging their relative position within the same groove. Hence, it can be concluded that the platform with the closed lid ensures that the cells are securely encapsulated inside the grooves and grow reliably in line. It was previously shown that LT-HSCs gives rise to HSCs with more-limited self-renewal potential (ST-HSCs) and ST-HSCs further differentiate to generate multipotent progenitors (MPPs). While the LT-HSCs remain mostly in a quiescent state, ST-HSCs and especially MPPs divide more frequently[125,126]. We compared the proliferation kinetics of these three populations to assess whether the platform changed the proliferative behavior of these populations of cells (Fig. 4D-F). In line with previous study, the number of divisions changed dramatically from the LT-HSCs to MPPs with concomitant increase as we moved down in the hematopoietic hierarchy[73].

2.3.4 Temporal and phenotypic information mapping

To demonstrate the possibility of acquisition of the biologically relevant data during the cell culture experiments in our platform, we have correlated the kinetics of single live cell divisions (temporal mapping) with the distribution of the peroxisomal protein PMP70 between the pairs of daughter cells (phenotypic mapping) at the end of the 3-day long cell culture experiment (Figure 2.5). The phenotypic mapping is achieved by immunofluorescent staining of fixed cells, and the temporal information mapping is derived from time-lapse imaging of live cells. Thus, to correlate the kinetic and phenotypic information for the same cells, it is obligatory that the exact spatial positions of the cells can be unambiguously defined throughout the analysis of the experimental data. To demonstrate that our approach allows efficient preservation of the cells inside the same grooves within a platform to which they were seeded initially, throughout all washing and staining steps necessary for the immunofluorescent staining, we cultured HSCs for 1 day, fixed them and stained the cells with the anti-PMP70 antibody. Remarkably, even after multiple washing and incubation steps, cells remained at their initial positions, as illustrated in Figure 2.5B. Having proved that our platform can be used for the correlation of the temporal and phenotypic information within the same cells, we used this assay to study asymmetric division in HSCs. Such asymmetric division gives rise to two functionally distinct progenies of the same mother cell[127]. It was previously shown that PPAR-δ activation with GW501516 agonist increases the number of asymmetric division events in LT-HSCs[128] (i.e., where one cell retained stem cell phenotype and the other acquired more committed phenotype) *in vitro*, and that this phenomenon is associated with an increase of fatty acid oxidation (FAO)[128]. Therefore, we used PPAR-δ activation as a way to induce asymmetric division in LT-HSCs cultured in our platform, and analyzed the temporal and phenotypic information during these divisions. We hypothesized that peroxisomes might be distributed non-homogeneously in asymmetrically dividing HSCs and may influence the fate of the daughter cells derived from the same mother HSC. In congruence with this hypothesis, we found that comparison of cousin cells (defined as two daughter cells derived from two different mother cells, while these mother cells themselves are derived from the same cell, see also Figure 2.5E) showed significant increase in the asymmetry of peroxisome distribution in the cells undergoing temporally asymmetric divisions. We defined as temporally asymmetric those divisions in which, within the pair of two daughter cells derived from the same mother cell, at least one cell had divided, and necessarily within at least 6h since this division the second daughter cell had not yet divided (Figure 2.5C). Such temporally asymmetric divisions have been proposed to be a phenomenon associated with increasing rate of asymmetric stem cell divisions[129]. Additionally, when the cells treated with GW501516 were compared to non-treated cells, the frequency of temporally asymmetric divisions was higher in cells exposed to GW501516 (Figure 2.5C). Analysis of the PMP70 protein expression in several cell generations also revealed that the cellular peroxisomal mass is increased after one division in the GW501516-treated cells, but with significant subsequent decrease in the following generations (Figure 2.5D). These findings suggest that peroxisomes may indeed play an important role in HSC fate decision; however, the exact mechanisms behind this influence are still not clear.

Overall, the correlation between temporal and phenotypic information (cell division kinetics and peroxisomal mass distribution, respectively) suggests that peroxisomes are non-homogenously distributed during asymmetric division in LT-HSCs.

2.4 Conclusions

The general aim of the present study was to design and investigate a new cell culture platform, which enables single cell tracking and multi-lineage progeny analysis for a small number of sensitive cells. We were able to successfully culture HSCs, overcoming the major challenges that had proved to be problematic for most previously developed devices. In contrast to previous approaches that require complicated tubing, micro-pumps and other expensive instruments to achieve cell progeny tracking, the platform presented here is not based on fluidics and is simple to use. It relies only on gravity to trap the single cells inside the closable microgrooves. The platform can be modified to track the progeny of other cell types, and the length of the grooves can be readily extended for longer-term cell tracking. Finally, we have shown the proof-of-concept possibility of modification of the cell-contacting surface of the hydrogel with protein molecules. Such surface modification can be used to influence the fate of cultured cells via numerous bioactive cues.

2.4.1 Acknowledgements

We thank the Center of MicroNano Technology (CMI, EPFL) for providing access to the clean room facility, the Flow Cytometry Core facility (FCCF, EPFL) for cell sorting, and Saba Rezakhani, Andrea Manfrin and Mukul Girotra for helpful discussions.

Supplementary Information for chapter 2

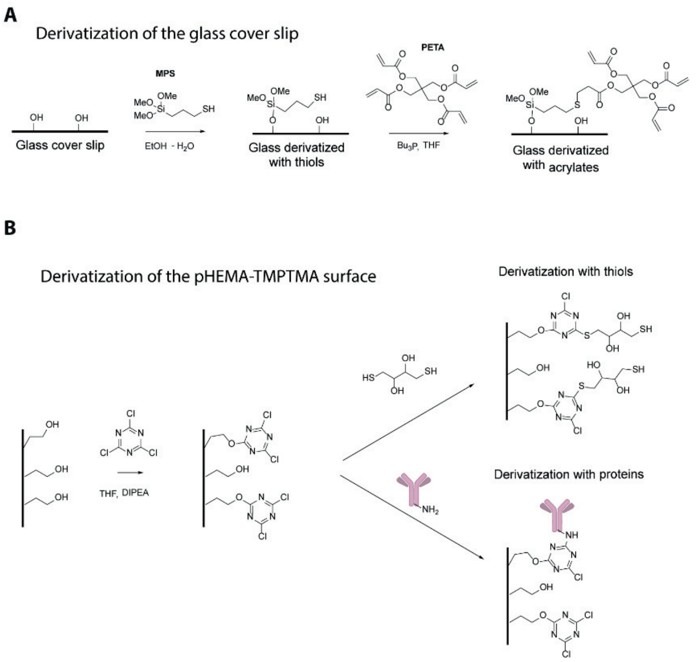
A
Derivatization of the glass cover slip
MPS
PETA
Glass cover slip
EtOH - H$_2$O
Glass derivatized with thiols
Bu$_3$P, THF
Glass derivatized with acrylates
B
Derivatization of the pHEMA-TMPTMA surface
THF, DIPEA
Derivatization with thiols
Derivatization with proteins

Figure S 2.1: (A) Derivatization of the glass cover slip in order to obtain acrylate groups on the surface. (B) General approach for pHEMA-TMPTMA functionalization with thiol or proteins. Chlorine substitution with hydroxyl groups occurs on the pHEMA-TMPTMA polymer surface. Then biomolecules or DTT is added and second chlorine substitution occurs.

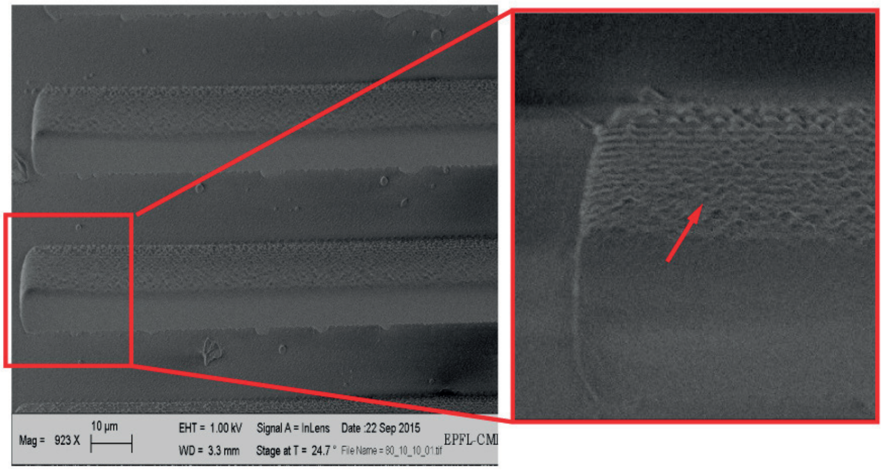
Mag = 923 X
10 µm
EHT = 1.00 kV
WD = 3.3 mm
Signal A = InLens
Stage at T = 24.7 °
Date :22 Sep 2015
File Name = 80_10_10_01.tif
EPFL-CMI

Figure S 2.2: Surface topography of pHEMA-TMPTMA obtained via scanning electron microscopy (SEM). Red arrow shows sub-micron ridges in the groove that were produced as a consequence of the previous production step.

Chapter 3 Automated algorithm for the lineage tracking of single hematopoietic stem cells

Abstract

In vitro experiments based on tracking of single cells and their lineages provide useful biological data, such as proliferation kinetics and single cell lineage tree construction. Additionally, these experiments allow following the movements of the cells, detection of changes in their size as well as registering cell death events. The tracking is generally performed by acquiring images at fixed time intervals using time-lapse microscopic imaging. This method generates a large number of images, and the manual analysis of this data is tedious and time-consuming. Today, computer-based algorithms are capable of performing single cell tracking, which is followed by automatic construction of the lineage tree. Such algorithms are usually designed to excel in analysis of a particular type of experimental data, and often perform poorly with other types of data. Here, we implemented a semi-automated method for detection, tracking and construction of the lineage trees for single hematopoietic stem cells (HSCs). The algorithm was specifically designed to be used in combination with a micro-groove array platform that enables high-throughput lineage tracking of the single cells. Our algorithm provided robust and efficient cell detection, while the average error in cell tracking accuracy was only 0.03 per 100 images. We demonstrated the usability of this tool for practical biological applications by analyzing the behavior of HSCs exposed to three different drugs. The preliminary data obtained in these experiments encourages further investigation of the importance of peroxisomal fatty acid oxidation in HSCs.

3.1 Introduction

Time-lapse microscopy allows temporal measurement of critical events or processes that take place during the life of a cell, such as mitosis, migration, morphological changes, interactions with other cells and death[99,130]. Tracking cell progenies over several generations allows building of the lineage trees, in which every cell division represents a new branch and cell death results in the termination of a branch[2]. Lineage trees provide useful information on division dynamics, cellular phenotype and fate. Such data is particularly valuable for studying hematopoietic stem cells (HSCs). Indeed, the nature of the single HSC lineages was shown to be intertwined, to some extent, with their respective fate choices (i.e., self-renewal, differentiation, quiescence and death)[58,73,111,129,130]. Lineage tree analysis during the exposure of HSCs to various drugs would be ideal to reveal how these drugs influence HSCs' fate. It was recently demonstrated that modulation of the metabolism via exposure to certain drugs could modulate HSC fate; consequently, the potential to manipulate HSC expansion *in vitro* in a way that allows preservation of their healing potential for clinical applications provides an exciting field for further research[32,50,51,131]. However, there are currently no reliable *in vitro* technologies that allow tracking HSCs and analyzing their lineages automatically in a high-throughput fashion.

Construction of the single cell lineages by tracking the cells through visual image inspection is a tedious task, because it requires visualization and manual linking of the lineage-related cells in hundreds of thousands of images. Such an approach not only greatly limits the throughput of the method, but is also highly prone to human error. Thus, several lineage tracking programs have been developed in recent years, which aim to perform automatic lineage tracking[132–136]. Common steps include preprocessing the image data, applying a segmentation algorithm to separate the cells from the background, associating cells between successive time points (i.e., frames) and analyzing output data[133,134,137]. Tracking algorithms are dependent on specific parameters, that are usually accurate only for a given problem and therefore are likely to fail for another one. A representative example involves the detection of cell division across various cell types. In the case of adherent cells like fibroblasts, the shape of the cells is a reliable readout, because fibroblasts undergoing mitosis become round. Hence measuring the circularity of a cell, frame by frame, provides sufficient information for confident detection of the cell division[132]. In contrast, non-adherent cells like HSCs practically do not change their shape during mitosis, which makes it problematic to determine which cells have divided and which have not. Moreover, the time interval between two image acquisitions needs to be small enough to resolve cellular shape changes (i.e., 4-5 min)[60]. A time-lapse interval of 4-5 min is not suitable for experiments that last for days or demand the observation of a small number of cells, due to the number of images generated for each experiment[99]. Another interesting aspect that deserves consideration is the cell culture setup. In conventional culture, cells can freely move and divide in all directions. Therefore, during time-lapse experiments, when images are acquired at a fixed position it is likely that the cells would enter or exit the field of view (FOV). In the case of an exit, the follow-up of the cell is interrupted and the subsequent lineage of this cell is lost. A cell that enters the FOV cannot be considered, as its previous proliferating history is unknown. The main challenge for the algorithm, in this case, is to discriminate whether a certain cell has divided or a new cell has entered the FOV. In fact, if the number of cells in the FOV has diminished, the algorithm is challenged to distinguish between the cell death event and the exit of a certain cell from the current FOV. These events lead to tracking errors and increase the complexity of problems that must be overcome to develop a robust tracking algorithm[137]. One possible solution is to change the field of view, following the moving cell, but this is not possible if one wants to follow more than one cell or an entire cell lineage, because certain daughter cells might move in the opposite direction in comparison to the mother cell. Alternatively, instead of increasing the algorithm complexity, the culture platform itself can be modified, for example by constraining cells into micro chambers[138]. Not only does this remove the problem of cells entering and exiting the FOV, but it also keeps single cell lineages isolated from others. Indeed, in such conditions a microwell would contain colonies, deriving exclusively from a unique cell[57,139]. Nevertheless, although this approach solves the aforementioned problems, lineage tracking is by no means trivial to achieve in the context of microwells, due to the possibility of movement of the cells in all directions. This imposes a demand for very frequent, if not continuous, image acquisition, in order to precisely track cells.

Here we aimed to solve these limitations by combining a state-of-the-art culture platform with the development of a tracking software, tailored for HSCs. The platform contains a micro-groove array that enables HSC culture during long-term experiments with lineage tracking (Trachsel et al., Submitted). In contrast to microwell-based approach, micro-grooves constrain cells on all axes except one, which forces cells to grow and move in line. Therefore, it allows studying the lineages derived from single HSCs, unambiguously, even if image acquisition is performed infrequently. In regard to implementation of the tracking algorithm, the use of a micro-groove approach diminished the complexity of the algorithm, while retaining all the key capabilities of a lineage tracking program (i.e., building of the lineage trees, monitoring of the cellular size and movements). Unlike other tracking algorithms that need optimization of a few parameters before being able to do cell tracking[132], here we implemented a program that by default doesn’t need any user intervention for tracking HSCs.

The purpose of this study was primarily to facilitate the tracking and analysis of the lineages derived from single HSCs, by combining the algorithm, specifically designed for HSC detection, with the advantages of the micro-groove platform. We assessed our algorithm by analyzing 55 single HSCs, cultured during 85h (during which time ~200 frames per sequence were acquired). A sequence (or image sequence) represents all images acquired during the experiment at a particular position. We found an average tracking accuracy error of 0.03 per 100 frames. To validate the potential of our approach we performed a multi-dimensional assay, where we automatically measured the proliferation kinetics and cell morphology and detected the events of differentiation into megakaryocytes for 163 HSCs exposed to three different drugs that specifically affect their metabolism. We found a notable difference in HSC behavior between the studied conditions. This finding highlights the practical utility of our approach.

We believe that our automatic tracking algorithm, combined with the micro-groove technology, is a powerful tool to decipher HSC fate decisions, especially in the context of drug screening. Such an approach would help to understand fundamental mechanisms underlying HSCs’ fate choice.

3.2 Materials and Methods

3.2.1 Isolation of LT-HSCs

Hematopoietic stem and progenitor cells were isolated from crushed bone marrow of 8-16 weeks C57Bl/6 mice. Erythroid cells were eliminated by incubation with red blood cell lysis buffer (Biolegend). Lineage depletion (CD3, B220, Ter-119, CD11, Gr-1) was performed using the Hematopoietic Progenitor Cell Enrichment set (BD Biosciences). Cells were stained with SAV-PO (Life Technologies), Kit-PE-CY7 (2B8, BioLegend), Sca1-PE (D7, BioLegend), CD150-BV784 (TC15-12F12.2, BioLegend), CD48-PB (GM48-1, BioLegend), CD34-eF660 (RAM34), eBioscience). LT-HSCs were sorted as Lin− C-kit+ Sca1+ (LKS) CD150+ CD48− CD34− compartment, ST-HSCs as LKS CD150+ CD34+ and MPP as LKS CD150- CD34+. After extraction, cells were seeded onto platformsm, and time-lapse microscopic imaging was performed. HSCs were cultured in a serum free medium StemlineII (Sigma-Aldrich, St. Louis, USA), supplemented with 100ng/ml stem cell factor (SCF) and 2ng/ml Flt-3 ligand (R&D Systems, Minneapolis, USA). For the drug screening assay, 20nM of PPAR-δ agonist (GW50516, SigmaAldrich) or antagonist (GSK0660, SigmaAldrich), or 20nM of 10,12-tricosadiynoic acid (TDYA, SigmaAldrich) were present in the medium.

3.2.2 Time-lapse microscopy

Micro-groove arrays were fabricated and used as described (Trachsel et al., Submitted). Freshly isolated HSCs and multipotent progenitors were cultured in the platform for 85h. Cells were imaged every 15, 30min or 1h using a Zeiss Observer microscope.

3.2.3 Automated cell tracking and reconstruction of the lineage tree

The program was written in Java language and used as a plugin in ImageJ and can be obtained on demand.

3.2.4 Statistical analysis

Pairwise comparisons were performed using Student's t test and multi-comparaisons by one-way Anova followed by Bonferroni's test.

3.3 Results and discussion

3.3.1 Development of an automated lineage tracking algorithm for HSC analysis

To follow single cells and their progeny *in vitro*, we used a platform that forces the cells to grow in line (Trachsel et al.). We acquired images over 85h using a time-lapse microscope. We also developed an automated system that is able to find cells and cell-cell association over frames (i.e., through image sequences). We tested the robustness of our algorithm by experimental tracking of single HSCs. The main steps of the program are schematically shown in Figure 3.1. Briefly, grooves, containing single cells, were manually selected with a single mouse click per groove. This selection is the only non-automatic step of the procedure. The images are then segmented to detect cells. The segmentation involves a feedback loop that adjusts the process in order to minimize detection error. Once cells are detected, a comparison of the number of cells between neighboring frames allows the detection of cell division or cell death events. Finally, cell-cell associations are completed and the program saves the extracted data (i.e., lineage tree, cellular size, cell position (centroid), tracking robustness index (that is the value of the matching function described below), cell differentiation into megakaryocyte). We applied the program to 55 image sequences (with a total number of ~11,000 images) and obtained an accuracy of 0.05±0.001 errors per 100 frames.

3.3.2 Cell segmentation

Cell segmentation is probably the most important step in the algorithm for cell tracking. It consists of partitioning an image into multiple sets of pixels. Obviously, the objective here is to extract pixels, representing the cells, and to convert the images into binary masks. A straightforward approach is to use the difference of intensity between a cell and its surroundings by applying an intensity threshold. For this purpose, segmentation can be achieved by using the bright field or fluorescent images. An advantage of fluorescent over the bright field image is the high signal to noise ratio of the cellular area in comparison to the background. Typically, fluorescent dyes such as Qtracker®, CellTracker® or fluorescent protein reporters are used for lineage analysis[140,141]. However, exposure of cells to high intensity light (required for the excitation of the fluorophore) might induce stress and deleterious cellular damage (i.e., phototoxicity), including the production of reactive oxygen species (ROS) and free radicals[64,103]. It is especially important to minimize phototoxicity in the case of sensitive cells such as HSCs[142]. HSCs are highly susceptible to an elevated ROS level[32]. In contrast, bright field image acquisition involves softer light exposure, but produces poorly contrasted images which may cause inconsistent segmentation. Therefore, there exists a controversy as to the requirements of image quality for cell segmentation and cell health during image acquisition[64]. We found an excellent compromise by implementing a method that permitted producing highly contrasted images of HSCs by collecting bright field images at three different z-positions (z-stack). We noticed that an image of HSC, acquired 10µm above (defined as A1) or below (A3) a cell center, produced a darker or brighter spot, compared to the same cell in focus (A2) (Figure 3.2A). By applying a gaussian blur (defined as σ) and then a standard deviation projection (STD) to the z-stack, we obtained the projected images, where the cells became bright (high STD) whereas the background area consisted of dark pixels (low STD). We applied an adaptive intensity threshold[143] to segment cells (Figure 3.1B(4)) and obtained a binary image “C1”. We found that this method was extremely robust in finding the cells, but could also introduce false positive areas (pixels, that were falsely considered as cells) due to the high STD value in the area between two cells that are close to each other. To eliminate these areas, we applied a gaussian blur on image A3 and found its local maxima (Figure 3.2B(5)). Then we selected only the areas from C1 in which local maxima were found (Figure 3.2B(7)). We further filtered unwanted areas by applying thresholds to the size and circularity of segmented areas, which typically eliminated particles (dust) that would be falsely considered as cells otherwise.

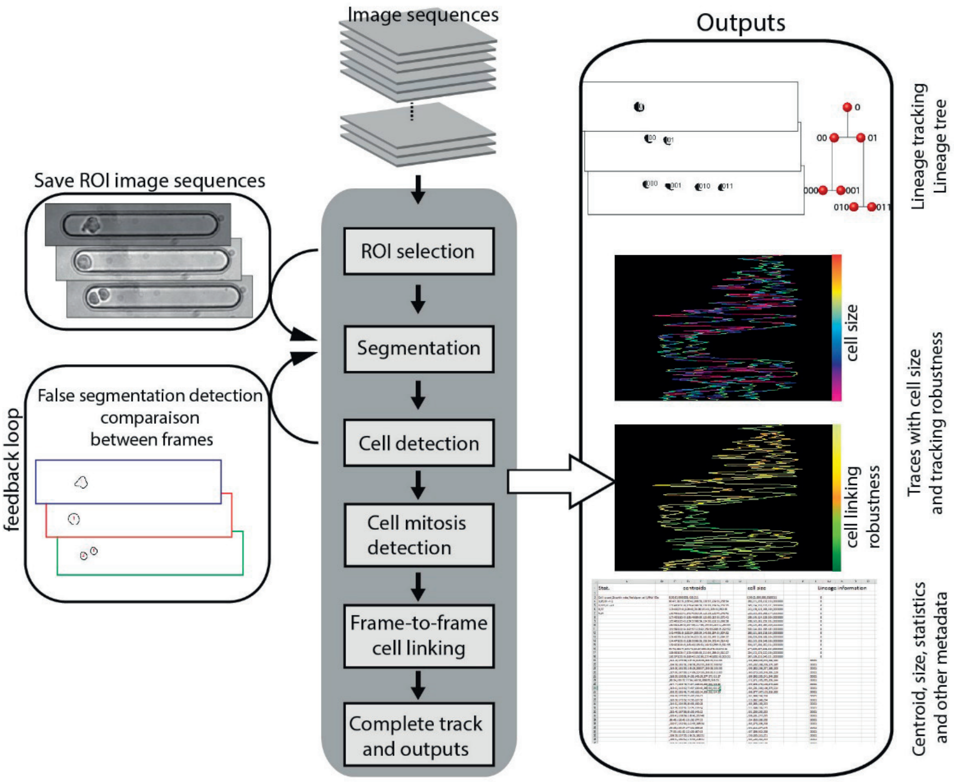
Image sequences
Outputs
Save ROI image sequences
ROI selection
Segmentation
Cell detection
Cell mitosis detection
Frame-to-frame cell linking
Complete track and outputs
False segmentation detection comparaison between frames
feedback loop
0
00
01
000
001
010
011
Lineage tracking
Lineage tree
cell size
cell linking robustness
Traces with cell size and tracking robustness
Centroid, size, statistics and other metadata

Figure 3.1: Schematic description of the algorithm with its output data. The algorithm consists of six modules: 1. Manual groove selection (ROI selection), 2. Segmentation, 3. Cell detection (with feedback loop), 4. Cell mitosis/death detection, followed by 5. Cell linking. Finally, image sequences and lineage tree of the tracking are created. The boxes on the left illustrate the feedback loop and boxes on the right the outputs provided by the algorithm.

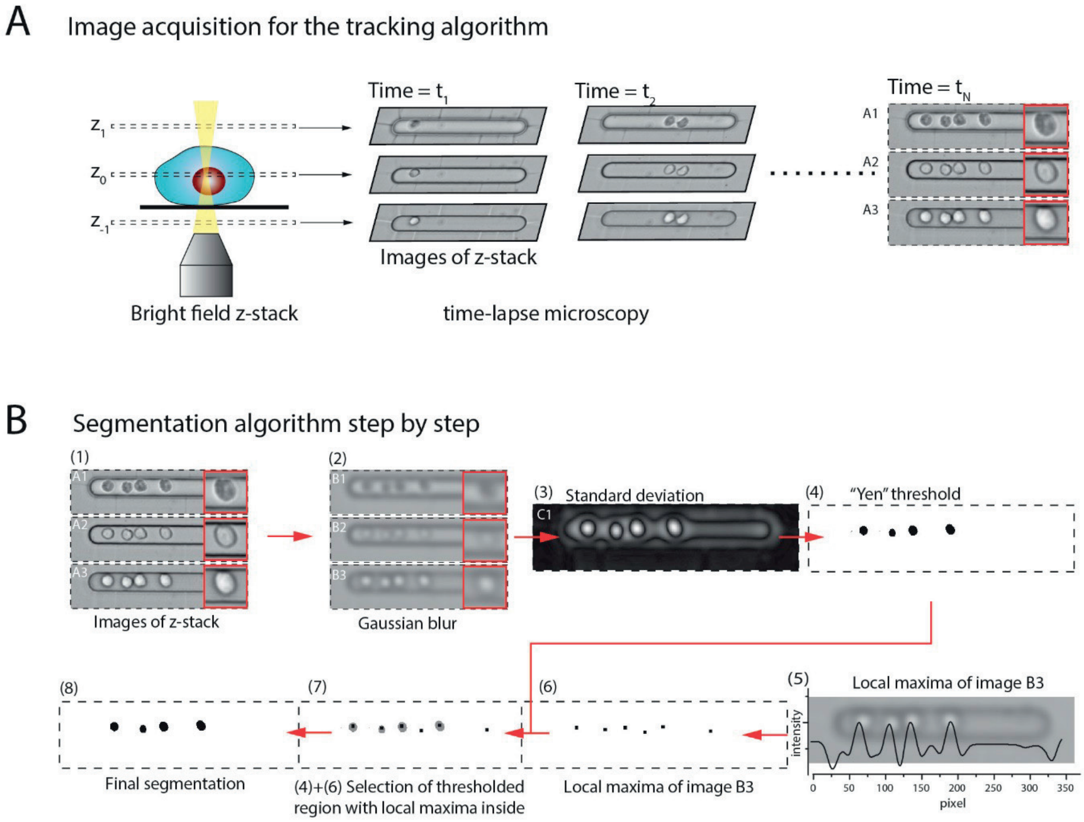
A
Image acquisition for the tracking algorithm
Z_1
Z_0
Z_{-1}
Time = t_1
Time = t_2
Time = t_N
A1
A2
A3
Images of z-stack
Bright field z-stack
time-lapse microscopy
B
Segmentation algorithm step by step
(1)
A1
A2
A3
Images of z-stack
(2)
B1
B2
B3
Gaussian blur
(3) Standard deviation
C1
(4) "Yen" threshold
(5) Local maxima of image B3
intensity
0
50
100
150
200
250
300
350
pixel
(6)
Local maxima of image B3
(7)
(4)+(6) Selection of thresholded region with local maxima inside
(8)
Final segmentation

Figure 3.2: Schematic description of the segmentation process. **(A)** Time-lapse microscopy is used to generate image sequences of a single cell and its progeny. Three images per z-stack are acquired with a step of ±10um from the cell center in focus. **(B)** Z-stacks are processed in order to extract cells from the background. Raw images (1) are blurred (2) and standard deviation is applied on the z-stack (3). Cells are segmented via an intensity threshold ("Yen-threshold"[143]) (4). In parallel local maxima are found (5-6) and added to the thresholded image (4) in order to discard false positive areas (7-8).

We implemented a "control" feedback loop that compared the number of segmented areas found in a frame at a time interval t to those in the previous frame at a time interval t-1 (respectively defined as N_t and N_{t-1}), as illustrated in Figure 3.3. We considered three different scenarios: 1) when $N_t = N_{t-1}$, cells only moved, and the program continued; 2) when $N_t > N_{t-1}$, division(s) occurred; 3) when $N_t < N_{t-1}$, either a false negative event happened or a cell died. A false negative event happens when a cell is rejected by the size or circularity threshold during segmentation. If the falsely rejected cell has a size or circularity that is very close to the threshold value, it is possible to find these cells by increasing or decreasing the gaussian blur σ. The Gaussian blur slightly changes the size and circularity of the segmented areas. Therefore, the feedback loop incrementally changes the gaussian blur σ by a step that can be changed if necessary by the user (±Δσ), and compares the number of cells N_t and N_{t-1}. If N_t becomes equal to N_{t-1}, the algorithm concludes that a cell was found, the new number of cells is validated, and the algorithm continues. If N_t is still lower than N_{t-1} despite the change in the blur value, the program concludes that “the missing cell” is not a false negative, but a cell that died (dying or dead cells are usually small and/or dark and are rejected by the algorithm) (Figure 3.3).

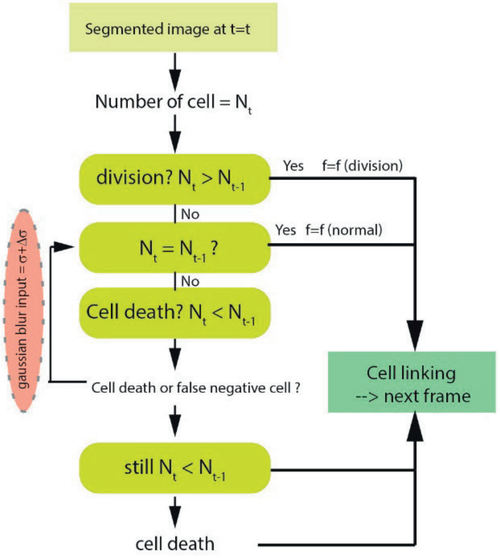
Segmented image at t=t
Number of cell = N_t
division? $N_t > N_{t-1}$
Yes f=f (division)
No
$N_t = N_{t-1}$?
Yes f=f (normal)
No
Cell death? $N_t < N_{t-1}$
gaussian blur input = $\sigma+\Delta\sigma$
Cell death or false negative cell ?
Cell linking --> next frame
still $N_t < N_{t-1}$
cell death

Figure 3.3: Schematic description of the feedback loop implemented in the segmentation algorithm.

We analyzed 55 representative image sequences (i.e., 11,000 frames), in which we observed all fates seen during HSC culture *in vitro* (Figure 3.4), and found error of segmentation in 1.8% of these image sequences (0.009±0.0001 errors per 100 frames). After visual inspection of the movies, we observed that problems appeared when a cell died after it had divided. The error is probably due to a wrong conclusion of the feedback loop, that may occur in case of division events and cell death. We also assessed whether the segmentation looks different, if HSCs had proliferated, died or differentiated into MK, or remained quiescent (Figure 3.4). The segmentation was consistent throughout the sequence of frames for all conditions, with the exception of MK cells (Figure 3.4), where the segmentation did not always produce accurate areas.

3.3.3 Detection of the differentiation into megakaryocytes

As previously mentioned, some HSCs differentiated into large cells that were considered as megakaryocytes (MK, Chapter 3 of this thesis and [111]). We implemented our program to detect MKs by applying a size threshold, above which a cell is considered as MK. By default, a cell is detected as MK when its initial size has increased by 30% (this threshold is tunable). MKs were manually identified in image sequences and the results were compared to the algorithm outputs. We obtained a MK detection specificity of 85% (i.e., true negative rate) and a sensitivity of 88% (i.e., true positive rate).

3.3.4 Cell linking

Cell linking is a process that iteratively associates a cell from one frame to the same cell or its daughter cells in the next frame. There are two general approaches to finding the good association of cells, using images. The first involves segmenting the images independently, followed by the cell association between consecutive frames. While this approach can be easily implemented for cell tracking, such a method is prone to tracking error because it relies entirely on the segmentation efficiency. The second approach involves segmenting the cell in the first frame and tracking these cells in the following image sequence. However, this approach does not naturally handle cell division events[135]. We designed our algorithm based on the first approach, because our segmentation method produced robust and accurate results. Our cell linking algorithm is a simplified version, similar to the one already described by Al-Kofahi et al.[135]. Briefly, all possible associations of a cell on one frame to the next frame are weighted using a “matching function. Then if the number of cells over two frames remains constant, mathematically, the problem can be summarized as follows. For a number of N cells at a time t and N cells at a time t+1, and an N x N matrix “S” containing the matching index value for one cell to its corresponding cell, we should find the overall minimum matching value while assigning each cell at time t to exactly one cell at time t+1 (Figure 3.5B).

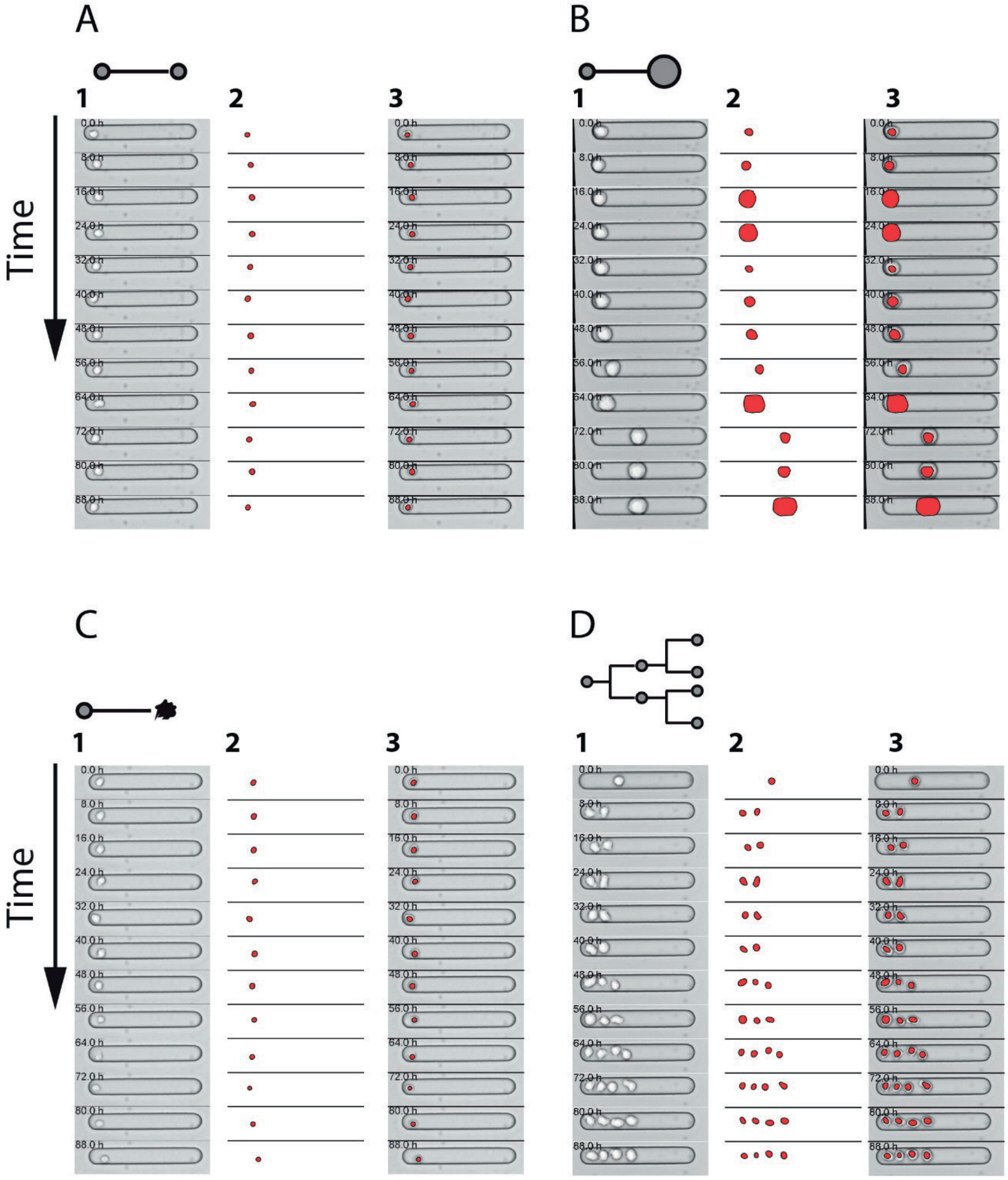

Figure 3.4: Representative image sequences, illustrating the bright field images (1), the corresponding segmented images (2) and the overlay of the two (3). Examples of segmentation of cells that (A) remained quiescent, (B) differentiated into MK, (C) died, (D) proliferated.

We found the best matching assignment between cells in matrix S by applying the Hungarian algorithm[144]. However, when a cell has divided, there are different cell numbers in adjacent frames and the Hungarian method cannot be applied directly, as it requires a square matrix (i.e., for this algorithm one cell at time t cannot be matched to 2 cells at time t+1). To solve this problem, we created a division matrix “D”, where we placed composite cells made from a hypothetical pair daughters (i.e., two cells at time t+1 are merged together to create a new one) (Figure 3.5C). Once the best match in matrix D is found, the rest of the assignment matching is performed in the square matrix S (Figure 3.5A) using the Hungarian algorithm.

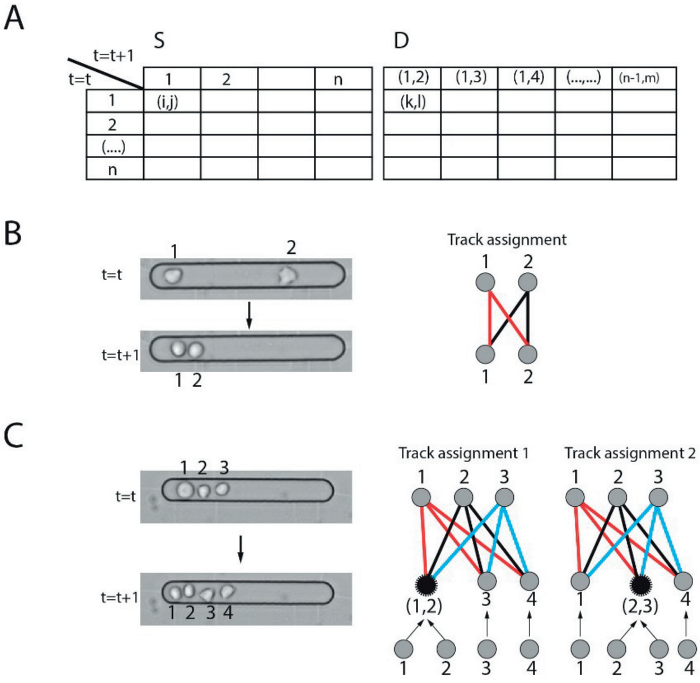

Figure 3.5: Cell linking through frames. (A) Representation of the two matrices, used for the cell-cell association with division (D) or without division (S). Each position of matrices (i,j) represents the index value of a cell at time t (i) to another cell at time t+1 (j). The matrix is filled by calculating matching index values with cost functions described in the results section. The best matching assignment among all possible associations is found by using the Hungarian algorithm. (B) Example of possible tracks between cells without divisions. (C) If a division occurred, an additional step is performed so that each cell at time t finds only one correspondence at time t=t+1. All possible daughter cell pairs are therefore virtually merged together (as illustrated in schemes on the right) and for each of them a matching index value is calculated and placed in the matrix D.

The matching values for matrix S are evaluated through a function f_{ij}^{S} that calculates an assignment value of a cell i at time t (c_i^t) and its corresponding cell j at time t+1 (c_j^{t+1}). For each cell i at time t, we find its centroid in terms of pixel position ($X_i^t = (x_i^t, y_i^t)$) and its area A_i^t. We then model the matching index as follows:

$$f_{ij}^{S} = \frac{f^{S}(A) * \delta_1 + f^{S}(X) * (1 - \delta_1)}{2}$$

Where $f^{S}(A) = \frac{|A_i^t - A_j^{t+1}|}{A_{norm}}$ and $f^{S}(X) = \frac{|X_i^t - X_j^{t+1}|}{X_{norm}}$ represent respectively the absolute difference of area and the distance between c_i^t and c_j^{t+1}. A_{norm} and X_{norm} are local normalization factors (defined for each frame) so that $f^{S}(A)$ and $f^{S}(X) \leq 1$. δ_1 represents the weight factor between the area and the distance values.

Similarly, for the matching index for matrix D, one cell c_i^t should be assigned to a pair of cells c_k^{t+1} and c_j^{t+1}. These cells are merged together to form one composite cell (c_{jk}^{t+1}) so that c_i^t is assigned to only one cell. We then calculated the centroid of c_{jk}^{t+1} that is the mean value of the cells' centroid: $X_{jk}^{t+1} = \frac{1}{2}(x_j^{t+1} + x_k^{t+1}, y_j^{t+1} + y_k^{t+1}))$, and similarly for the area $A_{jk}^{t+1} = \frac{1}{2}(A_j^{t+1} + A_k^{t+1}, A_j^{t+1} + A_k^{t+1}))$. We then model the matching index as follows:

$$f_{ijk}^{\mathrm{D}} = \frac{f^D(A) * \ \delta_2 + f^D(X) * (1 - \ \delta_2)}{2}$$

Where $f^D(A) = \frac{\left|A_i^t - A_{jk}^{t+1}\right|}{A_{norm}} \ and \ f^D(X) = \frac{\left|X_i^t - X_{jk}^{t+1}\right|}{X_{norm}}$. δ_2 represents the weight factor between the area and the distance during a division.

A representative example of cell-cell association is shown in Figure 3.6 and in Supplementary Figure S3.1. When a cell was wrongly associated to another cell or daughter cells in the next frame, we considered it an error in tracking an event. We found 8.3% error in image sequences (or 0.04 errors per 100 frames).

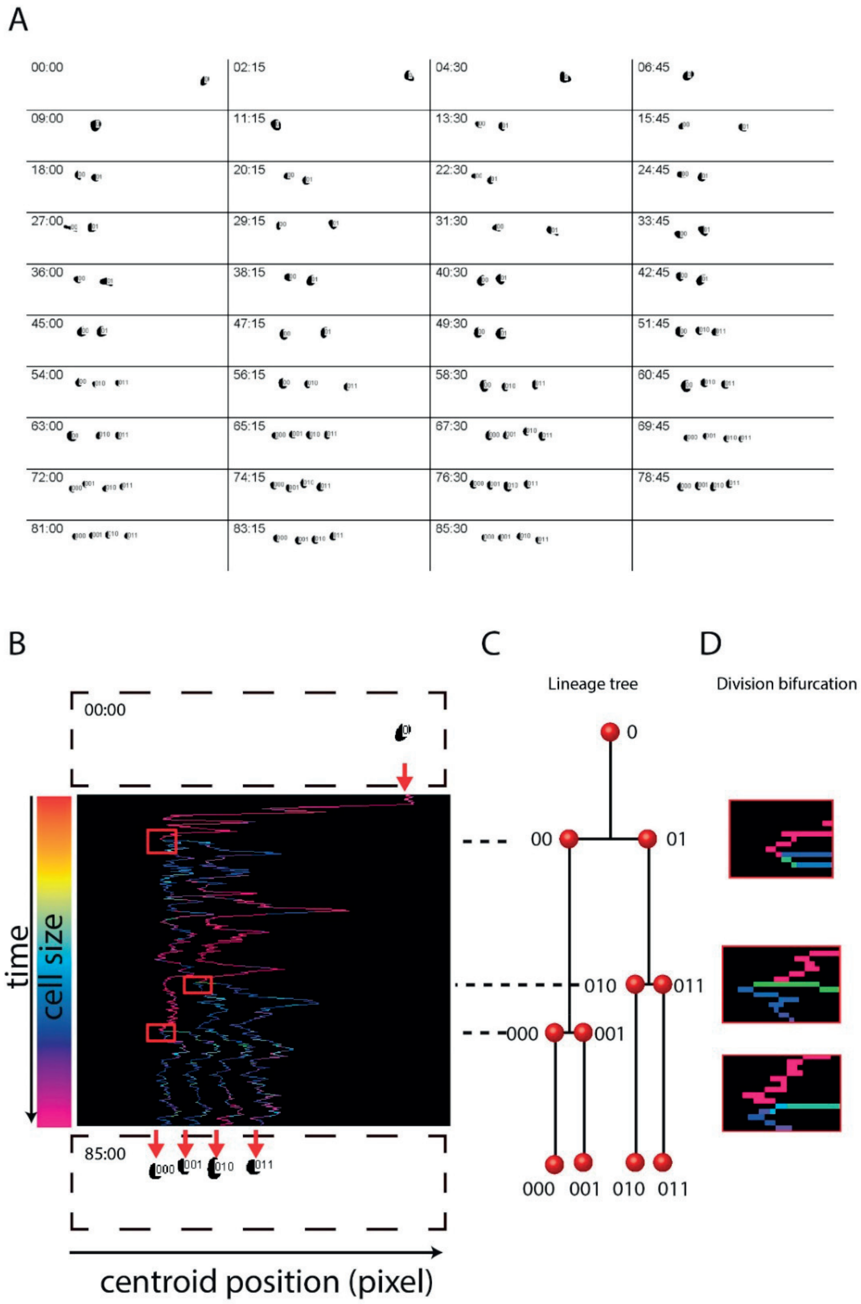
A
00:00
02:15
04:30
06:45
09:00
11:15
13:30
15:45
18:00
20:15
22:30
24:45
27:00
29:15
31:30
33:45
36:00
38:15
40:30
42:45
45:00
47:15
49:30
51:45
54:00
56:15
58:30
60:45
63:00
65:15
67:30
69:45
72:00
74:15
76:30
78:45
81:00
83:15
85:30
B
00:00
time
cell size
85:00
000
001
010
011
centroid position (pixel)
C
Lineage tree
0
00
01
010
011
000
001
000 001 010 011
D
Division bifurcation

Figure 3.6: Automatic tracking with generation of lineage trees. (A) Representative example of lineage tracking of a proliferating single HSC. Each cell is labelled with 0 and 1 and the number of digits represents the generation. For example, the first seeded mother cell (generation 0) is labeled with a "0". The first daughter cells (generation 1) will have two digits "00 and 01", daughter cells from cells "00" will be "000 and 001". (B) Same image sequence of (A) shown in regard to the cell displacement (centroid position). Tracks are colored according to cellular size. From small to large size: red, yellow, green, light blue, dark blue and purple. (C) Corresponding lineage tree from (A). (D) Zoom on tracks during a division. The difference of colors shows that daughter cells are smaller than the mother cell.

3.3.5 HSCs' analysis in the presence of drugs

Here we report an experimental strategy to analyze automatically the effects of drugs on HSCs. As a proof of concept, we focused on several readout parameters: the proliferation kinetics (average number of cells per groove, time spent prior to first division and the proportion of asynchronous divisions), cell viability, differentiation into MK, cell size and the mean cell displacement before the first division. Asynchronous divisions are defined as those where one daughter cell divides 6h before its sister cell does. For this experiment, we selected three drugs that affect fatty acid oxidation (FAO) of HSCs. FAO occurs in mitochondria and in peroxisomes[145], and was found to be an interesting target that allows modulation of HSC fate. Indeed, it has been established that mitochondrial FAO (mitoFAO) stimulation via activation of PPAR-δ promotes asymmetric divisions in HSCs[51]. However, FAO modulation in HSCs was never characterized during *in vitro* culture. Thus, we used GW501516, a PPAR-δ agonist used in 2012 by Ito et al.[51], to increase the number of asymmetric divisions in HSCs; GSK0660, a PPAR-δ antagonist that negatively regulates FAO; and finally we treated HSCs with 10,12-tricosadiynoic acid (TDYA), a specific inhibitor of peroxisomal FAO (peroxFAO)[146]. TDYA irreversibly blocks the first enzyme of peroxFAO, namely ACOX1. As illustrated in Figure 3.7, we observed notable changes in our readout parameters upon treatment with drugs, as compared to basal medium (control). While the doubling time was 83h for non-treated cells, PPAR-δ antagonist and PPAR-δ agonist markedly decreased the doubling time to 56h and 53h, respectively (Figure 3.7A). TDYA treatment had a mild effect on the average number of cells per groove, as compared to the basal medium. These results may be explained by the fact that the number of MK cells is higher in the basal and TDYA supplemented media, and because these cells do not proliferate they lowered the overall proliferation kinetics (Figure 3.7F). This hypothesis is confirmed by analysis of the cumulative histogram of the time spent by a cell prior to the first division (Figure 3.7B). Here, PPAR-δ antagonist and PPAR-δ agonist-treated cells showed only a slight increase in division time (respectively 1h and 4h) in comparison to basal medium conditions. Intriguingly, TDYA seems to affect the time of first and second divisions significantly, as compared to the basal medium (+7h and +13h, respectively) (Figure 3.7B-C). This is an interesting result, because HSCs are marked by slower cell cycling, as compared to progenitor cells[14]. In addition, HSCs treated with TDYA demonstrated a significant increase in the proportion of asynchronous cell divisions (58%) as compared to HSCs in the basal medium (33%), which suggests that TDYA increased the number of asymmetric divisions (Figure 3.7D).

As mentioned previously, PPAR-δ agonist was shown to promote asymmetric divisions in HSCs[51]. In agreement with this observation, we found an increase in the number of asynchronous divisions (48%) upon PPAR-δ agonist treatment (Figure 3.7D). However, PPAR-δ antagonist had no effect on asynchronous division, as compared to control. While the viability seems not to be affected by PPAR-δ agonist and TDYA, the presence of PPAR-δ antagonist increased the number of cell death events (Figure 3.7E). Overall, TDYA effect on HSCs is intriguing. Interestingly, Zeng et al.[147] found that the inhibition of peroxFAO in liver cells activates mitoFAO. In homeostatic conditions, PeroxFAO produces acetyl-CoA that can be transformed into malonyl-CoA[148], which in turn negatively regulates mitoFAO through inhibition of CPT-1A[147]. In the presence of TDYA, peroxFAO is blocked, which might decrease the cellular malonyl-CoA concentration and, consequently, activate mitoFAO[146,147]. This could explain the higher proportion of asynchronous divisions observed with TDYA treatment. This hypothesis needs to be interpreted with caution, and the observation made in liver cells must first be verified in HSCs before final conclusion.

In certain circumstances, cell size and mean displacement could be meaningful readout parameters. Typically, when the substrate on which cells are grown is modified with bioactive molecules (for example, niche-like proteins), the cells might adhere to this substrate differently and, as a consequence, would change their movement speed. Their size could also change[73,149]. Therefore, we compared cell sizes and mean cell displacements prior to the first division between the three drug treatment conditions (Figure 3.7G-H). We found a significant decrease in cell size in all conditions, as compared to the basal medium. Also, cells subjected to TDYA treatment moved slightly more than in the control conditions. These preliminary results illustrate the potential of the cell lineage tracking algorithm, when it is used in combination with the micro-groove array-based cell culture platform.

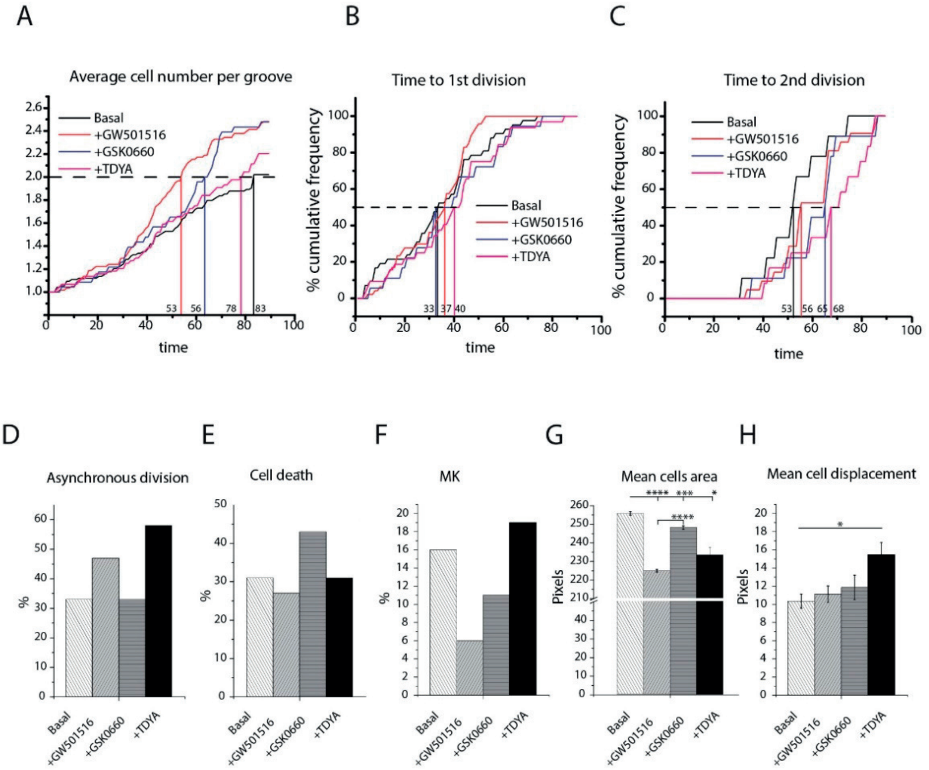

Figure 3.7: Analysis of HSCs cultured in the presence of various drugs. (A) Average proliferation rates measured for single live cells in each condition and (B-C) Cumulative histogram of time spent prior to first or second division for indicated population. (Basal n= 48; GW501516, n=49; GSK0660, n=23; TDYA, n=43; dead cells excluded). (D) Frequency of asynchronous divisions per condition. (E) Viability. (F) Frequency of differentiation into MK events. (G) Mean cell area. Numbers show average and SEM. Statistical analysis was performed using one-way Anova followed by Bonferroni’s test. ****$p< 0.0001$, ***$p< 0.001$, **$p< 0.01$, *$p< 0.05$

3.4 Conclusions

In the field of HSCs, scientists still face a lack of high-throughput tools that allow studying single HSCs and their lineages. In this study, we presented a new algorithm for lineage tracking and progeny analysis. Tracking was performed using bright field microscopy in order to minimize phototoxicity during time-lapse imaging. We showed that the algorithm can efficiently detect and track HSCs and also demonstrated its applicability to the drug screening experiments. The implementation of the algorithm to this task demonstrated the high accuracy of cell lineage tracking. In line with Ito et al.[51], we found that PPAR-δ agonist (GW501516) increases the number of asymmetric divisions.

TDYA, a drug specifically inhibiting the peroxisomal FAO, surprisingly increased the number of asynchronous divisions in HSCs, besides increasing the duration of time spent prior to the first division. These preliminary findings raise the intriguing possibility that peroxisomal FAO might have an important role in governing the HSC fate decisions. Overall, we think that this study lays the groundwork for future high-throughput analysis of HSCs *in vitro*.

3.5 Acknowledgements

We thank Jean Haizmann, Daniel Schmitter and Daniel Sage for their support with the implementation of the tracking algorithms.

Supplementary Information for chapter 3

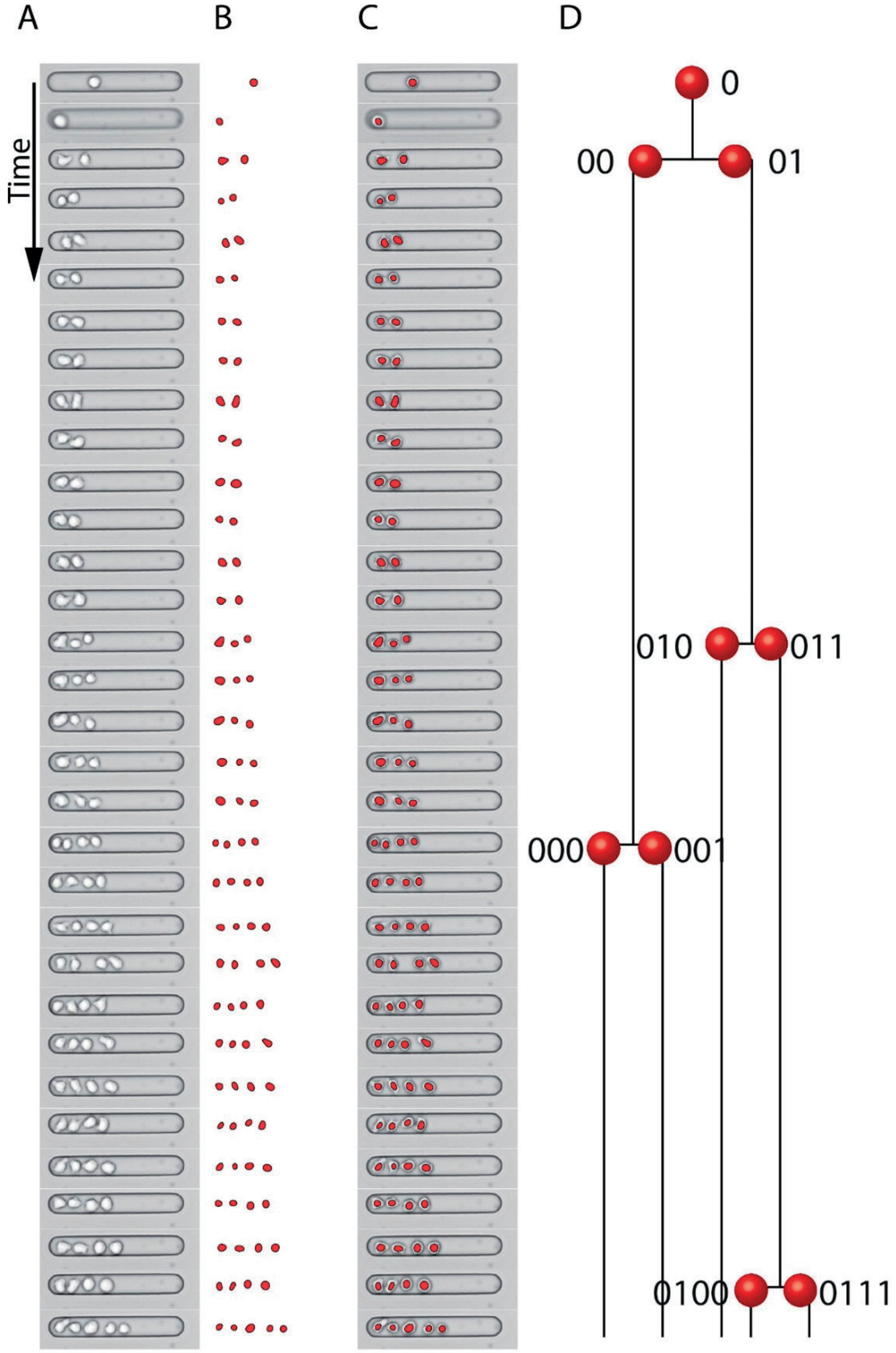
A
B
C
D
Time
0
00
01
010
011
000
001
0100
0111

Figure S 3.1: Image sequences in bright field (A) with corresponding segmentation (B), overlay of the two (C) and lineage tree (D).

Chapter 4 Monitoring of mitochondrial mass of HSCs in culture

Abstract

Currently, the identities of the hematopoietic stem cells (HSCs) and progenitors cells have not yet been defined in *in vitro* culture as the result of a lack of markers that would correlate their phenotypes to their fate. Previously, we developed a state-of-the art single cell tracking platform that enables the imaging of single cells and their lineages during long-term experiments (up to 5 days) *in vitro* and simultaneous study of the individual cell division kinetics. We applied these techniques to study the purified but still heterogeneous long-term murine hematopoietic stem cells (LT-HSCs) defined as Lin- ckit+ Sca1+ CD150+ CD48- CD34-. We measured the mitochondrial mass in single LT-HSCs and its distribution between their lineages and found that the mitochondrial mass in LT-HSC progeny correlates with the LT-HSC fate. Moreover, our results indicated that mitochondria are distributed asymmetrically in the daughter cells that undergo temporally asynchronous divisions (with a time difference of at least 24 h between the corresponding divisions). In contrast, a more symmetrical mitochondrial mass distribution was observed in the cells that undergo temporally synchronous divisions. This observation signifies the existence of a mechanism that selectively distributes mitochondria during asymmetric divisions in LT-HSCs, which is likely linked to the LT-HSC fate choice.

4.1 Introduction

Currently, the *in vitro* expansion of hematopoietic stem cells (HSCs) is confounded by the rapid loss of their stem cell function. One of the main reasons behind this is an inability to provide the correct biological signals to HSCs during their culture outside the natural niche. Depending on the nature of signaling, HSCs are forced to undertake various cell fate decisions including self-renewal, hematopoietic lineage commitment, quiescence or apoptosis[150,151]. In practice, HSCs rapidly differentiate during *in vitro* culture, which limits their use in clinical therapy[152]. In order to understand the mechanisms underlying the HSCs fate choices, it is essential to track the lineages of individual stem cells[62,153,130].

Here, we used a platform that enables tracking of single HSC lineages. First, by characterizing HSCs behavior on the platform, we demonstrated that it permits the study of HSCs during the culture in serum-free medium. Importantly, the high throughput nature of our platform allowed observation of 614 individual cells in just 3 experiments. Secondly, following the recent evidence of mitochondrial involvement in HSC fate decision[128,154], we used the platform to monitor mitochondrial mass in cell lineages to better understand its connection with HSC fate. It was demonstrated that HSCs rely more on glycolysis for ATP production than mitochondrial oxidative phosphorylation (OXPHOS)[28,155]. Consistent with these results, Vannini et al. showed that functional HSCs are marked by low mitochondrial activity and mass while committed progenitors, in contrast, preferentially produced ATP by mitochondrial OXPHOS and have a higher mitochondrial mass[156,50]. These observations have been recently challenged by Almeida et al. who demonstrated contradictory results (i.e. higher mitochondrial mass in HSCs in comparison to committed progenitors cells)[157]. This experiment was, however, performed on a highly heterogeneous populations of hematopoietic cells (Lin-ckit+CD48-) that also contains progenitor cells[14]. Nevertheless, although the mitochondrial metabolism is currently a major focus of research in the field of HSC, the mechanistic link between mitochondria and the HSC fate is still poorly defined[158]. To characterize how mitochondrial mass is correlated to HSC fate *in vitro*, we used the micro-groove platform to quantify the mitochondrial mass in individual LT-HSCs and further the distribution of mitochondria in corresponding single cell lineages.

Interestingly, our results showed that mitochondrial mass evolution in lineages over time is different regardless of whether the HSCs had differentiated, remained quiescent or proliferated.

In addition, we found a striking asymmetric distribution of mitochondria between daughter cell pairs that had divided asynchronously (i.e., when one daughter cell divides 24 h before its sister). As this phenomenon was proposed to be correlated with asymmetric division (AD) of HSCs[129], our results support that mitochondria is tightly linked with AD and that a distribution mechanism of mitochondria during AD might take place in HSCs.

4.2 Materials and Methods

4.2.1 Isolation of LT-HSCs

Hematopoietic stem and progenitor cells were isolated from crushed bone marrow of 8-16 weeks C57Bl/6 mice or r26-mitoEGFP mice. Erythroid cells were eliminated by incubation with red blood cell lysis buffer (Biolegend). Lineage depletion (CD3, B220, Ter-119, CD11, Gr-1) was performed using the Hematopoietic Progenitor Cell Enrichment set (BD Biosciences). Cells were stained with SAV-PO (Life Technologies), Kit-PE-CY7 (2B8, BioLegend), Sca1-PE (D7, BioLegend), CD150-BV784 (TC15-12F12.2, BioLegend), CD48-PB (GM48-1, BioLegend), CD34-eF660 (RAM34), eBioscience). LT-HSCs were sorted as Lin− C-kit+ Sca1+ (LKS) CD150+ CD48− CD34− compartment , ST-HSCs as LKS CD150+ CD34+ and MPP as LKS CD150- CD34+. After extraction, cells were seeded on platforms and time-lapse microscopy was performed. HSCs were cultured in “Basal” medium defined as a serum free medium StemlineII (Sigma-Aldrich, St. Louis, USA) supplemented with 100ng/ml stem cell factor (SCF) and 2ng/ml Flt-3 ligand (R&D Systems, Minneapolis, USA) or in the differentiation-inducing medium, composed of the basal medium with the addition of 20ng/ml Il-3 and 100ng/ml Il-6 (R&D Systems, Minneapolis, USA).

4.2.2 Single HSC trapping and lineage tracking

Micro-groove arrays were fabricated and used as described (Trachsel et al., Submitted). HSCs were cultured in basal or differentiation media for 70h and bright field images were acquired every 30min or 1h on a Zeiss Observer microscope.

4.2.3 Mitochondrial mass measurement

For the live cell mitochondrial mass measurements, freshly isolated LT-HSCs from R26-Mito-eGFP, were seeded on the platform and visited every 24h during 5 days. Mitochondrial mass was quantified as the intensity-thresholded area of mito-eGFP signal. Images were processed in imageJ.

4.2.4 Colony Formation

Lin- cells (1000 per experiment) were cultured for 1.5 days on platforms or standard 96 well plate. Then cells were cultured in MethoCult GF (M3434, Stem Cell Technologies) and colony-forming cell mass was scored at day 8.

4.2.5 Statistical Analysis

Pairwise comparisons were performed using Student’s t test. For multi-comparaisons, one-way Anova followed by Bonferroni’s test was used.

4.3 Results and Discussion

4.3.1 Characterization of HSCs cultured on a micro-groove platform for lineage tracking

To study single HSCs and their subsequent progeny, we used a previously developed tracking platform (Figure 4.1A) (Trachsel et al., Submitted). The platform is briefly composed of an array of grooves that are closed after cell seeding with a permeable polyethylene glycol (PEG) hydrogel. The platform is designed in such a way that the single cells seeded into the grooves are encapsulated and forced to grow and move in a line. Such design does not allow cells to interchange their relative positions. Hence, the platform enables precise tracking of single cell progeny by optical microscopy even if the time elapsed between two consecutive image acquisitions is close to a full cell cycle (Figure 4.1B-C). We first characterized the fate of LT-HSCs (Lin- ckit+ Sca1+ CD150+ CD48- CD34-) cultured on the platform for 72h in three independent experiments. In line with previous studies, we found that the LT-HSC population is heterogeneous[111]. Indeed, 56.6% ± 11.1% of cells underwent proliferation, 13.2% ± 2.8% differentiated into very big cells (that were considered to be megakaryocytes[111,159]), 11.8% ± 4.1% never divided (a fate termed “quiescence”) and 18.4 ± 13.2% died. We next assessed division kinetics of the LT-HSCs on the platform (n=100) and compared it to the control conditions (n=248) when cells were cultured in PEG-microwells[149]. The principal difference between the culture in PEG-microwells and micro-groove platform is that in PEG-microwells, the cells are not encapsulated and can move freely in all directions whereas the HSCs’ movement in the micro-grooves is bidirectional. Importantly, the spatial confinement of HSCs, which is achieved when they are fully embedded in a hydrogel, was shown to change their proliferative behavior[160]. However, in our micro-groove encapsulation conditions, we observed remarkable similarity in the cell growth rates when compared to open PEG-microwells (Figure 4.1J). This demonstrates that the HSC proliferation kinetics are not affected. We next assessed the HSC response to supplementation of Il-3 and IL-6 cytokines, which are known to activate their cell cycling[42]. As expected, the cells proliferated faster in comparison to basal medium conditions (Figure 4.1K). The cell number doubling time of 55 h in the basal medium (ctrl, n=106) decreased to 37 h in IL3, IL6-induced differentiation conditions (n=45). We further assessed whether the culture in the platform could influence the colony forming potential of hematopoietic cells when compared to a culture in standard plastic well plate (Figure 4.1L). The statistical analysis revealed no significant difference between the two conditions, both for the colonies derived from the more committed progenitors such as megakaryocyte and erythroid colonies (MK/E), granulocyte and/or macrophage colonies (G, M, GM) and the highly proliferative colonies derived from the most primitive cells (GEMM). Taken together, these results suggest that the HSCs cultured on the tracking platform have similar proliferation kinetics and potential than the control culture in PEG or plastic well. Therefore, the platform is suitable for studying HSCs.

4.3.2 Mitochondrial mass measurement in LT-HSCs and their lineages

It is well established that mitochondria play a role in the homeostasis of HSCs[161,162]. While HSCs have low mitochondrial mass and rely on glycolysis for energy generation, progenitor cells rely on mitochondrial oxidative phosphorylation[50]. However, the amount of mitochondria in functional HSCs has been recently questioned due to the limitation of the dye-dependent methods used to measure mitochondrial mass. However, it has indeed been shown that the efflux of the dye from mitochondria increases in primitive HSC population, which might lead to erroneous conclusion[157]. For this reason, we employed a genetically modified mouse line (R26-mito-eGFP) that ubiquitously expresses enhanced green fluorescent protein (eGFP) in the mitochondria of all cells (Figure 4.2E). We were therefore able to measure the mitochondrial mass in single LT-HSCs seeded on the platform (n=174) and in all subsequent cells derived from them (cumulative total number of cells, n=1547) in an accurate manner without the use of fluorescent dyes. The mitochondrial mass of each cell was mapped on its respective lineage tree (Figure 4.2C-D), thus providing a correlation between the observed mitochondrial mass phenotype and the proliferation kinetics in single LT-HSCs and their progeny. It is to be noted that in order to observe whether mitochondrial monitoring affect cells, we compared the proliferation kinetics between the HSCs with mitochondrial mass acquirements (i.e. exposed to fluorescent light) and cells without and did not find any significant difference (Figure 4.2F-H).

4.3.3 Mitochondria are asymmetrically distributed in sister cells after divisions

We cultured single LT-HSCs until they underwent at least two divisions. This allowed us to define daughter and cousin cell pairs according to their lineages. Daughter cells are pairs of sister cells of the first generation (derived from the initially seeded mother cell). Cousins cells are the pairs of sister cells of the second generation when each of them is derived from the same daughter cell of the first generation (Figure 4.2C). We wanted to find out whether mitochondrial mass distribution is correlated to the type of division undergone by a single stem cell. We classified the division types as asymmetric divisions (AD) or symmetric divisions (SD)[162,163]. AD is a process during which a mother stem cell produces a pair of sister cells that have different cellular fates, for example, when one cell preserves a stem cell function and another becomes a committed hematopoietic cell. In contrast, SD will produce daughter cells with equal fate[127]. When the mother cells divide asymmetrically, its daughter cells will have certain different phenotypical aspects. Therefore, we decided to assess whether the sister cells produced by an AD would have a higher difference in its mitochondrial mass when compared to the sister cells produced by a SD. We defined the difference in mitochondrial mass between the two sister

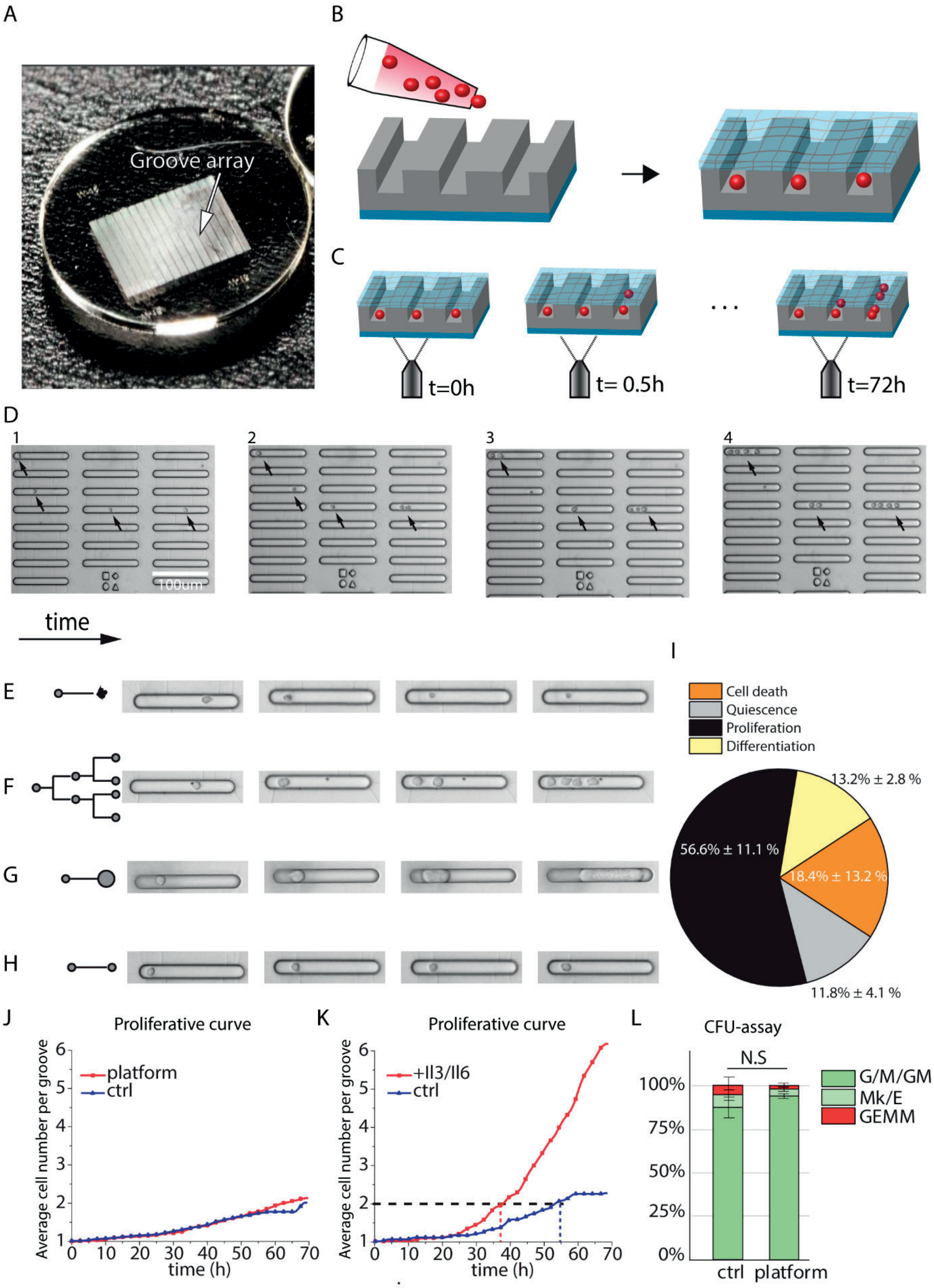
A
Groove array
B
C
t=0h
t= 0.5h
...
t=72h
D
1
2
3
4
100um
time
E
F
G
H
I
Cell death
Quiescence
Proliferation
Differentiation
13.2% ± 2.8 %
56.6% ± 11.1 %
18.4% ± 13.2 %
11.8% ± 4.1 %
J
Proliferative curve
platform
ctrl
Average cell number per groove
time (h)
0
10
20
30
40
50
60
70
1
2
3
4
5
6
K
Proliferative curve
+Il3/Il6
ctrl
Average cell number per groove
time (h)
L
CFU-assay
N.S
G/M/GM
Mk/E
GEMM
100%
75%
50%
25%
0%
ctrl
platform

Figure 4.1: Platform for single-cell trapping with multi-lineage tracking. (A) The platform is made of an array of grooves on the glass coverslips. (B) Single cells sediment in the groove by gravitation and are encapsulated by covering with a permeable lid. (C) Tracking is performed by acquiring time-lapse bright field microscopy images. Cells are forced to grow in a line within the corresponding groove. (D) Representative example of HSCs, cultured on the platform. Black arrows indicate cells at t=0, 24, 48 and 72 h. (E-I) Single cell analysis revealed significant heterogeneity in the HSC compartment. The quantification of cell fate choices observed in three independent experiments with a total number of 614 single cells. Percentages are given as average ± SD. (J) Average number per groove of progeny cells derived from single HSCs observed at the end of the experiment when cultured in polyethylene glycol (PEG) microwell – or in the tracking platform (blue line, n=248 and red line, n=100, respectively). Dead cells were excluded. (K) Average number per groove of progeny cells derived from single HSCs cultured in basal or differentiation medium (blue line, n=106 and red line, n=45, respectively). Dead cells were excluded. (L) The percentage of colony types (G/M/GM, green; Mk/E, light green; GEMM, red), measured by hematopoietic colony-forming assay at day 10 from 1000 Lin- cells, cultured 1.5 days on the platform or plastic well plate. (CFU-)G: Colony forming unit-granulocyte; (CFU-)M: Colony forming unit-macrophage; (CFU-)GM: Colony forming unit-granulocyte, macrophage; (CFU-)GEMM. Percentages are given as average ± SD from three independent experiments. N.S (Non-significant) in Student's t test.

cells or between two pairs of cousin cells as mitochondrial asymmetry (Figure 4.2E). This difference is calculated by subtracting the eGFP signal intensity of one cell from the corresponding value of another as shown by the black arrows in Figure 4.2E and in the formula below:

$$Asymmetry\ of\ daughter\ cells = |c_1 - c_2|$$

where $c_1\ and\ c_2$ are the values corresponding to two daughter cells. In order to compare two pairs of cousin cells, the average value for each pair of sister cells is taken as follows:

$$Asymmetry\ of\ cousin\ cell\ pairs = \left|\frac{c_1 + c_2}{2} - \frac{c_3 + c_4}{2}\right|$$

where $c_1\ and\ c_2$ are values of the first pair of sister cells and $c_3\ and\ c_4$ are values of the second pair of sister cells.

One of the key properties of HSCs is their slower cycling rate in comparison to the progenitors cells[164–166]. Therefore, we used this parameter to detect the AD *in vitro*. The difference in the time of division between daughter cells would indicate different cellular fate and, consequently, can be used to detect AD[129,138]. If the difference in time between two daughter cells divisions was 24 h or more, the division was defined as asynchronous (Figure 4.3D). Otherwise, the division was considered as synchronous[129]. In addition, if only one of the daughter cells had divided, we also considered this as an asynchronous divisions. We then grouped cell lineages according to the type of division (synchronous or asynchronous) and compared the mitochondrial mass distribution asymmetry between either daughter cells or pairs of cousin cells. Strikingly, the daughter cells that underwent an asynchronous division displayed a significantly higher mitochondrial mass distribution asymmetry as compared to the synchronous daughter cells (Figure 4.3A). Interestingly, the same pattern was observed when the mitochondrial mass distribution was analyzed for pairs of cousin cells that were themselves produced by asynchronous or synchronous divisions (Figure 4.3A). Thus, it could be hypothesized that the HSC fate decision occurs during the first division and that the subsequent pairs of cousin cells inherit the fate of the corresponding daughter cells. But this hypothesis remains to be confirmed. Our results also imply that the mitochondria are not randomly distributed during AD and that some mechanism of selective distribution of mitochondria between daughter cells exists for dividing HSCs. Interestingly, such a phenomenon has been observed in dividing budding yeast[153] and in germ line cells in Acricotopus[167]. Moreover, a remarkable experiment performed by Katajisto et al. showed that aged mitochondria are asymmetrically distributed after a division of human mammary stem-like cells and that cells that received fewer old mitochondria remained as stems[168].

4.3.4 Mitochondrial mass distribution asymmetry in different cell generations

To identify if the mitochondrial mass asymmetry in sister cells correlates to the number of divisions and the time of division, we analyzed the mitochondrial mass distribution asymmetry depending on the time spent until the division. Our analysis revealed that the mitochondrial mass asymmetry in the first generation of cell increases with the time spent until the division (Figure 4.3B). This result indicates that mother cells that divide later (i.e. remaining for a longer time in a dormant state) produce more asymmetric daughter cells. This observation is interesting as it was suggested that functional HSCs have slower cycling rates when compared to progenitor cells[166]. A higher mitochondrial mass distribution asymmetry in daughter cells derived from slower cycling mother cells corroborates this idea.

In contrast to what we observed in first generation daughter cells, the mitochondrial mass distribution asymmetry in the second generation remains independent on the time spent until the division and is significantly lower than the asymmetry in first generation daughter cells (Figure 4.3B). This

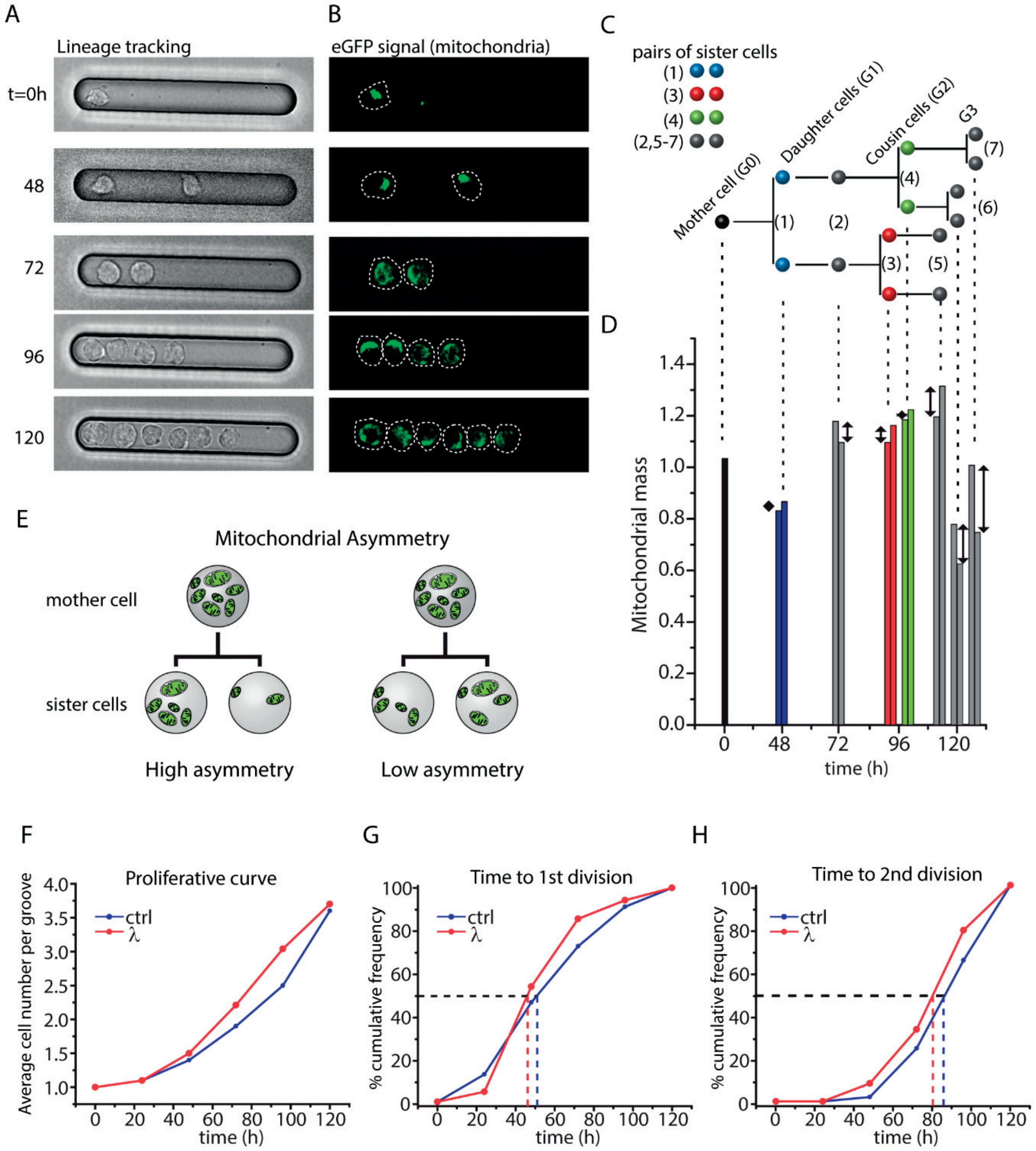

Figure 4.2: Single cell lineage tracking and mitochondrial mass measurement. (A-B) Representative images from time-lapse microscopy showing single LT-HSCs proliferating over 5 days. (B) Corresponding cells in eGFP (mitochondria) channel. (C) The corresponding lineage tree of (A). The scheme demonstrates how sister cell pairs are defined for mitochondrial asymmetry analysis. (D) Mitochondrial mass measurements from the eGFP signal of cells in (A). Black arrows indicate the difference of mitochondrial mass between sister cell pairs. (E) Illustration of mitochondrial asymmetry. (F-H) LT-HSC proliferation kinetics with mitochondrial mass measurement (fluorescence excitation exposure) (λ, red line, n=47 cells) or without mitochondrial mass measurement (ctrl, blue line n=70 cells). Dead cells are excluded. (F) Average cell number per groove. (G) Cumulative histogram of the time spent until the first division. At 50% of divided cells, there is a difference of 5 h between conditions. (H) The cumulative histogram of time spent until second division. At 50% of divided cells, there is a difference of 6 h between conditions.

result suggests that asymmetric divisions are more likely to occur during the first divisions in our *in vitro* system and are probably less common during the second divisions.

4.3.5 Mitochondrial mass distribution asymmetry, correlated to mitochondrial mass of the mother cell

Regression analysis was used to measure the correlation between the mitochondrial mass of mother cells and the asymmetry of mitochondrial mass distribution between their respective daughter cells. Since HSCs are marked by low mitochondrial mass[50], we hypothesized that mother cells with low mitochondrial mass would more likely undergo an asymmetric division[169]. However, no such correlation was found (Figure 4.3C), suggesting that the mitochondrial mass of mother cell on its own is not sufficient enough to predict the asymmetry of the mitochondrial mass distribution between daughter cells.

4.3.6 Initial mitochondrial mass marks LT-HSCs fate

Finally, we grouped single LT-HSCs and their corresponding lineages according to the following mother cell fate outcomes observed at the end of the culture: quiescence; proliferation limited to one division; proliferation (more than one division); direct differentiation into megakaryocyte (MK); symmetric differentiation “SD MK” (resulting in two daughters that both gave rise to MK); or asymmetric differentiation “AD MK” (resulting in one daughter that gave rise to MK and one that remained small).

We then observed how the mean mitochondrial mass of each of these mentioned groups fluctuated during culture. Interestingly, the mean mitochondrial mass is highly different between groups (Figure 4.3E). Overall, the megakaryocytic-fated cells’ mean mitochondrial mass show a notable increase over time in contrast to other groups whose mean mitochondrial mass remained more constant (Figure 4.3E). Moreover, at the beginning of culture, the quiescent cells have significantly lower mitochondrial mass (0.7±0.1) in comparison to other groups (MK=1.1±0.4, AD MK=1±0.2, Proliferation=1±0.2) (Figure 4.3F). The observed lower mitochondrial mass in these cells are in line with other groups[50,156].

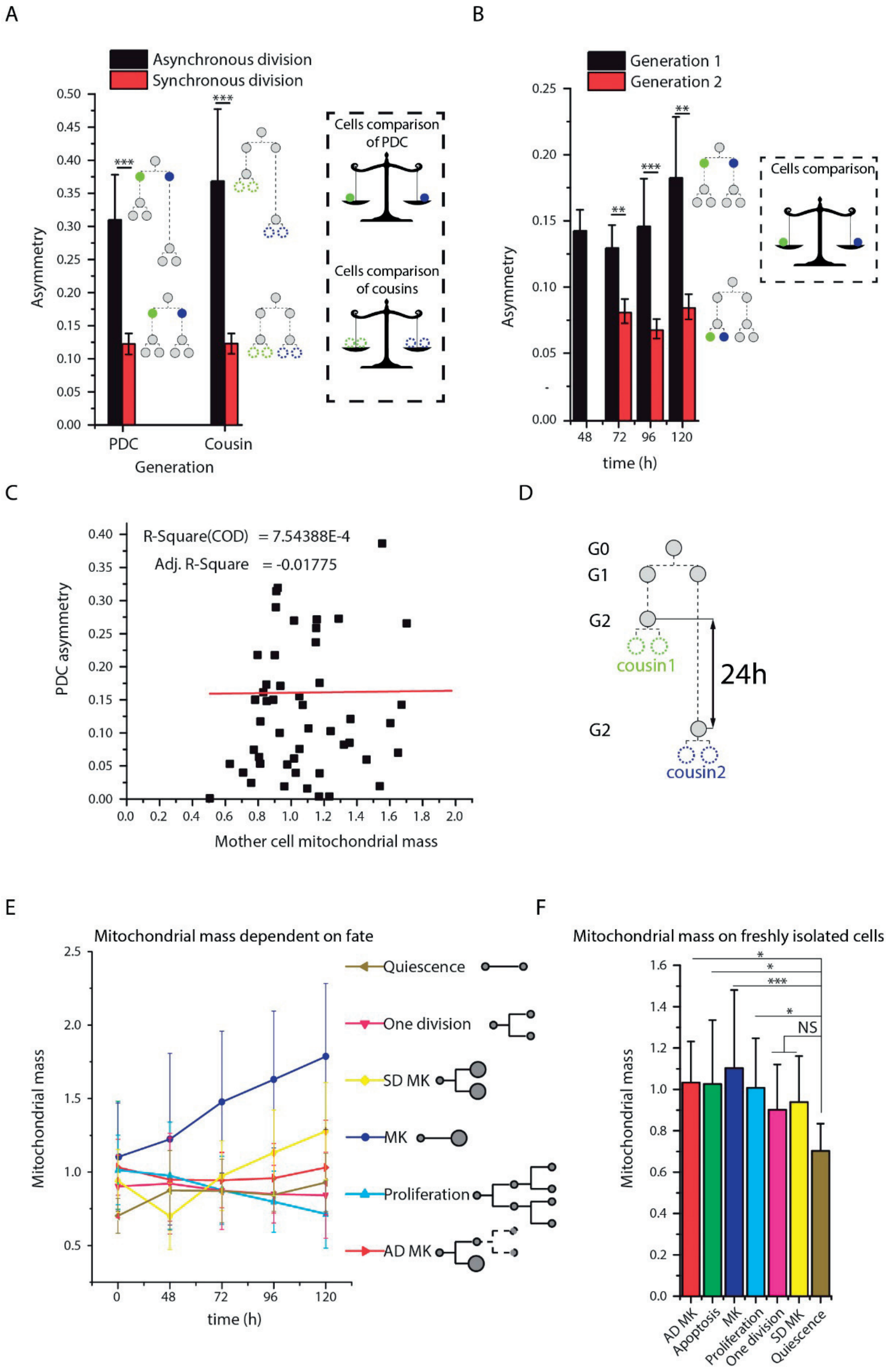
A
Asynchronous division
Synchronous division
Asymmetry
0.50
0.45
0.40
0.35
0.30
0.25
0.20
0.15
0.10
0.05
0.00
***
***
PDC
Cousin
Generation
Cells comparison of PDC
Cells comparison of cousins
B
Generation 1
Generation 2
0.25
0.20
0.15
0.10
0.05
0.00
**
***
**
48
72
96
120
time (h)
Cells comparison
C
R-Square(COD) = 7.54388E-4
Adj. R-Square = -0.01775
PDC asymmetry
0.40
0.35
0.30
0.25
0.20
0.15
0.10
0.05
0.00
0.0
0.2
0.4
0.6
0.8
1.0
1.2
1.4
1.6
1.8
2.0
Mother cell mitochondrial mass
D
G0
G1
G2
G2
cousin1
24h
cousin2
E
Mitochondrial mass dependent on fate
Mitochondrial mass
2.5
2.0
1.5
1.0
0.5
0
48
72
96
120
time (h)
Quiescence
One division
SD MK
MK
Proliferation
AD MK
F
Mitochondrial mass on freshly isolated cells
Mitochondrial mass
1.6
1.4
1.2
1.0
0.8
0.6
0.4
0.2
0.0
*
*
***
*
NS
AD MK
Apoptosis
MK
Proliferation
One division
SD MK
Quiescence

Figure 4.3: Mitochondrial mass analysis of 174 individual LT-HSCs. (A) Mitochondrial asymmetry in daughter cells or cousin cells correlated to synchrony. (B) Mitochondrial mass distribution in sister cells of the first (black) or second (red) generation. (A–B) The inset demonstrates which cells (in green and blue) are used for asymmetry calculation. Statistical analysis is performed by one-way Anova with Bonferonni post-hoc analysis: *p<0.05, **p<0.01, ***p<0.001. The asymmetry index for sister cells is calculated as the absolute difference of mitochondrial mass ($|c_1 - c_2|$) where c_1 and c_2 represent the sister cell values. Similarly, the difference of mitochondrial mass between cousin cells was taken as ($\left|\frac{c_1+c_2}{2} - \frac{c_3+c_4}{2}\right|$) where c_1 and c_2 are the values of two sister cells that are both the cousins of cells with values c_3 and c_4. (C) Correlation between mitochondrial mass of mother cells and the asymmetry of mitochondrial mass distribution between their respective daughter cells. (D) Scheme illustrating an asynchronous division (E) Mitochondrial mass evolution from day 0 to day 5 depending on the cell fate: no division (quiescence, brown line), one division (pink line), symmetric differentiation into megakaryocyte (SD MK), differentiation into megakaryocyte without division (MK), asymmetric differentiation into megakaryocyte (AD MK, one or more division) and proliferation (more than one division). Error bar shows standard deviation. (F) Mitochondrial mass on day 0, depending on subsequently defined cell fate.

4.4 Conclusion

The first aim of the present study was to characterize the LT-HSC behavior when cultured on our micro-groove lineage tracking platform. We successfully demonstrated that the platform is suitable for studying HSCs by demonstrating its similarity in various cellular parameters, including cell fate, proliferation kinetics and cell functionality, between the cells cultured on the platform and the cells cultured in standard conditions. We then used the platform to track the mitochondrial mass in HSCs throughout a period of 5 days. Collectively, our experiments revealed the existence of a specific distribution mechanism that segregates mitochondria, preferentially to one of the daughter cells, during an asymmetric division. These results further support the idea that the HSC fate is tethered to mitochondria[161]. This work encourages further studies that would assess mitochondrial mass distribution asymmetry in the presence of molecules known to increase the frequency of asymmetric divisions in HSCs[51] or, in contrary, direct HSCs toward symmetric commitment[42]. Additional investigation should also be carried out to distinguish whether the mitochondrial mass distribution during AD is also linked to the difference in the metabolic activity of these mitochondria.

4.5 Acknowledgement

We thank Thierry Laroche and Oliver Burri for their support with the confocal microscope.

Chapter 5 Analysis of asymmetric markers in the first generation of cells derived from murine HSCs

Mukul Girotra*, Vincent Trachsel*, Aline Roch, Sonja Giger, Matthias P. Lutolf

*- equal contribution

Abstract

Hematopoietic stem cells (HSCs) maintain their own population and produce committed daughter cells for the life-long production of all mature blood cells. Under homeostasis, HSCs in the native niche are believed to achieve this dual role by undergoing a process called asymmetric cell division (ACD), whereby one daughter cell maintains stem cell potential while the other differentiates to give rise to various blood cell lineages. Lack of critical instructive signals in the in vitro environment results in rapid loss of functional HSCs, making it extremely challenging to study self-renewal and ACD in a dish. Here, we explored the possibility to "pre-instruct" fate in activated HSCs directly in their in vivo niche in order to assess the fate choices for dividing HSCs in vitro in a cell-intrinsic manner. To this end, we pushed HSCs out of their dormancy by Interferon-α (IFNa) treatment and analyzed paired daughter cells (PDCs) by in vitro tracking of cell division, followed by multi gene and protein expression analysis at the single cell level. We demonstrate that IFNa treatment significantly increases the proportion of asynchronous divisions of HSC daughters, indicating a possible involvement of asymmetric cell divisions. The gene expression analysis of PDCs revealed a set of 12 asymmetrically expressed genes. We then confirmed these results by analyzing the asymmetric expression at the protein level, where we found three candidates to be highly asymmetric, namely, Glut1, JAM3 and HK2. Preliminary functional analysis by colony forming assays revealed that the combination of Glut1 and JAM3 allows reliable discrimination of a differentiated daughter HSC from a self-renewing one during an ACD.

5.1 Introduction

The maintenance of a hematopoietic stem cell (HSC) pool and a concomitant production of committed daughter cells for life long generation of mature blood cells is achieved by a well-orchestrated balance of HSC fate choices *in vivo*. This regulation restricts uncontrolled stem cell expansion or differentiation that could be detrimental for the organism. Asymmetric cell division (ACD) is an intriguing strategy that allows for both the maintenance of stem cell number as well as the production of differentiated progeny at the same time[170]. Previous studies on paired daughter cell (PDC) have revealed different colony forming potential[171,172] and *in vivo* reconstitution ability[38,173] in sister cells, suggesting the occurrence of ACD in HSCs. However, most *in vitro* methods lack critical instructive signals of the *in vivo* niche. Therefore, it is currently not possible to study niche-instructed HSC fate choices, especially ACD, in a dish. Here, we explore the possibility to 'pre-instruct' HSCs directly in the *in vivo* niche in order to assess the fate choices of dividing HSCs in a cell-intrinsic manner.

To this end, we used Interferon-α (IFNa) treatment to activate murine HSCs out of their dormancy in their native environment[174]. Intriguingly, the IFNa activated HSCs demonstrated a significant increase in the proportion of asynchronous cell divisions, suggesting the execution of ACD. Single cell gene expression analysis on PDCs revealed an asymmetric gene set and showed significantly higher "asymmetry index" values for IFNa activated HSCs. High resolution confocal imaging confirmed increased asymmetry for the three selected markers in IFNa treated HSCs. Furthermore, we characterized the expression of one of the markers, namely, Glucose transporter 1 (Glut1). In line with previous studies[175], the flow cytometry analysis revealed lower Glut1 expression in phenotypic HSCs. Using co-staining and functional assays, we found that post cell-division, daughter cell with low Glut1 and high JAM3 expression show a more primitive phenotype. Collectively, we established IFN-based activation as a useful model to understand the molecular mechanisms mediating ACD in murine HSCs and identified an asymmetric gene set that provides a first glimpse of the molecular players involved in ACD.

5.2 Materials and methods

5.2.1 *In vivo* activation of HSCs

HSCs were activated to exit dormancy by interferon-alpha (IFNa) treatment following published protocols[50,174]. Briefly, subcutaneous injections in C57Bl/6J mice were carried out with 10,000U of IFNa (R&D systems) 48 and 24 hours prior to bone marrow extraction. Control mice were injected with an equivalent volume of the vehicle (PBS + 0.1% BSA).

5.2.2 Antibodies

The following antibodies were used: cKit-PeCy7 (2B8, Biolegend), Sca1-APC (D7, Biolegend), CD150-PeCy5 (TC-15-12F12.2, Biolegend), CD48-PB (GM48-1, Biolegend), CD34-FITC (RAM34, eBiosciences), SAV-PO (life technologies). A mixture of biotinylated mAbs against CD3, CD11b, CD45R/B220, Ly-6G, Ly-6C and TER-119 was used as lineage depletion cocktail (BD Biosciences).

5.2.3 Cell cycle analysis

FACS sorted HSCs were fixed and permeabilized using Cytofix/Cytoperm plus kit (BD Biosciences), according to the manufacturer instruction. Cells were then stained overnight with Ki67 FITC (BD Biosciences) at 4°C, and 10 minutes with Hoechst 33342 (Invitrogen). Stained cells were run on a BD LSRII for cell cycle analysis.

5.2.4 Micro-groove array platform fabrication

Micro-groove arrays were fabricated and used as described (Trachsel et al., Submitted). Briefly, the platform is composed of two parts: one containing the groove array (bottom) and one used as a lid to close the groove (top). The lid covalently reacts with the bottom part, therefore cells seeded on the groove array are encapsulated allowing an unambiguous tracking of cells and their progeny. The bottom part is made in poly(2-hydroxyethyl methacrylate)-trimethylolpropane trimethacrylate copolymer (pHEMA-TMPTMA) and the permeable lid in self-assembling polyethylene glycol (PEG).

5.2.5 PEG microwell array fabrication

PEG microwells were formed at the bottom of 96-well micro plate (BD) or 4-well plate (Nunc) by crosslinking 4arm-PEG-thiol (PEG-SH, 10kDa) with 8arm-PEG-vinboneulfones (PEGVS, 10kDa) at 5%

w/v. Hydrogel films were micropatterned by soft embossing with PDMS (polydimethylsiloxane, VWR) stamps for one hour to create an array of microwells.

5.2.6 Single cell proliferation analysis by time-lapse microscopy

Freshly isolated HSCs were seeded on the platforms. Platforms were directly placed on the time-lapse microscope (Zeiss Axio Observer Z1 inverted microscope equipped with a motorized stage) for image acquisition. An incubation chamber maintaining temperature and CO_2 levels allowed for live cell imaging. The stage was programmed to scan the microwell array surface and acquire images of multiple positions every 3 hours (30 min or 1 hour for the micro groove platform) for the duration of the culture period. Single cell proliferation kinetics were assessed based on time-lapse movies.

5.2.7 Flow cytometry and cell sorting

Flow cytometry analysis of hematopoietic stem and progenitor cells was performed on freshly isolated bone marrow (BM) from 8-12 weeks old C57Bl/6J mice. BM was extracted from crushed femora, tibia and hip bone. Cell suspension was then filtered through a 70µm cell strainer and erythroid cells were eliminated by incubation with red blood cells lysis buffer (eBioscences). Lineage-positive cells were removed with a magnetic lineage depletion kit (Miltenyi Biotech). Cell suspensions were stained with a panel of specific antibodies for stem and progenitor cells and FACS-sorted on BD FACS Aria II. The hematopoietic stem cell (HSC) compartment was identified and sorted with the following cell surface phenotype Lin- Ckit+ Sca1+ (LKS) CD150+ CD48- CD34-.

5.2.8 HSC culture

All HSC cultures were maintained at 5% CO_2 at 37^o C in “Basal” media, Stemline II (Sigma) supplemented with 100ng/ml SCF (R&D Systems), 2ng/ml Flt3 ligand (R&D systems) and 0.5% P/S. “Differentiation” media was made by supplementing Basal media with 20ng/ml IL3 (R&D Systems) and 100ng/ml IL6 (R&D Systems). For uncoupler experiments, 5µM carbonyl cyanide 4-(trifluoromethoxy) phenylhydrazone (FCCP) (Sigma) was added to the “differentiation” medium every 24 hours.

5.2.9 Single cell proliferation analysis

Individual cells cultured in microwells were imaged on a Zeiss Axio Observer Z1 inverted microscope equipped with a motorized stage. An incubation chamber maintaining temperature and CO_2 levels allowed for live cell imaging. The stage was programmed to scan the microwell array surface and acquire images of multiple positions every 3 hours. Single cell proliferation kinetics were assessed based on time-lapse movies.

5.2.10 Micromanipulation of paired daughter cells for single cell analysis

Single cells in microwells having undergone one division to give rise to two daughter cells were identified after 40 hours in culture. Paired daughter cells were isolated by micromanipulation in 20µm diameter micro capillaries (Eppendorf). Single cells were ejected from the micro capillaries into lysis solution for subsequent single cell PCR.

5.2.11 Selection of candidate genes

47 candidate genes listed in Table 4.1 were selected for expression analysis in PDCs. Some of those genes were identified in a microarray analysis where they were differentially expressed in HSCs compared to MPPs[176], or compared to mobilized or leukemic HSCs[177]. These included, key cell surface molecules such as JAM3, Tie2, ProCR, and Esam1; intracellular adaptor proteins Grb10 and Fhl1;

and, cycling dependent kinase inhibitor p57[178]. After a careful review of published work we included, cell cycle genes p21, p27, and p130, which were shown to be important in HSC quiescence[179–181]; HSC maintenance genes b-cat[182], Pten[183], and Gata3[184]; and, important self renewal mediators, HoxB4[185] and c-myc[186,187]. With recent developments in the field that are strongly implying the role of metabolism in HSC fate choices, we included a variety of metabolic genes for our analysis. These included, a glucose transporter (Glut1), key glycolytic enzymes (HK2, PFKFB3, Ldha)[50,188], enzymes involved in TCA cycle (CS, Acyl, Aco1, Suclg1, Mdh2), and some key components of the oxidative phosphorylation machinery. Based on recent work that implicated fatty acid oxidation as a key to HSC maintenance[189], we included two acyl-coA dehydrogenases (MCad and Lcad) and an enzyme that facilitates the entry of fatty acids into the mitochondria (Cpt1a). With growing amount of information on the detrimental effects of ROS on HSC function, we included two key antioxidants (SOD2 and Cat) that were shown to be instrumental in keeping ROS levels low in HSCs[31,188].

Classification	Gene name		Classification	Gene name
House keeping gene	HPRT		**Glycolysis**	HK2
ECM proteins	Tgm2			PFKFB3
	Bgn			Glut1
Membrane proteins	Esam1			Ldha
	Tie2		**TCA cycle**	CS
	JAM3			Acly
HSC markers	CD150			Aco1
	CD48			Suclg1
	CD34			Mdh2
	C-kit		**Oxidative Phosphorylation**	Cyt-C
Intracellular adaptors	Grb10			NDUFA2
	ProCR			COX2 (Sdhd)
	Fhl1			ATP5g1
	b-catenin			COX1
Cell cycle regulators	P57 (cdkn1c)			COX3
	P27 (cdkn1b)			COX4
	P21 (cdkn1a)		**Mitochondrial biogenesis**	Mfn2
	P130 (rab3gap)			Tfam
	Pten		**Antioxidants**	SOD2
Transcription factors	Pbx1			Catalase
	Gata3		**Fatty acid oxidation**	MCad
	c-myc			LCad
	Hoxb4			CPT1a
DNA repair	Gadd45			

Table 5.1: List of genes tested in single cell multi gene expression analysis. Table from Dr. Mukul Girotra's thesis

5.2.12 Single cell qRT-PCR

Micromanipulated single cells were ejected in 0.2ml PCR tubes containing 10µl of Lysis solution (9µl single cell lysis solution+ 1µl single cell Dnase I). Cells were incubated in the lysis solution at RT for up to 30min followed by addition of 1µl of single cell stop solution and incubation at RT for up to 20min. The samples were then stored at -20°C. Reverse transcription and pre-amplification were performed sequentially on the lysed cell sample using Single Cell-to-Ct Kit (Life Technologies). Conditions for reverse transcription were 10min at 25°C, 60min at 42°C, and 5min at 42°C. Gene Expression TaqMan Assays (Life Technologies) corresponding to the gene set (Table 4.1) were pooled and diluted at 0.2X in 1X TE buffer pH8.0 for pre-amplification. Samples were incubated for 10min at 95°C and pre-amplified for 14 cycles of 15 sec at 95°C and 4 min at 60°C on a thermal cycler. The pre-amplified samples were diluted 1:15 in 1X TE buffer pH8.0 and stored at -20°C. Real-time quantitative PCR was performed with Gene Expression TaqMan Assays (Life Technologies) on a 7900HT system (Applied BioSystems). Conditions for amplification were 2 min at 50°C and 10 min at 94.5°C followed by 40 cycles of 5sec at 97°C and 1min at 59.7°C. Expression values over the threshold of the machine were set to 40 (ct=40).

5.2.13 Immunostaining and images analysis in the multi groove platform

At the end of the culture period, cells were fixed (4% PFA) and permeabilized (0.1% TritonX) before blocking with 10% goat serum on the platform. Immunostaining was performed using Glut1-AlexaFluor 647 (1:500) (cat no: ab195020 Abcam), JAM3-FitC (1:100) (clone CRAM-18 F26, cat:no MCA5935F BioRad), and HK2 (1:500) (cat no: ab76959 Abcam) with a secondary antibody AlexaFluor 555 (1:500) (cat no: A-21425 Thermofisher scientific). Z-stacks of paired-daughter cells were obtained using a confocal spinning-disk microscope (NikonTi, Crest spinning disk with ANDOR EMCCD camera). Sum of pixels value of z-stack images were calculated to obtain the total protein expression of a cell. Image analysis was performed with ImageJ.

5.2.14 Glut1 staining for FACS analysis

Freshly sorted/cultured cells were stained with anti Glut1-PE (cat no: NB110-39113PE) for 1 hour at 4°C followed by washing with PBS before being used for analysis.

5.2.15 Transplantation

Double congenic (CD45.1/45.2) marker system was used for transplantations. CD45.2 female mice were lethally irradiated (850RAD) and transplanted with donor cells isolated from CD45.1 mice and competitor cells from CD45.1/45.2 mice. Glut1 low and high subpopulations in LT-HSCs were FACS sorted. 75 donor cells were transplanted together with 250 $*10^3$ BM competitor cells. Recipient mice were bled at 4, 8 and 16 weeks post-transplant and peripheral blood was stained with specific antibodies to determine donor-derived chimerism.

5.2.16 CFU assay

Freshly isolated LT-HSCs were cultured for 3 days and directly stained with Glut1 (cat no: NB110-39113PE, NovusBiologicals) and JAM3 (cat no: MCA5935, BioRad) antibody. Stained cells were re-sorted based on Glut1 and JAM3 low and high signals. 35 collected cells of either population were plated in complete M3434 methylcellulose (Stem Cell Technologies) following the manufacturer's instructions. Colony-forming cell mass was scored at day 8 and 10 using STEMvisionTM (an automated colony counting machine, StemCell technolgies). Colony categories (erythroid and/or megakaryocyte progenitor cells CFU-MK/E, granulocytes and/or macrophage progenitor CFU-M/G/GM, and multi-potential progenitors (CFU-GEMM) were evaluated by visual inspection.

5.2.17 Statistics

Data was statistically analyzed by student t test, Mann-Whitney test, Spearman's rank correlation coefficient was determined for correlation analysis.

5.3 Results

5.3.1 *In vivo* activation of HSCs by IFNa increases asynchronous cell divisions

We used interferon-α (IFNa) treatment as a model to push HSCs out of their dormant state in vivo[50,174]. HSCs from IFNa treated and control mice were FACS sorted based on a combination of cell surface markers regularly used in the field, such as Lin-ckit+Sca1+ (LKS) CD150+CD48-CD34-[13,166,190], and immediately fixed and stained to determine their cell cycle status (Figure 5.1A). As previously shown, the IFNa treatment resulted in a significant increase in the proportion of cycling HSCs (Ki67 positive) (Figure 5.1B). We next assessed the proliferation kinetics of freshly isolated control and IFNa-activated single HSCs using a platform with micro-grooves array made in pHEMA-TMPTA in combination with live cell imaging (Trachsel et al., Submitted; Vannini et al., In preparation). The platform was developed to allow single cell trapping and lineage tracking of rare and sensitive cells (such as HSCs). In brief, single cells were captured in individual micro-grooves by gravity and were restricted to grow in a line. To avoid a cell from interchanging its position with other cells, the micro-grooves were closed with a permeable lid made in self-assembling polyethylene glycol (PEG) polymer. Therefore, this platform allows unambiguous tracking of single cells over multiple generations. Using the platform, we measured single cell behavior and division dynamics in high throughput over a period of up to five days (Figure 5.1D-F). As expected, the IFNa-activated HSCs carried out the first division faster when compared to the control HSCs (Figure 5.1F). The time until half of the population had carried out a cell division was around 53 hours for control HSCs and was shortened by approximately 8 hours in IFNa treated cells (Figure 5.1F), confirming the IFNa treatment as a reliable model for HSC activation in their native bone marrow niche. Moreover, the proliferation curves showed similar average expansion over a period of five days (Figure 5.1E), demonstrating that acute IFNa treatment leads to transient activation and not an uncontrolled proliferation of HSCs, as shown by previous studies[174]. We observed similar division kinetics on the PEG microwell platform[73,111,120,129], confirming our results on two different single cell platforms (Supplementary Figure S5.1)

One key property of the HSCs is their slower cycling rates as compared to their progenitors[111,164–166]. Therefore, we hypothesized that an analysis of the proliferation kinetics of the first generation of HSC daughters could reveal information on the maintenance of stem cell properties such as slower cycling rates. We assessed the difference in time of division of PDC to define the synchrony of cell division (ΔT). A pair of daughter cells was defined here as asynchronous if the ΔT was longer than 6 hours (Figure 5.1G). We observed that the proportion of asynchronous divisions was higher (Figure 5.1H) and the average asynchrony time was significantly longer in IFNa-activated HSCs when compared to controls (Figure 5.1I). Corresponding analysis on the PEG microwell platform confirmed this observation (Supplementary Figure S5.1). This increase in asynchrony suggested a possible increase in asymmetric division where one daughter retains stem cell potential (slow cycling) whereas the other daughter undergoes commitment (fast cycling), supporting earlier evidence in the field for the production of two non-identical daughter

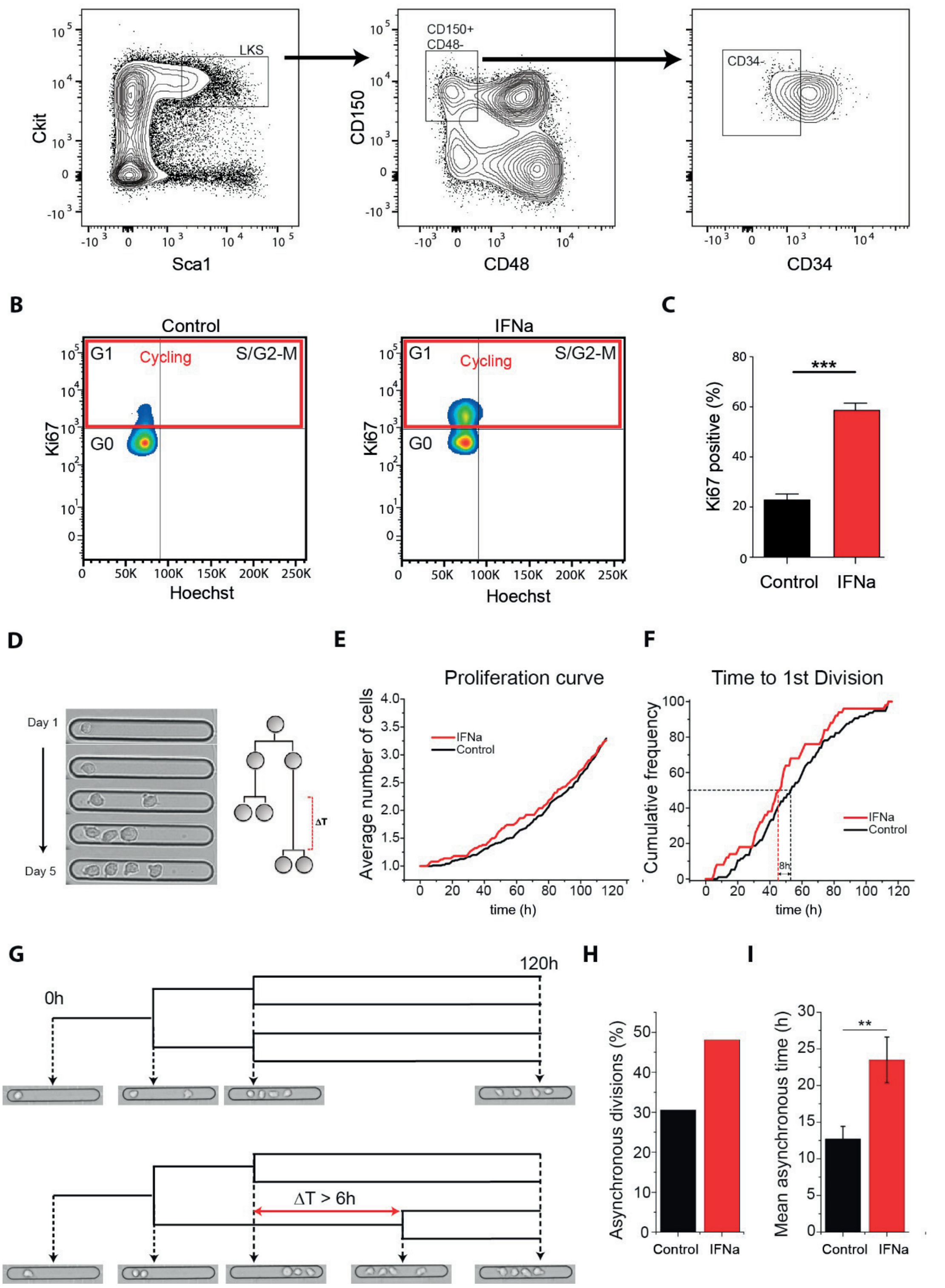

Figure 5.1: *In vivo* activation of HSCs by IFNa increases asynchronous cell divisions. (A) HSCs were freshly isolated from the bone marrow using Lin- cKit+ Sca1+ CD150+ CD48- CD34- markers.

(B) Cell cycle analysis using Ki67 and Hoechst staining on freshly isolated HSCs from control and IFNa treated mice. Cells in red box (Ki67 positive) constitute a fraction of HSCs in a cycling state (G1+S/G2-M phase). (C) HSCs isolated from IFNa treated mice show a significant increase in the cycling fraction (Ki67 positive cells). (D) Single cell proliferation kinetics analysis using live cell imaging of HSCs pHEMA-TMPTA micro-grooves platform (Trachsel et al., Submitted. (E-F) Proliferation kinetics of live and dividing HSCs isolated from control and IFNa administered mice. The average proliferation over 5 days remains similar in the two conditions, with IFNa activated cells carrying out the first division much faster (~8h) when compared to control HSCs. (G) Representative example of synchronous division (top) and an asynchronous division (below) with $\Delta T \geq 6$ hours being used as a threshold. (H) IFNa activated HSCs show a notable increase in the proportion of asynchronous divisions. (I) IFNa activated HSCs show a significant increase of asynchronous-time division between daughter cells. ***$P < 0.001$, **$P < 0.01$ and *$P < 0.05$

cells with different colony forming and blood reconstitution levels *in vitro*[38,171–173].

5.3.2 Identification of the asymmetric gene set using PDC gene expression analysis

We, and others, have previously demonstrated how acute activation by IFNa results in HSC self-renewal without the loss of stem cell potential[50,174]. Since IFNa mediated activation occurs in the native bone marrow niche without loss of stem cell potential and leads to an increase in asynchronous divisions *in vitro* (Figure 5.1H, Supplementary Figure S5.1E), we hypothesized that this could be a suitable system to study niche-instructed HSC fate choices and, specifically, the process of ACD. To test this, we performed the multi-gene expression analysis in PDCs and compared the gene expression profiles of sister cells. To this end, we isolated IFNa-activated HSCs from the bone marrow and cultured them as single cells in PEG microwells in basal serum-free culture condition in order to follow their proliferation kinetics (Supplementary Figure S5.2A). The PEG microwell system is an open system that allows easy access to cells for their collection. Upon division, the PDCs were isolated from microwells by micromanipulation (Supplementary Figure S5.2B) and analyzed for their gene expression profile using single cell quantitative RT-PCR. We shortlisted 47 candidate genes for expression analysis (described in experimental methods) on every cell. These genes belonged to various metabolic pathways or were earlier identified as important regulators of HSC function. All candidate genes were analyzed in 24 sets of PDCs. Strikingly, when the $\text{Log}_2(\text{Ct})$ values of the two cells were plotted against each other, different genes showed distinct patterns of expression. The qualitative analysis revealed that, on one hand, some candidate genes demonstrated symmetric expression behavior with almost all pairs found close to the diagonal (Supplementary Figure S5.3A). On the other hand, various genes were asymmetrically expressed (Supplementary Figure S5.3B), with one cell of the pair expressing the gene at higher levels (low Ct) and the other at lower levels (high Ct). However, for most of these potentially asymmetric genes, a sub population of pairs that appeared close to the diagonal (Supplementary Figure S5.3B) remained, suggesting that not all pairs are carrying out ACD.

In order to identify the most asymmetrically expressed gene set, we assigned a quantitative value to every gene to determine where it ranked in comparison to the others. To this end, we obtained the average ΔCt for every gene across all pairs and designated it as "*Gene score"*.

$$Gene\ score = \frac{1}{n}\left(\sum_{i=1}^{n\ pairs} (\Delta Ct)\right) \qquad where\ \Delta Ct = |Ct\ Cell_a - \ Ct\ Cell_b|$$

A gene score of 1 indicated an average 2-fold difference in expression in the PDCs, which incremented to 4-, 8-, 16- and 32-fold with gene scores of 2, 3, 4 and 5. We found a huge range of this score with some genes as low as 0.195 (~1.15 fold difference) and others as high as 5 (~32 fold difference) (Figure 5.2B). We applied a stringent (although arbitrary) threshold of 10-fold difference to identify a set of most highly asymmetric genes from our candidate list. 12 genes were found to be above this threshold (Figure 5.2B (in red), Figure 5.2C). This set included genes controlling different metabolic pathways such as glycolysis and TCA cycle as well as conventional HSC markers such as JAM3 and CD150.

Having identified a set of asymmetrically expressed genes, we next checked the asymmetry associated in individual pairs linked to this gene set. To obtain a single quantitative readout of symmetry for a pair, we calculated the Euclidian distance between the two sister cells by summing up the square ΔCt value for all genes in the “asymmetric” gene set and calculating its square root. We called this value the (A)symmetry index (A.I) for a pair. Here, a higher value of A.I reflected a greater asymmetry in expression.

$$A.I_{gene} = \sqrt{\left(\sum_{i=1}^{N\ genes} (Ct\ \{cell\ a\} - Ct\ \{cell\ b\})^2\right)}$$

Pairs with high A.I value (representative examples shown in Supplementary Figure S5.3) had asymmetric expression of these genes, and, very often, the expression was restricted to only one cell of the pair (Supplementary Figure S5.3) whereas, in pairs with low A.I value (representative examples shown in Supplementary Figure S5.3), most genes were expressed symmetrically and were found very close to the diagonal (Supplementary Figure S5.3). A comparative analysis revealed that IFNa-activated pairs had significantly higher values of A.I than their control counterparts (Figure 5.2D), suggesting that it can be used as a suitable model to study the link between expression and asymmetric fate in HSCs.

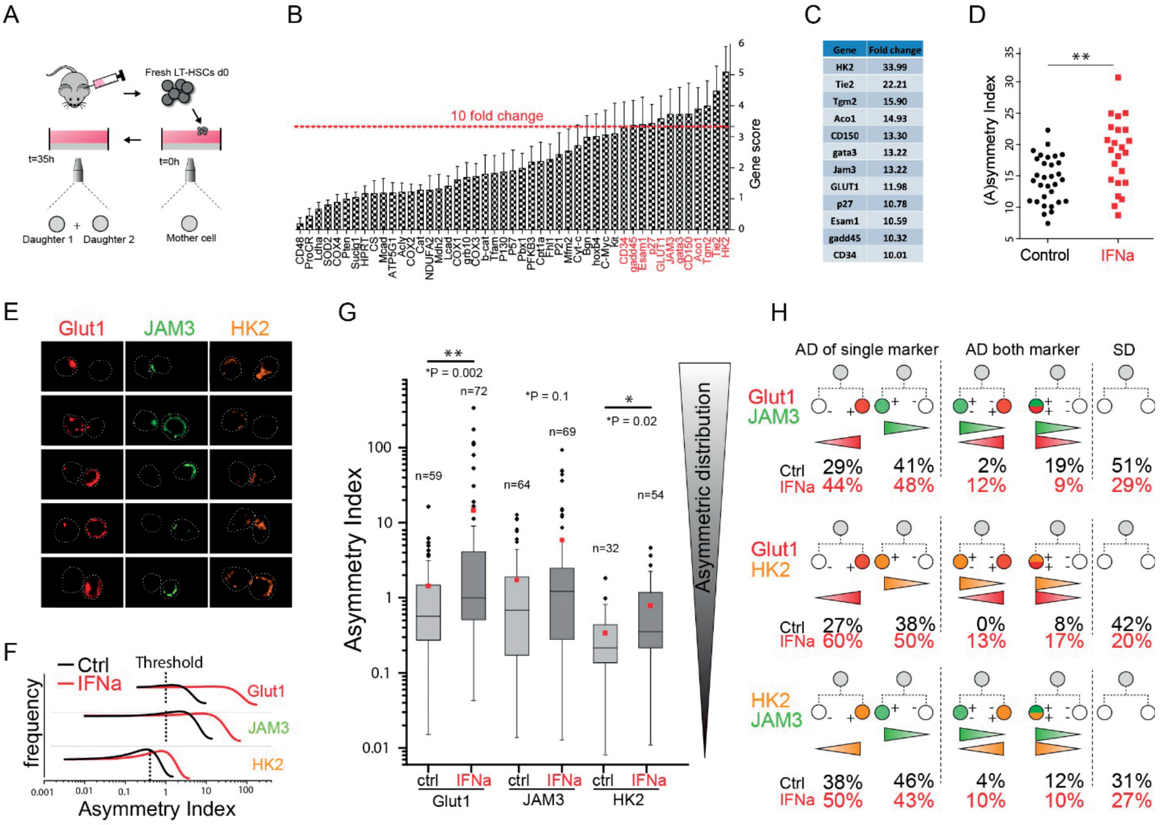

Gene	Fold change
HK2	33.99
Tie2	22.21
Tgm2	15.90
Aco1	14.93
CD150	13.30
gata3	13.22
Jam3	13.22
GLUT1	11.98
p27	10.78
Esam1	10.59
gadd45	10.32
CD34	10.01

Figure 5.2: Identification of asymmetric gene and protein expression in PDCs. (A) Freshly isolated HSCs tracked during culture until first division (35h) using a time-lapse microscope. A microwell array platform was used for the gene expression analysis and a microgroove platform for protein expression analysis (Figure S2). (B) The gene score values show a wide variation from one gene to another. A stringent threshold (average 10-fold difference in gene expression between PDCs) was put to identify the "asymmetric gene set". (B-C) Figures adapted from Dr. Mukul Girotra's Thesis (C) Table showing 12 candidate genes that were seen to cross the 10-fold threshold (fold change values in table). (D) IFNa treated PDCs show a higher asymmetry when Index compared to control PDCs. (E) Representative immunofluorescent images showing asymmetric expression of Glut1, JAM3 and HK2 in 5 PDCs. (F-G) Analysis of PDCs asymmetry for Glut1 (n=59 control, n=72 IFNa), JAM3 (n=64 control, n=69 IFNa treatment) and HK2 (n=32 control, n=54 IFNa) with IFNa treated cells or control. (F) PDCs asymmetry in frequency with threshold defining "asymmetric protein expression" used in (H): Glut1=1, JAM3=1, HK2=0.3. (G) PDCs asymmetry. Boxplot's interquartile range from 25th to 75th percentile. Line and red square shows respectively median and mean, and the error bar is SD (outliers lower or upper inner fence is equal to 1.5 the interquartile range) (H) The protein expression pattern in PDCs (all PDCs considered) for Glut1, JAM3 and HK2. Asymmetry with one marker (first column) are shown in total percentage (without considering other markers). A double asymmetry (two asymmetric proteins) analysis is showed in the second column. An asymmetry comprising two proteins (for example "P1" and "P2") on two daughter cells (defined by ca and cb) may be either "coinciding"—a cell having high expressions of both proteins "A" "B" (phonetically defined by $c_a\,{}^{P1}_{P2} == {}^{+}_{+}$, $c_b\,{}^{P1}_{P2} = {}^{-}_{-}$)—or "diametrical"—a cell having more than one protein "P1"" but less than of "P2" $c_a\,{}^{P1}_{P2} = {}^{+}_{-}$ and, conversely, his sister more than one protein "P2" and less than "P1" $c_b\,{}^{P1}_{P2} = {}^{-}_{+}$. ***P< 0.001, **P< 0.01 and *P< 0.05.

5.3.3 Analysis of the protein expression of Glut1, JAM3 and HK2 by immunofluorescent staining

Having identified a list of 12 highly asymmetric candidates using gene expression analysis, we further went on to analyze whether this asymmetry holds true at the protein level. We selected three candidates, namely, Glut1, JAM3 and HK2, to check their expression in paired daughter cells.

To this end, we used the micro-groove platform, which allows high throughput tracking of single cells (Figure 5.1 and Supplementary Figure S5.2). Single cells were seeded onto the grooves and followed by time-lapse microscopy. Upon division, the PDCs were fixed and stained for immunofluorescence (Supplementary Figure S5.2C). Importantly, the closed micro groove platform allows cell encapsulation without a mix up of cells between different grooves during various staining steps. This results in a high throughput analysis of PDCs that is currently lacking in the field (Trachsel et al., Submitted). We compared the protein expression between sister cells (denoted by $c_a \ and \ c_b$) using confocal microscopy and obtained an index of asymmetry at the protein level, calculated as follows:

$$A.I_{protein} = \frac{c_a - c_b}{c_b}, \text{with } c_a > c_b \ .$$

The preliminary analysis revealed that some PDCs are very symmetric ($A.I_{protein}$<0.01) (Supplementary Figure S5.4) while others are extremely asymmetric (Figure 5.2E) ($A.I_{protein}$>100) both in control and IFNa-treated cells. In total, we analyzed 131 pairs for Glut1, 133 for JAM3 and 86 for HK2. To the best of our knowledge, this is the first study in which such a high number of HSC daughter pairs are analyzed for their protein expression by immunofluorescence at the single cell level. Our analysis revealed that with the IFNa treatment, PDCs exhibit significantly higher levels of asymmetry in Glut1, JAM3 and HK2. Particularly, Glut1 and JAM3 showed very high asymmetry values, suggesting their importance in mediating an asymmetric cell division in HSCs. Surprisingly, HK2, which was the most asymmetric candidate identified in the gene expression analysis, showed only a mild increase (although significant) in the protein asymmetry associated with IFN treatment (Figure 5.2G). In line with our asynchrony data (Figure 5.1) that suggested an increase in ACD with IFNa treatment, we found a concomitant increase in the frequency of high asymmetric segregation of all the three markers in the IFNa condition (Figure 5.2F).

To obtain a more comprehensive phenotype of PDCs, we analyzed co-stainings of Glut1, JAM3 and HK2 (n=69 IFNa n=63 control for Glut1/JAM3, n=30 IFNa n=26 control for Glut1/HK2, n=30 for IFNa, n=26 for control JAM3/HK2). We applied a threshold of $AI_{protein}$ equal to 1 (this corresponds to one sister having 100% more expression over the other) to identify asymmetric PDCs. However, since the overall asymmetry with HK2 was smaller, we lowered the threshold for HK2 to 0.3 (this corresponds to one sister having 30% more expression over the other) (Figure 5.3F).

As expected, we found that in the IFNa condition, Glut1 and JAM3 are more asymmetric individually (Figure 5.3H top and middle left panel). We next looked within these asymmetric pairs for double "diametrical" asymmetry and found it in 12% of IFNa PDCs (2% in control). This shows that one daughter cell exhibits higher expression of one marker and lower expression of the other when compared to its sister cell (i.e., first daughter has Glut^{high} JAM3^{low} while the second daughter has Glut^{low} JAM3^{high}). In contrast to diametrical asymmetry, only 2% of IFNa PDCs had a "coinciding" asymmetry (both markers expressed more on the same daughter cell) and 12% in control. Interestingly, both markers were symmetrically expressed in 51% of control PDCs and only 29% of IFNa PDCs. This data suggested a different signature in asymmetry expression in control and IFNa cells. Previous studies have shown higher JAM3[73,191,192] and lower Glut1 expression[175] on functional HSCs.

Therefore, we hypothesized that PDCs with Glut1^{low} JAM3^{high} phenotype could represent a more primitive cell type when compared to other combinations.

Moreover, we think that cell surface markers Glut1 and JAM3 can be used as reliable markers in functional assays for future analysis. Nevertheless, we tried co-staining with the other combinations (i.e., Glut1/HK2, JAM3/HK2) and confirmed the increase in asymmetry in the IFNa-treated PDCs (Figure 5.3H middle and bottom panel).

5.3.4 Characterization of Glut1 and JAM3 as markers for ACD in mHSCs

Many previous studies have highlighted the critical role of glycolytic metabolism in HSC fate determination[32,50,156,188]. Therefore, we further analyzed the protein expression levels of Glut1 whose glucose transporting activity would directly impinge upon the glycolytic and mitochondrial oxidative phosphorylation activities in the cell. Moreover, as a cell surface protein, it serves as an ideal candidate that allows the simultaneous estimation of protein expression levels by flow cytometry and stem cell potential through various functional assays. To this end, we first estimated the Glut1 expression by flow cytometry in different cell populations of the hematopoietic hierarchy. Strikingly, we found a stepwise increase in the Glut1 expression from the most primitive population (HSCs: LKS CD150+CD48-CD34-) to the more committed cell types (ST-HSC: LKS CD150+CD48-CD34+ and MPP: LKS CD150-) (Figure 5.3A). This agrees with previous studies estimating Glut1 levels in HSCs[175]. To test if the lower Glut1 imparts better functionality to HSCs, we sub-fractionated the HSCs into Glut1 low and high and transplanted them in irradiated recipients. We found that the Glut1 low subpopulation of HSCs shows higher long-term blood reconstitution potential (Supplementary Figure S5.5). The differential expression pattern of Glut1 in HSCs and progenitors plus higher stem cell potential of Glut1 low subpopulation suggested that it could be used as a potential marker to identify asymmetric cell division.

We further assessed the Glut1 expression in HSCs after 3 days of *in vitro* culture in pre-defined conditions. HSCs cultured in the Basal media showed a small decrease in the Glut1 low fraction (Figure 5.3B). Strikingly, the HSCs cultured in differentiation inducing “IL3/6” condition (Vannini et al., 2016) showed a dramatic increase in the Glut1 expression, almost resulting in the disappearance of the Glut1 low fraction. Intriguingly, the addition of a chemical uncoupler “FCCP” to these differentiation inducing conditions, previously shown to maintain stem cell potential (Vannini et al., 2016), completely reverts the profile of Glut1 expression (Figure 5.3B). This observation provides an indirect link between Glut1 expression and HSC fate.

To further characterize the “diametrical” asymmetry that we observed in Glut1 and JAM3 (Figure 5.2H), we sorted out the four populations after 3 days of *in vitro* culture (ensuring that the cells had divided). 35 sorted cells of each population were plated on methylcellulose and assessed for the ability to form different colonies. We found Glut1^{low} JAM3^{high} to be the only population showing emergence of GEMM colonies at 8 and 10 days post plating (Figure 5.3C), clearly indicating that the primitive cells post division are residing in this population. This phenotype is in line with previous studies showing high JAM3 and low glut1 in functional HSCs[73,175,191,192].

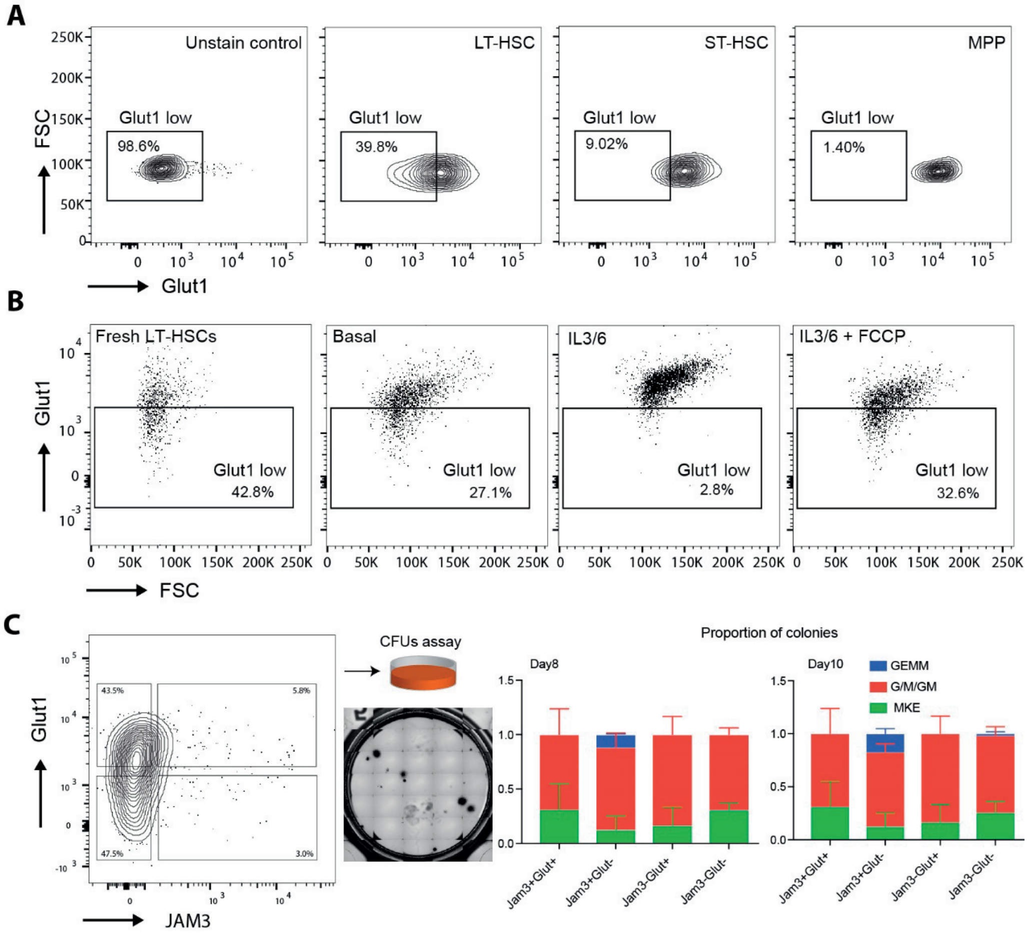

Figure 5.3: Characterization of Glut1 and JAM3 as markers for asymmetric division in HSCs. (A) Expression of Glut1 was tested in different populations of the hematopoietic hierarchy using flow cytometry. Long term HSCs (LT-HSCs: LKSCD150+CD48-CD34-), short term HSCs (ST-HSCs: LKSCD150+CD48-CD34+) and multipotent progenitors (MPPs: LKSCD150-) were identified using a combination of cell surface markers and stained with Glut1 to be analyzed by flow cytometry. Glut1 levels changed dramatically from the LT-HSCs (Glut1 low ~40%) to ST-HSCs (Glut1 low ~9%) to MPPs (Glut1 low ~1.5%) with concomitant increase as we moved down in the hematopoietic hierarchy. (B) Glut1 expression in LT-HSCs after 3 days of *in vitro* culture was assessed using flow cytometry. HSCs cultured in Basal media showed a small loss of Glut1 low fraction as compared to fresh uncultured LT-HSCs. Differentiation inducing (IL3/6) condition shows a striking loss of Glut1 low fraction with the overall Glut1 levels going up. The addition of FCCP (mitochondrial uncoupler) to the IL3/6 condition reverts this loss of Glut1 low fraction and brings down the level of Glut1 expression. (A)-(B) From Dr. Mukul Girotra's thesis (C) LT-HSCs were cultured for three days and were sorted based on Glut1 and JAM3. The stem cell potential of these sorted cells was determined by their Colony forming (CFU assay) ability. Glut1 low JAM3 high cells showed a significant increase in the proportion of more primitive (GEMM) colonies and concomitant decrease in the less primitive (Mk/E) colonies, suggesting that Glut1 low JAM3 high cells are more primitive than other populations (i.e., Glut1 high JAM3 low, Glut1 high JAM3 high, Glut1 low JAM3 high). (CFU-)G: Colony forming unit-granulocyte; (CFU-)M: Colony forming unit-macrophage; (CFU-)GM: Colony forming unit-granulocyte, macrophage; (CFU-)GEMM: Colony forming unit-granulocyte, erythrocyte, macrophage, megakaryocyte); Mk/BFU-E: Megakaryocyte/Burst forming unit-erythroid. (D) Bone marrow from healthy adult human ortheopedic donors were stained with different HSC and progenitor markers. The Glut1 low fraction reduced dramatically from the HSC containing population CD34+CD38-CD45RA- (~73%) to the progenitor populations CD34+CD38+ (56%) and CD34- (47%).

5.4 Discussion

Here, we report a unique experimental strategy to analyze niche-instructed fate choices in HSCs. IFNa mediated activation was used as a model to study ACD in murine HSCs. Live cell imaging revealed a significant increase in the asynchronous divisions in activated HSCs, suggesting the execution of a niche-instructed ACD program. Previous studies in invertebrates have elegantly demonstrated the role of the niche in orchestrating ACD. For example, in Drosophila, a close association with the niche (cap cell in the ovary and hub cell in the testis) is instrumental in the execution of the ACD of germline stem cells. Instructive cues from the niche lead to the activation of BMP (in ovary) or JAK-STAT (in testis) signaling, which eventually represses the differentiation in the daughter cell destined to maintain stemness [193–196]. PDC analyses in the hematopoietic system have revealed different colony forming potential[171,172] and *in vivo* reconstitution ability[38,173] in sister cells, suggesting the occurrence of ACD in HSCs. However, the precise mechanisms that regulate this fate choice are currently unknown.

Our single cell gene expression analysis in PDCs allowed the identification of an asymmetric gene set. Among them were some genes that have been described in the literature as important for HSC identification, such as CD150[13], Tie2[197] and JAM3[73]. Interestingly, Tie2 (receptor of Ang1) has been previously used as an asymmetry marker[189]. We also identified some metabolic genes such as Glucose transporter 1 (Glut1), Hexokinase 2 (HK2) and Aconitase 1 (Aco1) as highly asymmetric in PDCs. Glut-1 facilitates the transport of glucose across the cell membrane and has been previously shown [175] to be expressed more in the progenitors as compared to HSCs. Moreover, HK2, a glycolytic enzyme involved in the conversion of glucose to glucose-6-phosphate, was shown to be upregulated by HIF1a[198], a key component involved in the HSC function[188]. The identification of these two candidates confirms earlier reports on the importance of glycolytic pathways in the regulation of HSC function[32,188]. The asymmetric expression of Aco1, an important TCA cycle enzyme in the mitochondria converting citrate to iso-citrate, fitting well with our previous finding implicates mitochondrial activity as a determinant of the HSC fate[50].

Our results on the gene expression asymmetry were quite striking. We went ahead and explored if this asymmetry is maintained at the level of protein expression. To this end, we employed a platform that allowed us to quantify protein expression in paired-daughter cells using immunofluorescent staining. The asymmetric expression analysis at the protein level revealed significantly higher asymmetric protein expression in the three chosen candidates, suggesting the maintenance of asymmetry post translation. Co-staining with two markers showed higher double asymmetry in IFNa treated cells, suggesting it to be a good model for studying ACD in HSCs.

Our functional analysis using CFUs revealed Glut^{low} JAM3^{high} to be the most primitive subset in culture. This is in line with previous reports showing lower Glut1[175] and high JAM3[73] in functional HSCs. To better understand the expression of Glut1, we sorted the different cells of the hematopoietic hierarchy and checked their Glut1 levels. Flow cytometry analysis revealed that the Glut1 expression systematically increases as one moves down in the hematopoietic hierarchy, which confirms the observations of Sarrazy et al.[175]. Moreover, HSCs with lower Glut1 expression showed higher long-term blood reconstitution potential (Supplementary Figure S5.5). Furthermore, when the HSCs were put in pre-defined *in vitro* cultures, the Glut1 expression was higher in differentiation-inducing conditions (IL3/6) as compared to conditions (IL3/6+FCCP) that we previously exhibited as conducive to stem cells in culture[50].

At first, the lower expression of Glut1 appears to be counter intuitive as HSCs have been previously shown to be more glycolytic when compared to progenitors[128,156,188]. However, HSCs are also known to express lower levels of global protein synthesis relative to differentiating progenitors[199] . We think our data does not reflect the glycolytic flux but, in general, a lower expression of Glut1 in functional HSCs maintained post an asymmetric division in culture.

We believe that having a mechanistic understanding of niche-instructed cell fate choices in HSCs is important in basic stem cell biology and also holds immense clinical potential to design future *in vitro* culture systems for a controlled expansion of HSCs.

Supplementary information for chapter 5

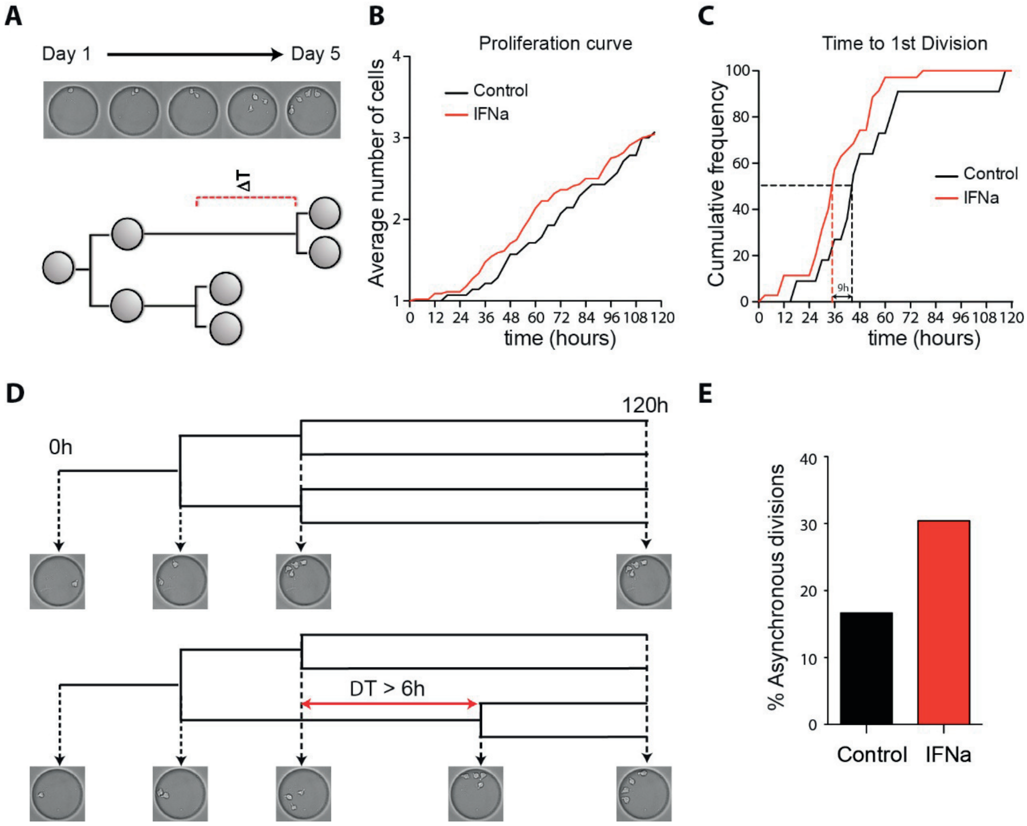

Figure S 5.1: *In vivo* activation of HSCs by IFNa increases the asynchronous cell divisions. (A) Single cell proliferation kinetics analysis using live cell imaging of HSCs in PEG microwells. (B-C) The proliferation kinetics of HSCs isolated from control and IFNa administered mice. The average proliferation over 5 days remains similar in the two conditions, with IFNa activated cells carrying out the first division much faster (~9h) as compared to control HSCs. (D) A representative example of synchronous division (top) and an asynchronous division (below) with ΔT 6 hours being used as a threshold. (E) IFNa activated HSCs show an increase in the proportion of asynchronous divisions. (Figure from Dr. Mukul Girotra’s Thesis)

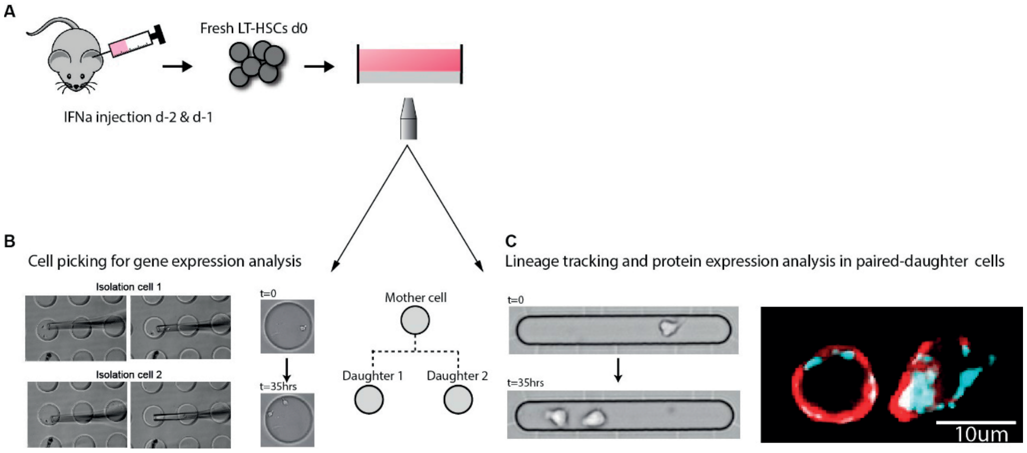
A
Fresh LT-HSCs d0
IFNa injection d-2 & d-1
B
Cell picking for gene expression analysis
Isolation cell 1
Isolation cell 2
t=0
t=35hrs
Mother cell
Daughter 1
Daughter 2
C
Lineage tracking and protein expression analysis in paired-daughter cells
t=0
t=35hrs
10um

Figure S 5.2: Gene and protein analysis of PDCs from IFNa-activated HSCs. (A) Freshly isolated HSC were cultured onto PEG microwells (B) (Lutolf et al., 2009) or pHEMA-TMPTMA micro-grooves (C) (Trachsel et al., Submitted) and allowed to carry out a division. (B) Micromanipulation of paired daughter cells (PDCs) generated from a single HSC after one division for multi-gene expression analysis using PEG microwell platform. (C) A protein expression analysis of PDCs generated from a single HSC after one division using pHEMA-TMPTMA micro-groove platform. Image (B) is adapted from Dr. Aline Roch's Thesis

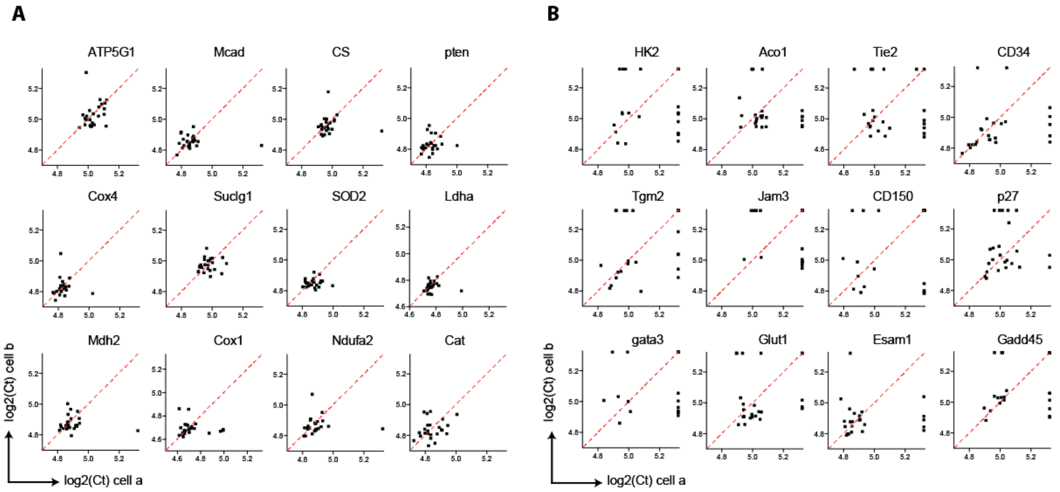

Figure S 5.3: Qualitative analysis of the distribution of gene expression in PDCs. Each gene is shown for the expression of 24 pairs of cells, with each dot representing a pair. (A) Representative examples of genes showing symmetric expression across most pairs. Most pairs appear close to the "symmetric diagonal" (in red). (B) Representative examples of genes showing asymmetric expression in pair daughter cells. Most pairs appearing far away from the "symmetric diagonal" (in red). Interestingly, most of these genes have a subpopulation of pairs that show symmetric behaviour. (Figure from Dr. Mukul Girotra's Thesis)

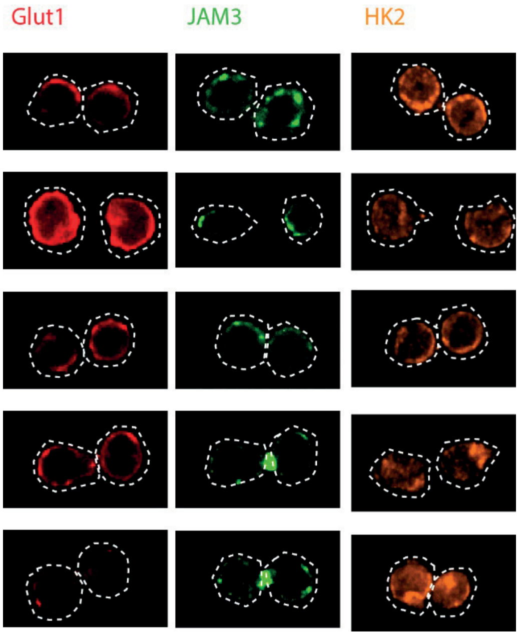

Figure S 5.4: Representative examples of symmetric expression of Glut1, JAM3 and HK2 in daughter cell pairs.

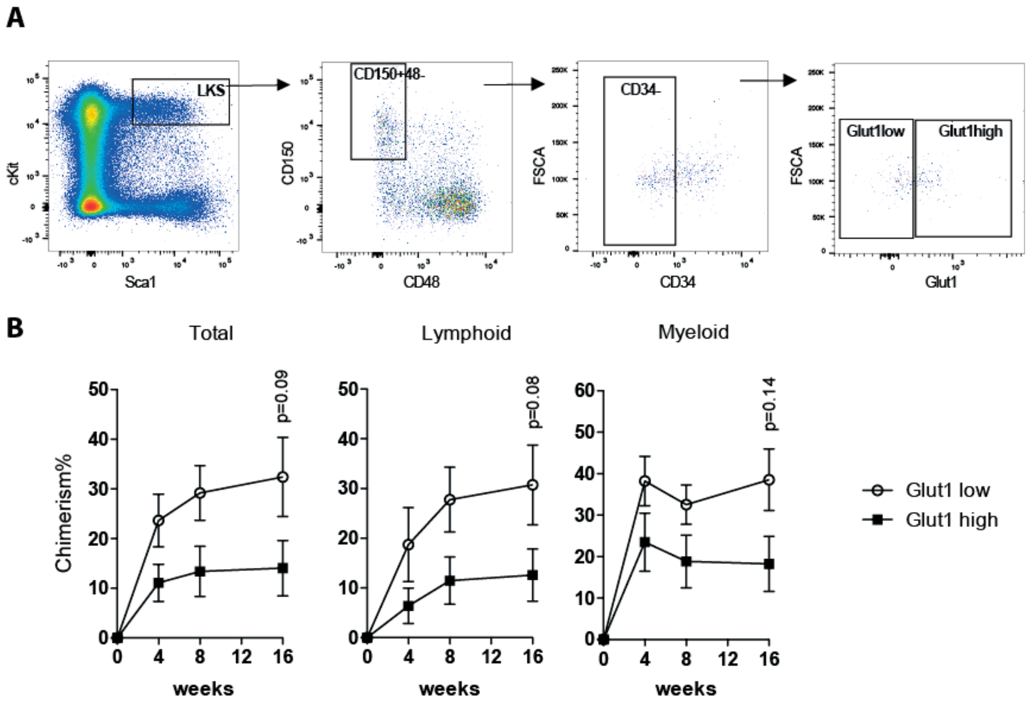

Figure S 5.5: Multi lineage blood reconstitution potential of Glut1low and high subpopulations. (A) Fresh LT-HSCs were sub fractionated in Glut1low and high populations. The two-sorted fractions were injected in lethally irradiated recipients. (B) Glut1 low fraction shows higher levels of multi lineage long-term blood reconstitution potential.

Chapter 6 Fate analysis of CD8+ T cell at the single cell level

Abstract

A host organism mounts a well-orchestrated immune response upon microbial infection. Cytotoxic T lymphocytes (CD8+ T cells) are an important arm of this immune response and generate various subsets to protect the organism against the pathogen. It was recently shown that these different T cell subsets, namely, the effector and memory cells, emerge from a common CD8+ T cell ancestor. However, it remains to be elucidated when and how this cellular diversity arise from a single T cell precursor. It was recently proposed that asymmetric cell division could be one mechanism through which two distinct daughter cells are generated as early as the first division. In the present chapter, we proposed a novel method that allows further characterization of T cells progeny in order to understand when and how this fate decision happens. We tracked single cells to observe if the first division is polarized during antigen presenting cell (APC) mediated activation. Moreover, we demonstrated that the immunological synapse (contact between T cell and APC) could also be studied using with our method.

6.1 Introduction

It has recently been shown that a single CD8+ naive T cells can give rise to effector and memory T cell progenies[200–202]. While the effector cells are short-lived and mediate acute protection against the pathogen, memory T cells have long lives and provide long-term protective immunity. However, how and when these different fates arise from a single cell (i.e., the diversification) remains a mystery. Moreover, the underlying mechanisms guiding this process are not fully understood. Suggested mechanisms are that T cells divide asymmetrically at a certain time or that a subset of T cell progressively diverge from the effector pool to form the memory T-cell population. Asymmetric division (AD), where one daughter proliferates and differentiates whereas the other daughter remains identical to the mother (maintaining the stem cell pool), is a process that has been well-established for stem cells. This allows rapid expansion of a cell population without compromising the integrity of the precursor cell. This phenomenon could potentially occur during multiple phases upon lymphocyte activation by an antigen-presenting cell (APC)[203]: 1) during the initial divisions after its activation, 2) during the T cell proliferation, or 3) during the contraction phase where cells die and only a small subset of cell remains alive to form the memory T cell pool[204]. One hypothesis envisages “the late divergence model” where the T cell diversification (appearance of memory T cells) happens after the expansion phase. In contrast, the “early divergent model” proposes that some T cells are already primed as memory T cells after the first division[205]. It is important to note that these models are not mutually exclusive. Recently, Chang et al.[206] compared two daughter cells arising from the first T cell and found notable differences in their protein expression. Strikingly, they were able to correlate these differences with a tendency of cells toward effector or memory fates, suggesting that the cells are already pre-instructed toward a distinct lineage during the first division. Chang et al.’s[206] observations are particularly in support of the early divergent model. Since the diversification may happen as early as the first division while one cell is still in contact with the APC, it was proposed that APCs could provide cues that promote AD. In line with this hypothesis, the same authors showed that the position of cells with respect to the APC seems to determine which daughter cell will acquire an effector fate and which one will take on the memory fate. The proximal cell (close to the APC) possessed more CD8 and CD44 proteins, were larger in size and expressed low level of CD62L, a profile consistent with “pre-effector” lineages[206]. In contrast, the distal daughter cell had a memory-like profile with a high level of CD62L but low CD44 expression; additionally, they were small[206]. Consequently, it is possible that the contact between a T cell and an APC (called the immunological synapse) that precede the first T cell division trigger the different fates between daughter cells. In line with this hypothesis, King. et al. demonstrated that the strength and affinity of T cells with APCs directly influences T cells polarization and, consequently, causes an asymmetric division[207].

Current experiments that allow the observation of daughter T cells require the addition of drugs to arrest the cells in the final phase of mitosis (i.e., Cytochalsin B or Nocodazole)[206,208,209]. Consequently, the two daughter cells are still connected and have not mixed with the rest of the cells in the culture, which leads to unambiguous asymmetry studies. However, an inhibition about mitosis prevents the analysis of subsequent lineages derived from each daughter cell. Lineage tracing analysis would greatly help to correlate the observations made on the asymmetric distribution of proteins between daughter cells after the first division with their respective progeny.

As previously explained, the interaction between the T cell and an APC at the immunological synapse seems to dictate the fate of daughter T cells[205,210]. Therefore, being able to observe the immunological synapse with a concomitant analysis of daughter cells would enable new understandings about their interactions. To this aim, Oliaro et al.[211] proposed a method that permitted the study of protein expression in daughter cells and an immunological synapse with the APC. In this approach, the antigen presentation was performed *in vitro* by seeding naive CD8+ T cell on pre-fixed antigen-primed dendritic cells. Cells were then fixed and stained for quantification, and the protein expression quantifications were made on cells that were in late-telophase. This experiment provided new insights into the role of APC to modulate the asymmetric division of T cell. This approach could not prevent the proximal and distal cell from changing their respective position and, therefore, can lead to inaccurate conclusions. More importantly, it was not possible to track daughter cell lineage after the first division. Collectively, these studies outline the critical need for a device that enables single T cell tracking over several generations in order to study the T cell fate.

To overcome the current limitations on T-cell progeny analysis and T-cell interaction with the APC, we attempted to establish a new methodology to observe and analyze the T cell lineages at the single cell level. The general aim is to observe the entire process, from the antigen presentation in a T cell to its proliferation. To enable T cell activation and lineage tracking, a co-culture of T cell with an APC is performed on the micro-groove tracking platform (Trachsel et al., Submitted). Not only would it provide meaningful information on how the immunological synapse changes T cell fate, it would allow a more precise estimation of when and how the dissociation between effector and memory cell happens. Here, we showed the first steps toward the achievement of this general aim.

6.2 Material and method

6.2.1 CD8+ T cells extraction

OT-I transgenic mice 20 weeks old were used for T cell extraction. Naïve CD8+ T cells were purified from spleens using the EasySep mouse CD8+ T cell Isolation Kit (Stem Cell Technologies). Briefly, spleens were disrupted in PBS and cell suspension was then filtered through a 70 µm cell strainer. Erythroid cells were eliminated by incubation with red blood cells lysis buffer (eBioscences). Cells were incubated with a cocktail of antibodies that target non-CD8+ T cell followed by a second incubation with streptavidin-coated magnetic beads. Cell suspension was placed in an Easysep magnet and negative selection of CD8+ T were then performed by collecting cell suspension in a new tube.

6.2.2 EG7 cell culture

EG7 cells were maintained in RPMI 1640 supplemented with 10% (v/v) heat-inactivated fetal bovine serum (FBS), 50 µM β-mercaptoethanol, Penicillin-Streptomycin (all from Gibco, Switzerland) and 400 µg/ml G418 (Brunschwig). Cells were then cultured in an incubator at 37°C and 5% CO2.

6.2.3 EG7 irradiation dose titration

EG7 cell suspension were washed and place in Eppendorf tube at a concentration of 10^6cells/ml in PBS. Tubes were placed in a gamma irradiator and exposed to different doses as follow: 0, 10, 30, 40, 50, 60 and 70 Gy. To assess proliferation of EG7 post-irradiation, cells were stained with cell trace violet (CTV, Thermofisher) following manufacturer's information and then cultured in round bottom 96-well plates. Cells were harvested every 24h, stained with propidium iodide (PI, Thermofisher) and analyzed on a LSR Fortessa flow cytometer (Becton Dickinson).

6.2.4 Activation of OT-I CD8+ T cells and analysis

Freshly isolated CD8+ T cells from OT1 mouse were stained with CTV and co-cultured with irradiated EG7 (40Gy) cells at a ratio of 1:2. Cells mix was cultured in round-bottom 96-well plates in "activation medium" made of RPMI 1640 supplemented with 10% (v/v) heat-inactivated fetal bovine serum (FBS), 50 µM β-mercaptoethanol, Penicillin-Streptomycin (all from Gibco, Switzerland), 50U IL-2. Every 24h, cell mix was harvested stained with anti-CD8-Bv650, anti-CD44-APC-Cy7, anti-CD62L-FITC, anti-CD27-PerCPCy5.5, and anti-CD69-PE (all from Biolegend), PI and analyzed on LSR Fortessa cytometer (Becton Dickinson).

6.2.5 Time-lapse imaging

For the study of immunological synapse, freshly isolated CD8+ T cells and irradiated EG7 cells (40Gy) were mixed at a concentration of 10^5 cells/mL at a ratio of 1:1 and cultured on the micro-groove platform (Trachsel et al., Submitted) (in activation medium). Brightfield images were captured every 30mn on a Zeiss Axio Observer microscope using a 10x air objective.

For the study of CD8+ T cell progeny, freshly isolated CD8+ T cells and irradiated EG7 cells (40Gy) were mixed at a concentration of 10^5 cells/mL at a ratio of 1:1 and cultured for 18h (in activation medium). Cells were then seeded onto a micro-groove array platform (Trachsel et al., Submitted) and cultured for 1 day in activation medium containing 150U IL2. Brightfield images were captured every 30mn on a Zeiss Axio Observer microscope using a 10x air objective. Alternatively, for fluorescent imaging a Nikon Ti microscope were used. Anti-CD8a conjugated to AF647 (BioLegend) and CD62L-AF488 (BioLegend) were added to the culture medium. Z-stack images were acquired prior and after cell divisions at 60x.

6.2.6 Image analysis

Sum of pixels value of z-stack images were calculated to obtain the total protein expression of a cell. Image analysis was performed with ImageJ.

6.3 Result and discussion

In the present study, we explored a new methodology that enabled not only the study of the immunological synapse between a naive CD8+ T cell and an APC, but also an analysis of the progeny derived from the T cell after its activation. In contrast to standard *in vitro* culture where it is not possible to follow the progeny of T cell due to cell movement or cell cycle inhibitors, here, we used a platform that confined the cell in micro-groove (Figure 6.2A) (Trachsel et al., Submitted). Cells were encapsulated and restricted to move and grow along one axis, which prevented cells from interchanging their position with other cells. By selecting grooves containing one APC and one T cell, we first showed that the immunological synapse can be studied (Figure 6.2B) and then demonstrated using fluorescent immunostaining that protein expressions comparison could be achieved between different generations of cells or between sister cells (Figure 6.4). To promote T cell activation in our system, we used naive CD8+ OT1 TCR-transgenic T cells (OT1) that are specific for ovalbumin peptide (OVA), and, as APC, we selected OVA-transfected cell line, namely, EG7, which synthetizes and secretes OVA[212,213]. EG7 cells are derived from the T-cell lymphoma EL-4. Professional APC such as dendritic cells (DCs) may not have been used to activate OT1 as DCs are very motile, adherent and, more importantly, much larger than T-cell. To encapsulate DCs, the groove width must have been increased to the extent that the T cell would not be constrained and might freely move in all directions, leading to ambiguous tracking.

6.3.1 CD8+ T cell activation with EG7

Previous studies have demonstrated that EG7 cells can directly present OVA to OT1, which in turn activate them in the presence of IL2[212,214]. Nevertheless, to establish it in our system, we co-cultured cells to assess whether OT1 can be efficiently activated by EG7 cells. Activation markers (i.e. CD69, CD27 and CD8) were up regulated after the co-culture (Figure 6.1C and Supplementary Figure S6.1) with a concomitant cell proliferation and cell size increase (indicated by dilution of CTV and FSC profile, Figure 6.1A-B). This indicated that OT1 were already activated after 24 h of co-culture[209,215]. The CD8 expression was proposed as an asymmetric marker that can help distinguish the effector (CD8 high) and memory (CD8 low) lineages after the first division is Linked to CD8 high cell. The expression of CD69, CD27 and CD44 should also be upregulated and that of CD62L downregulated. In contrast, the CD8 low cells are CD69, CD27, CD44 low and CD62L high[206,208]. We wondered if we could replicate this observation using our system (Figure 6.1D). In line with the above description, we observed that the CD8 high population exhibited more effector-like phenotype than CD8 low due to an up-regulation of CD69, CD27 and CD44. However, a notable exception was the presence of CD62L (Figure 6.1) on CD8 high cells, which is a marker of memory T cells, an observation that is different from that of Chang et al.'s and others[208,216]. One possible explanation for this result is that Chang et al. used another protocol that involves *in vivo* CD8+ T cell activation and not *in vitro*, like in our study. The differences of protein expressions between CD8 low and CD8 high were not seen on non-activated cells (Supplementary Figure S6.2), which confirmed that a difference in marker expression is induced upon EG7 mediated activation and not already present in freshly isolated naive T cells. Overall, these results suggested that OT1 were activated by EG7 cells and that asymmetric divisions occurs; yet, the presence of CD62L on CD8 high cell also indicated that daughter cells after the first divisions are probably different in our approach than the ones of Chang et al.[206]

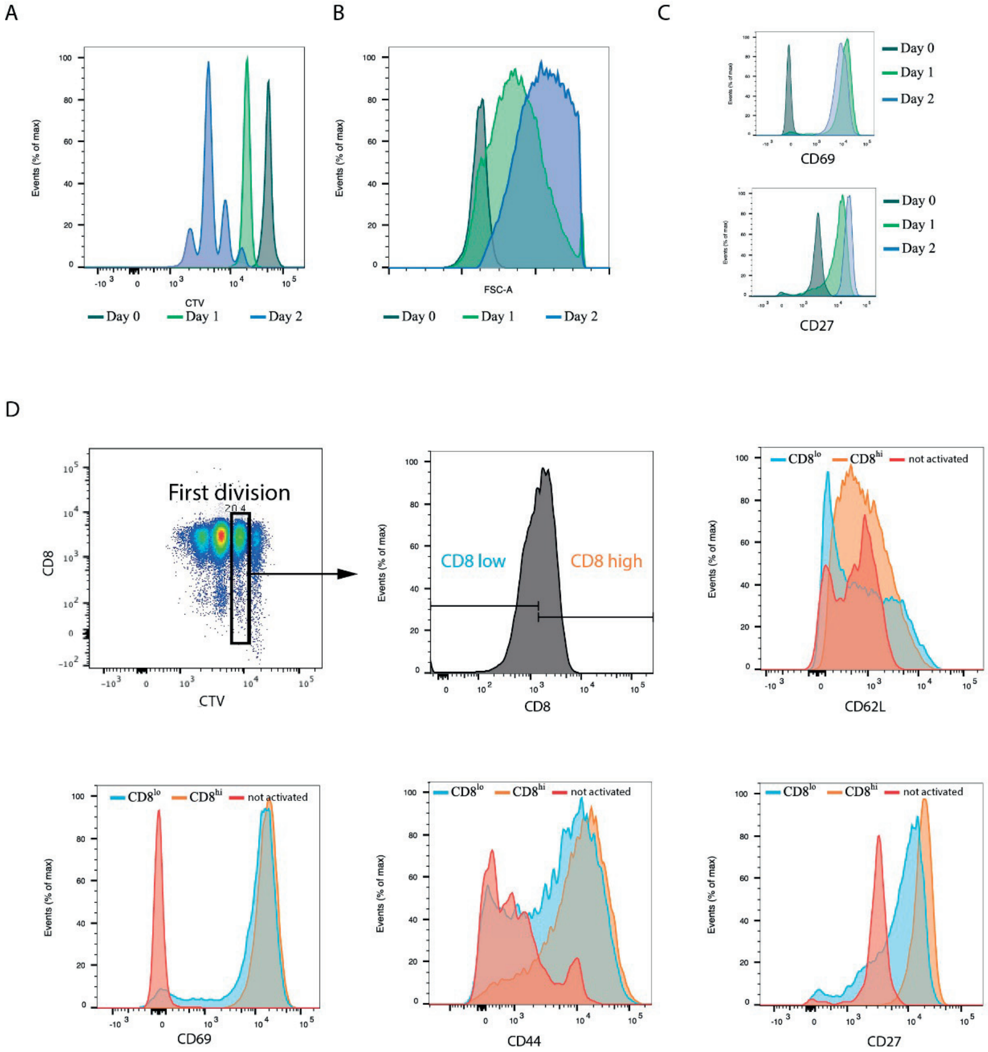

Figure 6.1: *In vitro* activation of OT1 CD8+T cell by EG7 cells. (A) CellTrace violet dilution of OT1 cells on day 0, 1 and 2 post co-culture with EG7. (B) Forward side scattering (FSC) profile of OT1 on day 0, 1, and 2 post co-culture with EG7. (C) Activation marker levels on day 0 (undivided cells),1 and 2. (D) Activated OT1 cells that divided one time were sub-fractioned in CD8 low and high populations and analyzed with CD62L, CD69, CD44 and CD27. Control is not activated in OT1 cells.

6.3.2 EG7 and OT1 culture on the micro groove platform

EG7 and OT1 cells were seeded on the micro-groove platform and observed by time-lapse microscopy (Figure 6.2). In general, the OT1 cells, alone or in multiple numbers, had very low viability in the absence of EG7. A possible explanation for this is that in contrast to standard well culture where the cells are touching each other, the cells here are spatially separated and probably suffer from a lack of signals that induce apoptosis (Figure 6.2C(3)). Although cell death was decreased when OT1 were in the presence of EG7, we still observed occasional cell death in these grooves (Figure 6.2C(1)-(2)). To observe immunological synapse, we selected grooves that contained one single OT1 and

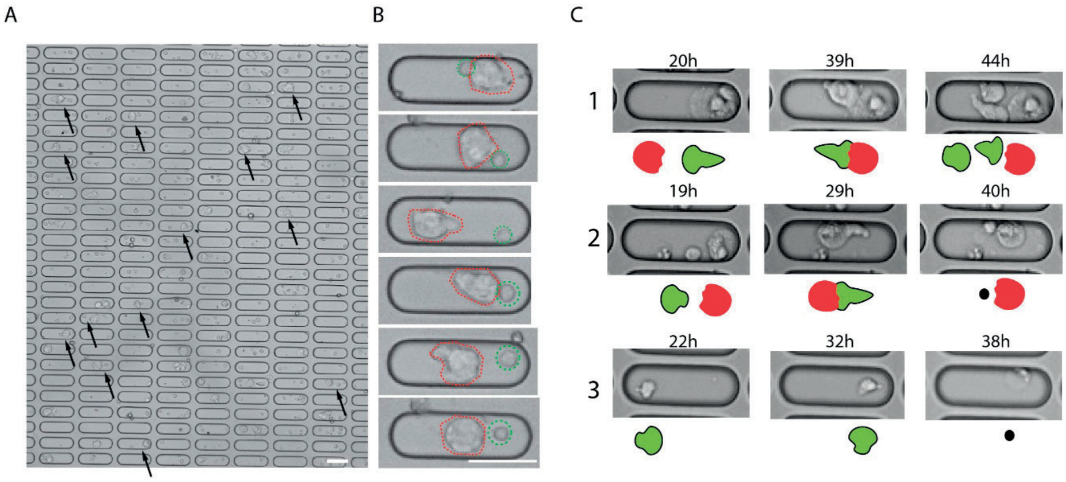

Figure 6.2: OT1 and EG7 cells co-culture in micro-groove array. (A) Micro-groove with OT1 and EG7 cells. Black arrows indicate groove containing one single cell of each type. (B) Representative example of groove filled with one EG7 (bigger cells in the red circle) and one OT1 (smaller cells in the green circle) cells. (C) Representative fate of OT1 in the groove, (1) OT1 cell doing an immunological synapse with one EG7 and proliferating, (2) OT1 with one EG7 but dying, (3) single OT1 dying. OT1 cells are depicted in green in schemes and EG7 in red. Scale bar = 25um

EG7 cell (Figure 6.3A-B) where the OT1 gave rise to two daughter cells (ensuring that the OT1 cells were activated).

We observed two modes of interaction between cells: a continuous (Figure 6.3A) and an intermittent contact (Figure 6.3B). These modes were already defined by Dustin et al. who proposed to call them as “immunological synapse” (continuous mode) and “immunological kinapse” (intermittent mode)[217]. After the synapse, the T cell divided and increased in size, indicating that they were activated[218].

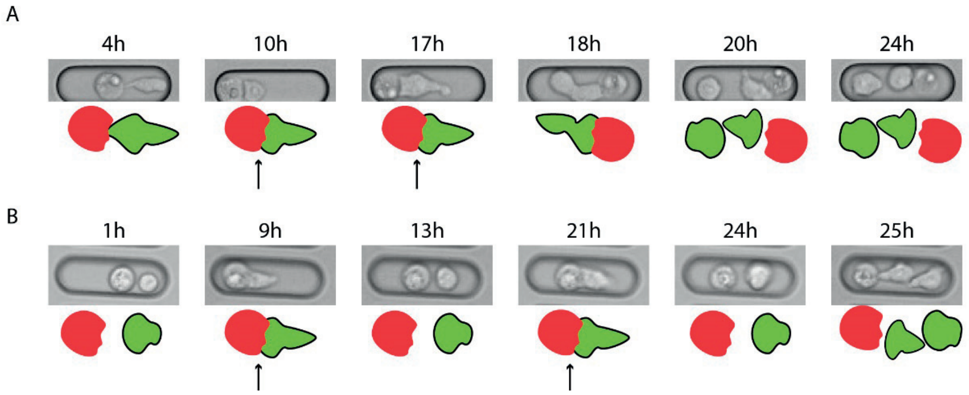

Figure 6.3: Representative images showing two different types of interaction between OT1 and EG7. (A) immunological synapse and (B) immunological kinapse (ON/OFF interaction) as defined by Dustin et al.[217]. Black arrows show the images where interactions occurred.

6.3.3 Analysis of asymmetry between daughter cells

To assess the asymmetric protein distribution between daughter cells upon T cell activation and division, we estimated the CD8 expression by antibody staining on live cells[102] (Figure 6.4). We selected CD8 as it is an established marker of asymmetric division for CD8+ T cell[206]. It is important to note that due to the massive cell death observed when OT1 and EG7 were directly placed on the tracking platform, here, we first co-cultured EG7 and OT1 in a standard cell culture plastic well plate overnight to provide better activation. We obtained 7 grooves through which we were able to track cells up to the second generations (Figure 6.4). We defined the first generation as pair daughter cells (PDCs) and the second generation as cousin cells. Cousin cells are, therefore, two pairs of sister cells (Figure 6.4B). We compared the CD8 distribution asymmetry of sister cells between these two generations and found that cousin cells exhibit significantly higher level of asymmetry than PDCs (Figure 6.5A). To assess if the CD8 expression level of the PDCs can influence the CD8 distribution asymmetry of cousin cells, we classified the cousin cells according to the CD8 expression of their mother cells (i.e., first generation cells) (Figure 6.5B). However, due to a large variability, we did not find the expression to be significantly different (Figure 6.5B). Finally, to see whether the first generation daughter cell that has a higher expression of CD8 produces more asymmetric second generation daughters, we compared the asymmetries of cousin cell pairs based on the CD8 expression of PDCs (first generation daughters) (Figure 6.5C). We found that the CD8 low first generation daughter cell produces cousin cells that have a significantly more asymmetric distribution of CD8 when compared to their respective CD8 high sister. Overall, our results are intriguing as they provide new information on T cell asymmetry. Firstly, Verbist et al. showed through FACS analysis that the two populations of CD8 high and CD8 low found after the first divisions dissipated after subsequent divisions[206,208], but the sister cell CD8's protein asymmetric distribution was never assessed. Here, we found that the second generation of cells exhibited more asymmetric CD8 distribution than the first generation. Another contrasting observation to the current dogma is how the daughter cell with low CD8 expression produces more asymmetric cell division[208]. Although still preliminary, we believe that these contradicting observations could arise from the use of non-standard plate culture conditions. The optimization of precise culture conditions in cell grooves will be needed in the future. Further analysis with more cell numbers would be needed to draw reliable conclusions from this methodology. However, to our knowledge, this is the first attempt to track T cell fate over several generations using *in vitro*.

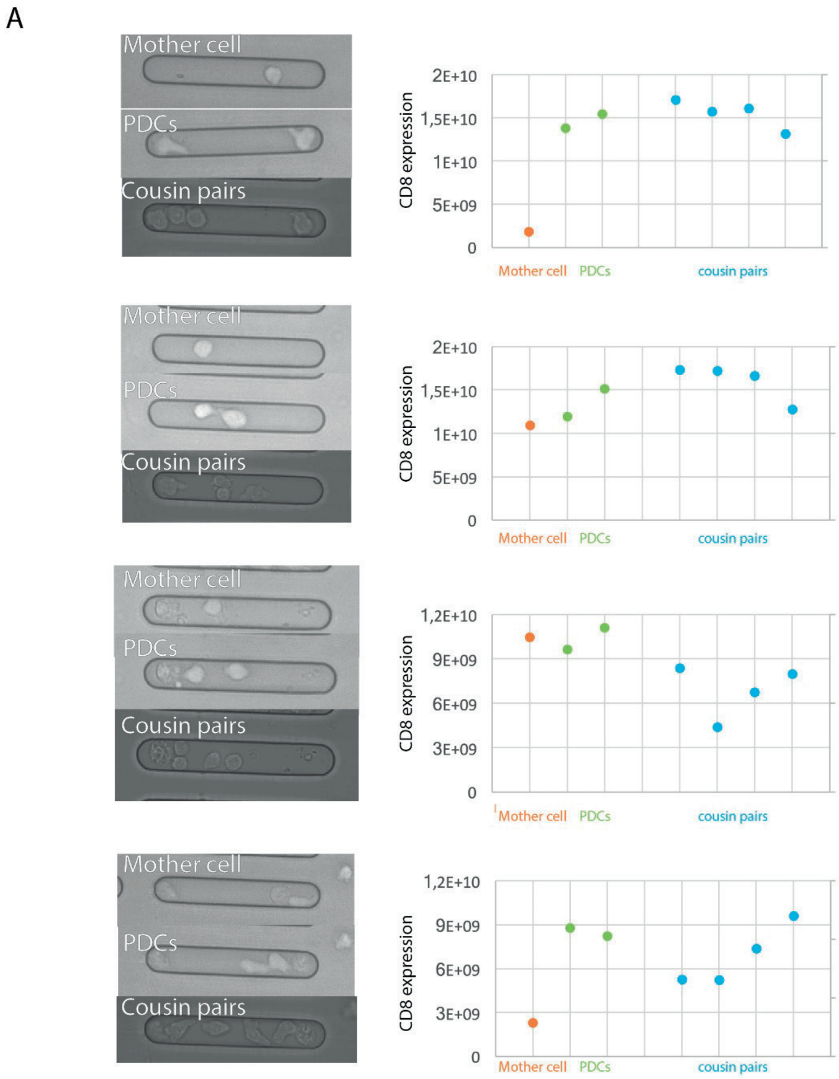

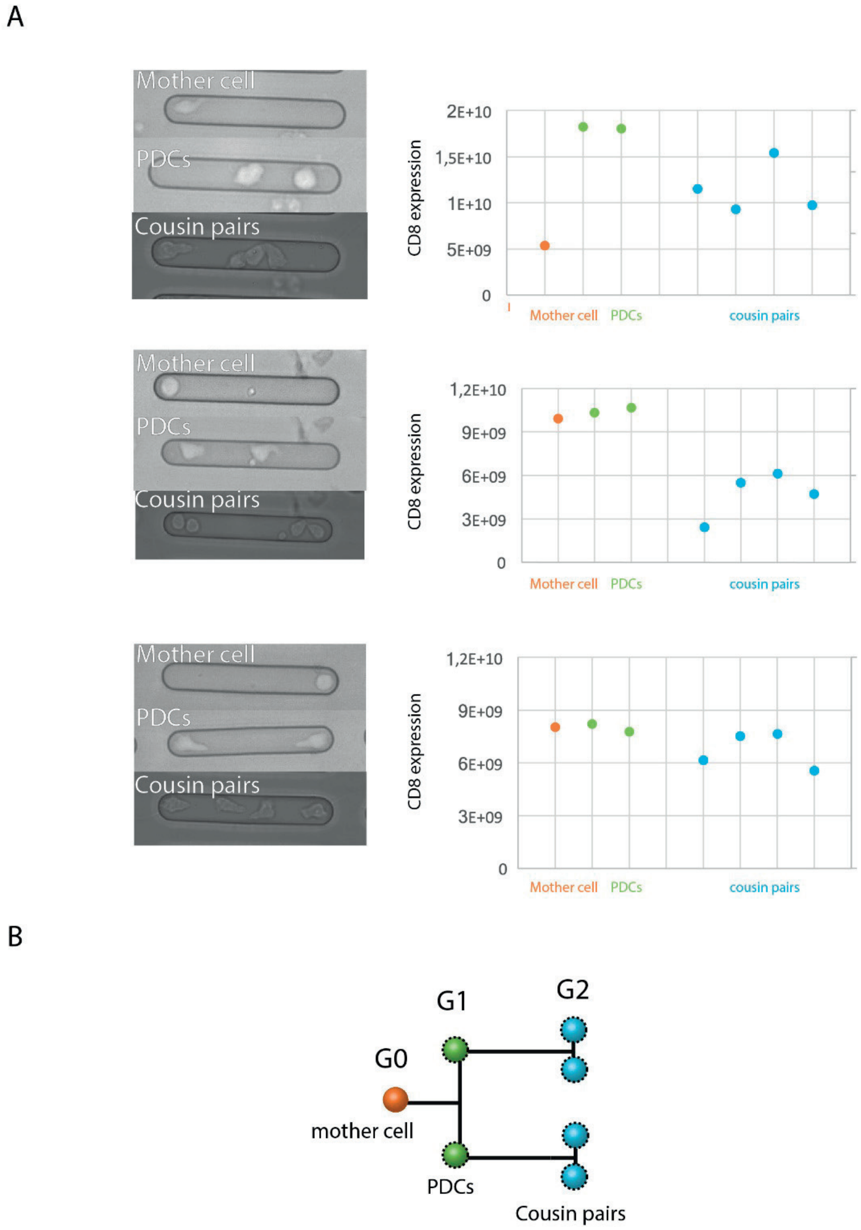

Figure 6.4: CD8 protein expression in OT1 cell lineages. (A) OT1 cells were co-cultured with EG7 for 24 h and placed on the micro-groove array platform. Single OT1 lineage were tracked (images on the left) and CD8 protein expression was measured for the mother, PDCs and cousin cells (Graphs). (B) The scheme demonstrates how sister cell pairs are defined.

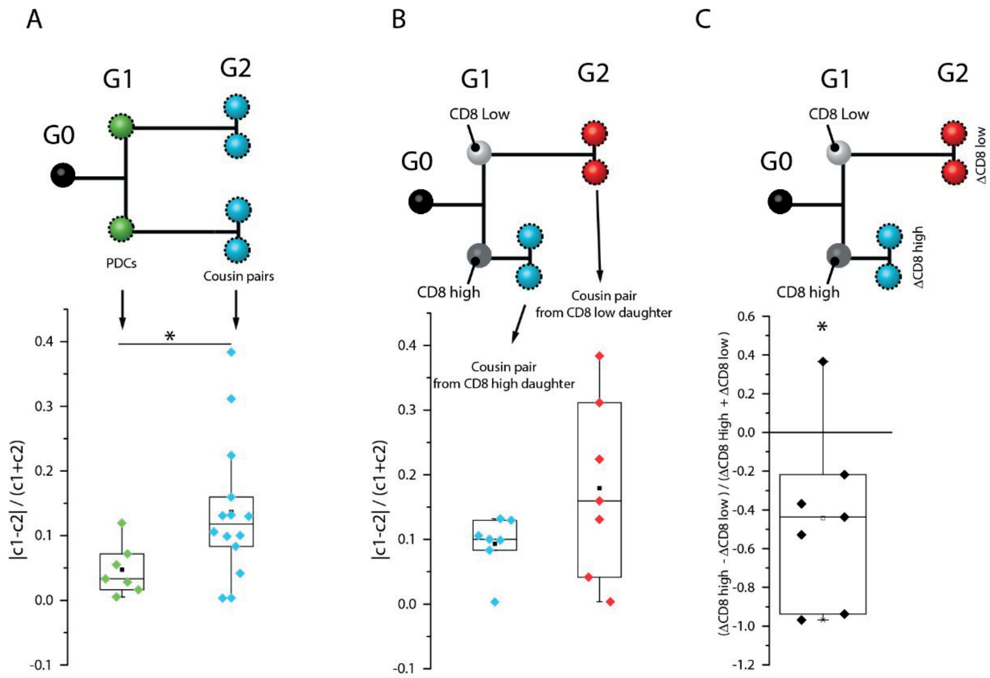

Figure 6.5: CD8 asymmetry in PDC and cousin cell pairs. (A) A comparison of CD8 asymmetry between PDC (green) and cousin pairs (blue). Statistical analysis is performed by Student t-test: *p<0.05 (B) Comparison of cousin pairs derived from a daughter with high CD8 expression (blue) or low CD8 expression (red).(A)-(B) Asymmetry in sister cells is calculated as follows $|c_1 - c_2|/(c_1 + c_2)$, where c_1 and c_2 represent the sister cell values. (C) The difference of asymmetry of cousin pairs derived from a CD8 high or CD8 low mother. $\Delta CD8\ high = |c_1 - c_2|$, where c_1 and c_2 represent the sister cell values derived from the CD8 high daughter cells and, similarly, $\Delta CD8\ low = |c_3 - c_4|$, where c_3 and c_4 represent the sister cell values derived from the CD8 low daughter cells.

6.4 Conclusion

With limited technical expertise available in the field to study immunological synapse and T cell progeny at the single cell level *in vitro*, we attempted to establish a method that is aimed at enabling the analysis of cell interaction between a CD8+ T cell and an APC combined with a lineage tracking. We successfully showed the occurrence of two types of interactions between OT1 and EG7—namely, the immunological synapse and kinapse. Furthermore, we demonstrated that in addition to reliable tracking, protein expression analysis could be performed with our method for up to two divisions. However, the viability of OT1 EG7 cocultures was surprisingly low in our platforms; thereby restricting high throughput analysis. One way of obtaining better survival rates could be to seed more EG7 cells ensuring that each groove contains multiple EG7 cells. We think that our method can be further optimized to yield reliable results on T cell fate tracking *in vitro*. Thus, although preliminary, our method is the first step towards a high-throughput analysis of T cells and their lineages.

6.5 Acknowledgements

We thank Nicola Vannini and Marcela Restrepo for providing OT1 cells and for the excellent discussions. We also thank Abla Benabderrazik for the help provided during the experiments.

Supplementary Information for Chapter 6

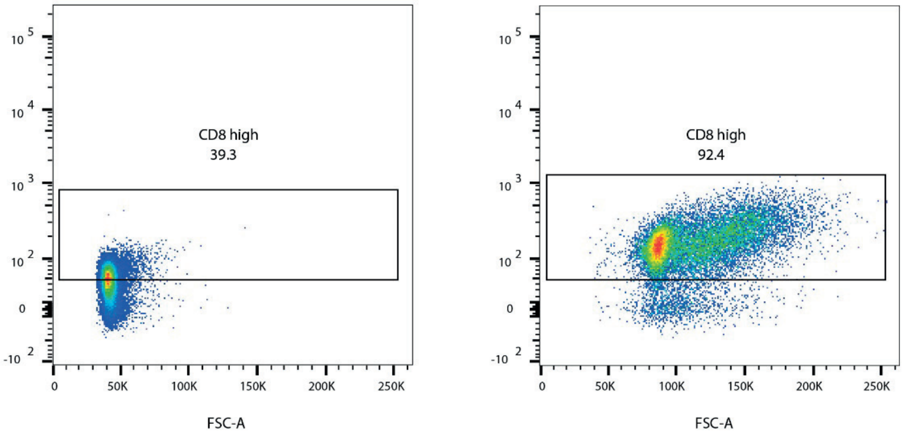

Figure S 6.1: Augmentation of CD8 expression after OT1 activation by EG7.

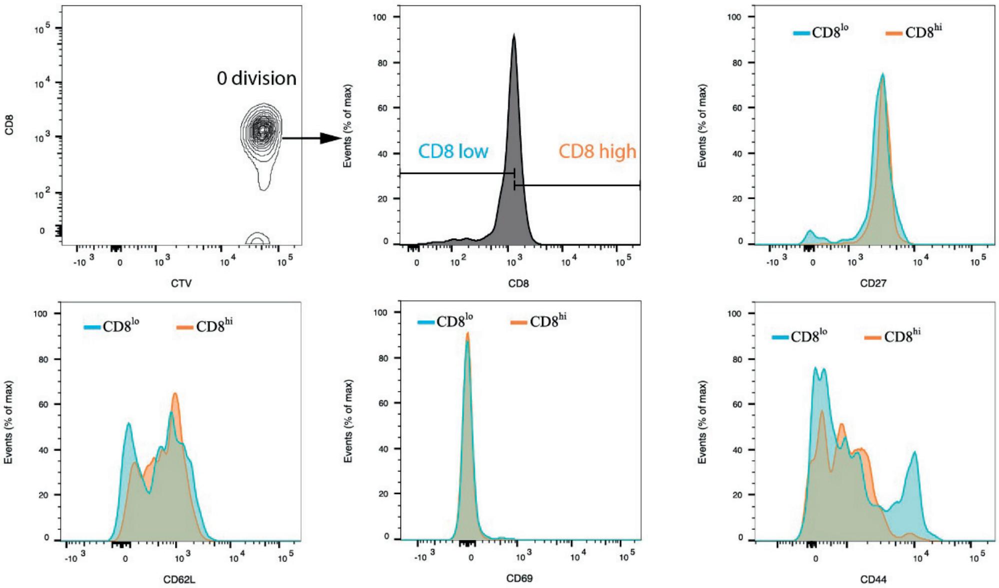

Figure S 6.2: Non-activated OT1 cells staining shows no difference between CD8high or CD8low cells.

Chapter 7 General discussion and outlook

For a better treatment of blood disorders, the number of HSCs must be expanded *in vitro*. However, the culture of HSCs is currently facing major problems due to the rapid loss of their functionality brought about by cell differentiation after initial divisions. This limits the usage of HSCs in regenerative medicine. In addition, freshly isolated HSCs once in culture either progressively lose their initial markers or become unreliable in the identification of functional HSCs[37]. This PhD thesis presents new methodologies using micro-technologies as a means to improve the analysis of HSCs *in vitro*.

7.1 Technological development (Chapters 2 and 3)

Current techniques only permit lineage tracking of extremely robust cells with the additional prerequisite of starting with a large number of cells (i.e. 20,000–50,000) [82,89,105]. Moreover, these platforms do not necessarily allow immunofluorescence staining on cell progenies. This is a major limitation to the detection of markers that could potentially allow the identification of distinct cell lineages.

In the first section of the thesis, a platform was developed to enable the high-throughput lineage tracking of primitive HSCs (chapter 2) with the possibility of conducting downstream analysis like immunostaining. The key difficulties to be solved during this task was the adoption of a methodology for (1) reliable and gentle single cell capture, (2) unambiguous cell lineage tracking and (3) immunofluorescence staining without the risk of flushing/mixing the cells. To achieve our aims, we designed a hybrid platform composed of two different hydrogels that can be bonded together upon cell seeding. The bottom layer was made of poly (2-hydroxyethyl methacrylate)-trimethylolpropane trimethacrylate copolymer (pHEMA-TMPTMA) and the top layer was made in a self-assembling poly(ethylene glycol) (PEG). The combination of these two different hydrogels permitted the encapsulation of single cells into grooves in a very gentle. Due to the porousness of the PEG-lid, nutrients reached the cells passively. For the same reason, we were able to perform immunostaining in order to quantify protein expression at the single cell level in different lineages.

The viability of HSCs cultured on the platform was the same as a conventional cell culture plate. We were therefore able to successfully culture HSCs, overcoming a major challenge that has plagued other state-of-the art devices. In contrast to previous approaches that require extensive tubings, micro-pumps and other expensive instruments to achieve cell progeny tracking, the platform presented here is not based on fluidics and is user friendly. It relies only on gravity to trap single cells inside closable microgrooves. The platform can be modified to track the progeny of other cell types, and the length of the grooves can be readily extended for longer-term cell tracking. Finally, we showed the proof-of-concept possibility of modification of the cell-contacting surface of the hydrogel with the protein molecules. Such surface modifications can be used to influence the fate of cultured cells via numerous bioactive cues. To our knowledge, this platform is the first successful attempt that allows the culture of the most primitive HSCs combined with the aforementioned requirements. To cope with the amount of data generated during time-lapse microscopy, we implemented a tracking algorithm designed for the detection and tracking of HSCs (Chapter 2). Our algorithm provided robust and efficient cell detection, while the average error in cell tracking accuracy was only 0.03 per 100 images. We demonstrated the usability of this tool for practical biological applications by analyzing the behavior of HSCs, exposed to three different drugs.

7.1.1 Suggestion for the enhancement of the current platform

The platform is closed with a PEG-lid after cell seeding. Although the platform closing is efficient, this procedure can be further optimized by implementing a more automatic closure protocol (i.e. deposition of the lid on the groove) that is not user-dependent. This procedure demands practice before being optimal. By the human hand, it is not possible to control the exact pressure that one exerts on the lid when closing the platform resulting in excessive pressure and in an increased possibility of cell-death. A simple tool made of a mechanical arm that would carry the lid and gently deposit it on the platform, for example, would permit a more reproducible closure. The aforementioned tool could address this limitation by applying constant pressure and in a more homogenous manner over the lid.

Lecault et al. developed a platform for *in vitro* HSCs' culture combined with a system that permitted the automated medium exchange (platform described in the introduction of this thesis). This platform permitted the identification of the time-window where HSCs are responsive to steel factor[79]. Change of media (i.e. media perfusion) is therefore a technical improvement that could be beneficial to the current groove-platform described in this thesis. This technology will offer another level of analysis to identify when cells are more responsive to cytokines and if combined with live-immunostaining[102], we could determine how cytokines are linked to the (dis)appearance of hematopoietic cell surface markers (e.g. CD34, CD48, CD150, Tie2, ckit, sca1[14,15,189]) or to metabolism.

An extremely useful read-out that could be targeted with this platform would be to assess the long-term potency of cultured HSCs by transplanting them into an irradiated recipient. To achieve this, single cells should be harvested from the platform through micromanipulation using microcapillaries. This approach is known to yield a low throughput but offers the precision required for single cell transplantations. Alternatively, this method could be used to study the gene expression of entire lineage of HSCs. Every time a cell divides, one daughter is harvested and its RNA would be sequenced. Difference of gene expression could be therefore quantified during HSCs' *in vitro* culture. An issue of practical interest is that the lid could potentially clog the needle of the microcapillary since it is made of a soft hydrogel. Hence, the operation of single cell micromanipulation should be first optimized.

7.2 Biological experiments (Chapters 4 to 6)

The aim of the platform (described in chapter 2) was to allow the tracking and analysis of HSC progenies. We demonstrated this concept by analyzing the protein expression for all cells generated during culture from freshly isolated murine HSCs. To observe distinct lineages arising from an asymmetric division (AD), we calculated the difference of protein expression between daughter cells of the first generation and combined this information with the temporally asymmetric divisions (i.e. asynchronous divisions). Since asynchronous division is a phenomenon associated with asymmetric cell divisions[129], we were able to locate proteins that are asymmetrically distributed during asymmetric division. This strategy is the first step towards the finding of reliable markers defining HSCs cell lineages *in vitro*.

In the following chapters of this thesis, we used the platform to study asymmetric protein (or organelles) distribution between sister cells. Asymmetric division is a process that is well-established for stem cells where one daughter proliferates and differentiates whereas the other daughter remains identical to the mother (maintaining the stem cell pool)[203]. Consequently, AD is the most relevant cell fate choice under homeostasis [170].

7.2.1 Chapter 4 "Monitoring of mitochondrial mass of HSCs in culture"

In chapter 4, we used a genetically modified mouse line that expresses enhanced green fluorescent (GFP) protein in mitochondria to measure mitochondrial mass and its distribution in daughter cells. Our experiments revealed the existence of a specific distribution mechanism that segregates mitochondria preferentially to one of the daughter cells during an asymmetric division. These results further support the contention that HSC fate is tethered to the mitochondria[161].

Using the same assay, an investigation can be carried out to distinguish whether mitochondrial mass distribution during asymmetric division is also linked to the difference in metabolic activity of these mitochondria. This experiment is performed in a serum-free medium supplemented of two cytokines (SCF and Flt3l, basal medium). Supplementation of IL3 and IL6 to the basal medium would lead to a decrease of asynchronous divisions and rapid proliferation associated to lineage commitment of HSCs *in vitro*[42,129]. Therefore, it would be interesting to see how mitochondrial mass is distributed during these symmetric commitment divisions.

7.2.2 Chapter 5 "Analysis of asymmetric markers in the first generation of cells derived from murine HSCs"

In chapter 5, we report a strategy to analyze the asymmetric expression of genes and proteins during AD. We used IFNa to promote the exit of HSCs out of their dormancy in their *in vivo* niche[174]. Thereby, dividing HSCs were "pre-instructed" in their *in vivo* environment. This is a major advantage provided by our method as HSCs in the absence of the right cues from the *in vivo* niche rapidly differentiate *in vitro*. This experiment provided numerous insights for HSCs phenotypic characterization *in vitro*. Our single cell gene expression analysis in paired daughter cells (PDCs) allowed the identification of an asymmetric gene set. Among them were some genes that have been described in the literature to be important for HSC identification such as CD150[13], Tie2[197] and JAM3[50,192]. Interestingly, Tie2 (receptor of Ang1) has been previously used as an asymmetric marker[51]. We also identified some metabolic genes such as Glucose transporter 1 (Glut1), Hexokinase 2 (HK2) and Aconitase 1 (Aco1) in highly asymmetric PDCs. We further explored the maintenance of this asymmetry at the level of protein expression. Protein analysis revealed significantly higher asymmetric protein expression in three candidates, namely Glut1, JAM3 and HK2, suggesting maintenance of asymmetry post-translation.

Our functional analysis using CFUs revealed Glut low JAM3 high to be the most primitive subset in culture. This is in line with previous reports showing lower Glut1[175] and high JAM3[50] in functional HSCs. Further *in vivo* functional assays should be undertaken to confirm that asymmetry at the protein level corresponds with the asymmetric fate of daughter cells. We believed that this experiment could be used to further characterize daughter cells during an asymmetric division in the future.

7.2.3 Chapter 6 “Fate analysis of CD8+ T cell at the single cell level”

A host organism mounts a well-orchestrated immune response upon microbial infection. Cytotoxic T lymphocytes (CD8+ T cells) are an important arm of this immune response and generate various subsets to protect the organism against the pathogen. It was recently shown that these different T cell subsets, namely the effector and memory cells, emerge from a common CD8+ T cell ancestor. In chapter 6, we attempted to establish a new methodology to observe and analyze T cell lineages at the single cell level. The primary aim was to observe the process of T cell activation and proliferation with its activation by an antigen presenting cells. We successfully observed two types of interactions between a T cell and an antigen presenting cells—the immunological synapse and kinapse. Furthermore, we also demonstrated that in addition to reliable tracking, protein expression analysis could be performed with our method for up to two divisions.

In the frame of this thesis, this experiment provided the proof that a co-culture can be achieved on the tracking platform and in the frame of a T cell. Our analysis further supports that the first initial division of T cells are asymmetric. In this last experiment, a few points can be optimized to yield more reproducible results. (1) The culture method should be optimized to provide a better cell viability on the platform. (2) Analysis of asymmetric protein expression after the second division should be carried out to investigate whether asymmetric division still occurs in subsequent division. (3) Other markers apart from CD8 should be used to more precisely characterize the difference between daughter cells. To achieve this aim we suggest starting with genes that were observed to be essential for asymmetric division of T cell, such as the Atypical protein kinase C (aPKC), Par3, Scrib and DlgF[208,209,211,219]. Moreover, a metabolic profiling of daughter T cells would surely provide interesting insights. In contrast to stem cells and in particular HSCs, where quiescent cells are marked by low mitochondrial mass[50,220], it was proposed that dormant memory T cells exhibit elevated mass of mitochondria while highly proliferating effector T exhibit low mitochondrial mass[221].

7.3 Future biological application

The number of experiments conducted to understand mechanisms underlying stem cell fate decisions using the platform developed in this thesis is infinite. The following sections include recommendations for further experiments to help develop a better understanding of cell fate decisions.

7.3.1 Mouse and human HSCs

For future studies with our platform, an obvious experiment to undertake would be to combine lineage tracking of HSCs when cultured in the presence of other cell types—typically, cells from the hematopoietic niche. *In vivo* observation of niche-cell interaction with HSCs followed by HSCs lineage tracking is currently not possible to implement[19]. However, *in vitro* co-culture of HSCs with niche cells can be undertaken with our platform to decipher mechanisms influencing HSCs’ fate after cell-cell interaction. Interestingly, bulk co-cultures in conventional plate have been performed with osteoblast and mesenchymal stem cells and already demonstrated exciting results for ex-vivo HSCs’ expansion[222–225]. Co-culture combined to further assays (i.e. immunostaining, qPCR), would permit a better characterization of key proteins involved in the niche and in the fate decision of HSCs. In chapter 5 of this thesis, we pointed out that the cell-cell protein JAM3 is expressed in the most primitive cells in culture[191] and can be used to identify HSCs *in vitro*. In the *in vivo* niche, JAM3 (expressed by HSCs) interacts with JAMB on bone marrow stromal cells[191]. Therefore, it would be extremely interesting to culture HSCs with genetically modified bone marrow stromal cells expressing less/more JAMB and to observe how this molecule changes HSC fates *in vitro*.

In addition to the co-culture experiment, relevant protein candidates of the extra-cellular matrix of the niche could be tethered in the grooves, as we have shown in chapter 2. Therefore, the next generation of the groove platform should facilitate the exposure of HSCs to “artificial niches” to find how protein in the niche can modulate HSC fate choices[120,129]. Such experiments were already performed but never in the context of entire lineages[120]. To achieve this, the protocol that was developed in chapter 2 should be adapted so that the platform can be still closable even in the presence of molecules on the groove-surface.

During this thesis, we primarily focused on the characterization of murine HSCs but we still do not know whether these results could be applied to human HSCs. A typical example of the difference between murine and human HSCs is the presence or absence of CD34 respectively on human and murine HSCs[190,226]. We think that the observation of human HSCs on the platform could be extremely interesting and straightforward with direct impact at the clinical level.

7.3.2 Suggestion of studies with other stem or tumor cells

Although the focal point of this thesis was the study of HSCs, the platform is not restricted to these types of cells. For example, the approach that was described in chapter 4 can be expanded to assess the pluripotency in progenies of other stem cells by using fluorescent reporter genes such as Lgr5 for intestinal stem cells[227], Nanog for embryonic stem cells[228] or induced pluripotent stem cells (iPS cells)[229]. Moreover, the progeny of stem cells can be stained on the platform to test the presence of other stem or lineage commitment markers. Similarly, the exact mechanisms of OCT4, SOX2, KLF4, c-MYC occurring during the reprogramming of somatic cells into iPS cells could be observed on the platform. Meanwhile, the cooperation of factors to reshape the epigenome and gene expression profile of somatic cells could be elucidated [230].

Tumor cells are highly heteregenous[231] but current therapies treat cancer as a homogeneous disease which often leads to an incomplete healing. Defining the pathways through which tumors progress in the presence of drugs could lead to a better characterization of these cells and would ultimately allow us to find new ways to treat cancer[232]. However, so far cancer cells are mostly studied by micro-array and flow cytometry technologies where the genealogical relationships of cells are lost. Therefore, we are still missing the exact mechanism underlying drug resistance of cancer cells. The platform presented in this thesis could address these limitations and permit the characterization of cancer development *in vitro*.

However, it should be noted that the bottom layer of the platform should be modified if other cell types are used. First, the width of the grooves must be scaled to fit the dimension of each cell type. The length of the grooves can be also modified depending on the number of cells of the progenies. For the analysis of adherent cells, moreover, a method to coat the platform to prevent cells’ adhesion has to be investigated. To achieve this, I propose the usage of a nonfouling polyethylene glycol-like film. Without this treatment, cells might escape from the groove even in the presence of the lid and might be difficult to track unambiguously.

References

1. Osawa, M., Hanada, K., Hamada, H. & Nakauchi, H. Long-term lymphohematopoietic reconstitution by a single CD34-low/negative hematopoietic stem cell. *Science* **273,** 242–5 (1996).

2. Farahbakhshian, E. *et al.* Angiopoietin-Like Protein 3 Promotes Preservation of Stemness during Ex Vivo Expansion of Murine Hematopoietic Stem Cells. *PLoS One* **9,** e105642 (2014).

3. Pietras, E. M., Warr, M. R. & Passegué, E. Cell cycle regulation in hematopoietic stem cells. *J. Cell Biol.* **195,** 709–20 (2011).

4. Kaushansky, K. Cell expansion and maintenance of stemness. *Blood* **111,** 4–5 (2008).

5. Mendelson, A. & Frenette, P. S. Hematopoietic stem cell niche maintenance during homeostasis and regeneration. *Nat. Med.* **20,** 833–846 (2015).

6. Weissman, I. L. Translating Stem and Progenitor Cell Biology to the Clinic : Barriers and Opportunities. **287,** 1442–1447 (2000).

7. Domen, J., Wagers, A. J. & Weissman, I. L. Regenerative Medicine 2006. *Natl. Institutes Heal.* 1–106 (2006).

8. Christensen, J. L. & Weissman, I. L. Flk-2 is a marker in hematopoietic stem cell differentiation: A simple method to isolate long-term stem cells. *Proc. Natl. Acad. Sci.* **98,** 14541–14546 (2001).

9. Morrison, S. J. & Weissman, I. L. The long-term repopulating subset of hematopoietic stem cells is deterministic and isolatable by phenotype. *Immunity* **1,** 661–673 (1994).

10. Xie, J. & Zhang, C. Ex vivo expansion of hematopoietic stem cells. *Sci. China Life Sci.* **58,** 839–853 (2015).

11. Crane, G. M., Jeffery, E. & Morrison, S. J. Adult haematopoietic stem cell niches. *Nature Reviews Immunology* **17,** (2017).

12. Moore, K. a & Lemischka, I. R. Stem cells and their niches. *Science* **311,** 1880–1885 (2006).

13. Kiel, M. J. *et al.* SLAM family receptors distinguish hematopoietic stem and progenitor cells and reveal endothelial niches for stem cells. *Cell* **121,** 1109–21 (2005).

14. Wilson, A. *et al.* Dormant and self-renewing hematopoietic stem cells and their niches. *Ann. N. Y. Acad. Sci.* **1106,** 64–75 (2007).

15. Arai, F. *et al.* Tie2/angiopoietin-1 signaling regulates hematopoietic stem cell quiescence in the bone marrow niche. *Cell* **118,** 149–61 (2004).

16. Fleming, H. E. *et al.* Wnt Signaling in the Niche Enforces Hematopoietic Stem Cell Quiescence and Is Necessary

to Preserve Self-Renewal In Vivo. *Cell Stem Cell* **2,** 274–283 (2008).

17. Haug, J. S. *et al.* N-Cadherin Expression Level Distinguishes Reserved versus Primed States of Hematopoietic Stem Cells. *Cell Stem Cell* **2,** 367–379 (2008).

18. Nakamura, Y. *et al.* Isolation and characterization of endosteal niche cell populations that regulate hematopoietic stem cells Isolation and characterization of endosteal niche cell populations that regulate hematopoietic stem cells. *Blood* **116,** 1422–1432 (2013).

19. Morrison, S. J. & Spradling, A. C. Stem Cells and Niches: Mechanisms That Promote Stem Cell Maintenance throughout Life. *Cell* **132,** 598–611 (2008).

20. Emerson, S. G. Thrombopoietin, HSCs, and the Osteoblast Niche: Holding On Loosely, but Not Letting G0. *Cell Stem Cell* **1,** 599–600 (2007).

21. Stier, S. *et al.* Osteopontin is a hematopoietic stem cell niche component that negatively regulates stem cell pool size. *J. Exp. Med.* **201,** 1781–1791 (2005).

22. Calvi, L. M. *et al.* Osteoblastic cells regulate the haematopoietic stem cell niche. 841–846 (2003). doi:10.1038/nature02041.1.

23. Bowers, M. *et al. Osteoblast ablation reduces normal long-term hematopoietic stem cell self-renewal but accelerates leukemia development*. *Blood* **125,** (2015).

24. Spradling, A., Drummond-Barbosa, D. & Kai, T. Stem cells find their niche. *Nature* **311,** 1880–1885 (2001).

25. Méndez-Ferrer, S. *et al.* Mesenchymal and haematopoietic stem cells form a unique bone marrow niche. *Nature* **466,** 829–34 (2010).

26. Omatsu, Y. *et al.* The Essential Functions of Adipo-osteogenic Progenitors as the Hematopoietic Stem and Progenitor Cell Niche. *Immunity* **33,** 387–399 (2010).

27. Ito, K. *et al.* Reactive oxygen species act through p38 MAPK to limit the lifespan of hematopoietic stem cells. *Nat Med* **12,** 446–451 (2006).

28. Karigane, D. & Takubo, K. Metabolic regulation of hematopoietic and leukemic stem/progenitor cells under homeostatic and stress conditions. *Int. J. Hematol.* **106,** 18–26 (2017).

29. Parmar, K., Mauch, P., Vergilio, J.-A., Sackstein, R. & Down, J. D. Distribution of hematopoietic stem cells in the bone marrow according to regional hypoxia. *Proc. Natl. Acad. Sci.* **104,** 5431–5436 (2007).

30. Spencer, J. A. *et al.* Direct measurement of local oxygen concentration in the bone marrow of live animals. *Nature* **508,** 269–273 (2014).

31. Takubo, K. *et al.* Regulation of the HIF-1α Level Is Essential for Hematopoietic Stem Cells. *Cell Stem Cell* **7,** 391–

402 (2010).

32. Ito, K. & Suda, T. Metabolic requirements for the maintenance of self-renewing stem cells. *Nat. Rev. Mol. Cell Biol.* **15,** 243–56 (2014).

33. Ansó, E. *et al.* The mitochondrial respiratory chain is essential for haematopoietic stem cell function. *Nat. Cell Biol.* **19,** 614–625 (2017).

34. Henig, I. & Zuckerman, T. Hematopoietic Stem Cell Transplantation—50 Years of Evolution and Future Perspectives. *Rambam Maimonides Med. J.* **5,** e0028 (2014).

35. Passweg, J. R. *et al.* Hematopoietic stem cell transplantation in Europe 2014 : more than 40 000 transplants annually. 786–792 (2016). doi:10.1038/bmt.2016.20

36. Uchida, N. *et al.* High doses of purified stem cells cause early hematopoietic recovery in syngeneic and allogeneic hosts. *J. Clin. Invest.* **101,** 961–966 (1998).

37. Zhang, C. C. & Lodish, H. F. Murine hematopoietic stem cells change their surface phenotype during ex vivo expansion. *Leuk. Lymphoma* **105,** 4314–4320 (2005).

38. Ema, H., Takano, H., Sudo, K. & Nakauchi, H. In vitro self-renewal division of hematopoietic stem cells. *J. Exp. Med.* **192,** 1281–8 (2000).

39. Miyazawa, K. *et al.* Membrane-bound Steel factor induces more persistent tyrosine kinase activation and longer life span of c-kit gene-encoded protein than its soluble form. *Blood* **85,** 641–9 (1995).

40. Kimura, S., Roberts, A. W., Metcalf, D. & Alexander, W. S. Hematopoietic stem cell deficiencies in mice lacking c-Mpl, the receptor for thrombopoietin. *Proc. Natl. Acad. Sci. U. S. A.* **95,** 1195–1200 (1998).

41. Solar, G. P. *et al.* Role of c-mpl in early hematopoiesis. *Blood* **92,** 4–10 (1998).

42. Peters, S. O., Kittler, E. L., Ramshaw, H. S. & Quesenberry, P. J. Ex vivo expansion of murine marrow cells with interleukin-3 (IL-3), IL-6, IL-11, and stem cell factor leads to impaired engraftment in irradiated hosts. *Blood* **87,** 30–7 (1996).

43. Reya, T. *et al.* A role for Wnt signalling in self-renewal of haematopoietic stem cells. *Nature* **423,** 409–414 (2003).

44. Seita, Jun; Weissman, I. L. Hematopoietic Stem Cell: Self-renewal versus Differentiation. *Wiley Interdiscip Rev Syst Biol Med* **2,** 640–653 (2010).

45. Kirstetter, P., Anderson, K., Porse, B. T., Jacobsen, S. E. W. & Nerlov, C. Activation of the canonical Wnt pathway leads to loss of hematopoietic stem cell repopulation and multilineage differentiation block. *Nat. Immunol.* **7,** 1048–1056 (2006).

46. Blank, U. & Karlsson, S. TGF-beta signaling in the control of hematopoietic stem cells. *Blood* **125,** 3542–3550

(2015).

47. Chiba, S. Concise Review: Notch Signaling in Stem Cell Systems. *Stem Cells* **24,** 2437–2447 (2006).

48. Suzuki, T. *et al.* Highly Efficient Ex Vivo Expansion of Human Hematopoietic Stem Cells Using Delta1-Fc Chimeric Protein. *Stem Cells* **24,** 2456–2465 (2006).

49. Suda, T., Takubo, K. & Semenza, G. L. Metabolic regulation of hematopoietic stem cells in the hypoxic niche. *Cell Stem Cell* **9,** 298–310 (2011).

50. Vannini, N. *et al.* Specification of haematopoietic stem cell fate via modulation of mitochondrial activity. *Nat. Commun.* **7,** 1–9 (2016).

51. Ito, K. *et al.* A PML–PPAR-δ pathway for fatty acid oxidation regulates hematopoietic stem cell maintenance. *Nat. Med.* **18,** 1350–8 (2012).

52. Goodell, B. M. A., Brose, K., Paradis, G., Conner, A. S. & Mulligan, R. C. Isolation and Functional Properties of Murine Hematopoietic Stem Cells that are Replicating In Vivo. **183,** (1996).

53. Okada, S. *et al.* In vivo and in vitro stem cell function of c-kit- and Sca-1-positive murine hematopoietic cells. *Blood* **80,** 3044–3050 (1992).

54. Schroeder, T. Hematopoietic Stem Cell Heterogeneity: Subtypes, Not Unpredictable Behavior. *Cell Stem Cell* **6,** 203–207 (2010).

55. Oguro, H., Ding, L. & Morrison, S. J. SLAM family markers resolve functionally distinct subpopulations of hematopoietic stem cells and multipotent progenitors. *Cell Stem Cell* **6,** 2166–2171 (2013).

56. Hodzic, E. Single-cell analysis: Advances and future perspectives. *Bosn. J. basic Med. Sci.* **16,** 313–314 (2016).

57. Lecault, V., White, A. K., Singhal, A. & Hansen, C. L. Microfluidic single cell analysis: From promise to practice. *Curr. Opin. Chem. Biol.* **16,** 381–390 (2012).

58. Sato, S., Rancourt, A., Sato, Y. & Satoh, M. S. Single-cell lineage tracking analysis reveals that an established cell line comprises putative cancer stem cells and their heterogeneous progeny. *Sci. Rep.* **6,** 23328 (2016).

59. Chen, Y. *et al.* Rare cell isolation and analysis in microfluidics. *Lab Chip* **14,** 626–45 (2014).

60. Eilken, H. M., Nishikawa, S. I. & Schroeder, T. Continuous single-cell imaging of blood generation from haemogenic endothelium. *Nature* **457,** 896–900 (2009).

61. Okamura, S., Crane, F., Jamal, N., Messner, H. A. & Mak, T. W. Single-cell immunofluorescence assay for terminal transferase: Human leukaemic and non-leukaemic cells. *Br. J. Cancer* **41,** 159–167 (1980).

62. Wang, Y. *et al.* Tracking hematopoietic precursor division ex vivo in real time. *Stem Cell Res. Ther.* **9,** 1–13 (2018).

63. Alber, A. B., Paquet, E. R., Biserni, M., Naef, F. & Suter, D. M. Single Live Cell Monitoring of Protein Turnover Reveals Intercellular Variability and Cell-Cycle Dependence of Degradation Rates. *Mol. Cell* **0,** 1–13 (2018).

64. Schroeder, T. Long-term single-cell imaging of mammalian stem cells. *Nat. Methods* **8,** S30-5 (2011).

65. Tuhin, F. T., Santra, S. & Prospects, F. *Essentials of Single-Cell Analysis*. (Springer, 2016). doi:1 F. T. Tuhin, S. Santra and F. Prospects, Essentials of Single-Cell Analysis, .

66. Beebe, D. J., Mensing, G. A. & Walker, G. M. Physics and Applications of Microfluidics in Biology. *Annu. Rev. Biomed. Eng.* **4,** 261–286 (2002).

67. Rettig, J. & Folch, A. Large-scale single-cell trapping and imaging using microwell arrays. *Anal. Chem.* **77,** 5628–5634 (2005).

68. Lutolf, M. P., Doyonnas, R., Havenstrite, K., Koleckar, K. & Blau, H. M. Perturbation of single hematopoietic stem cell fates in artificial niches. *R. Soc. Chem.* **1,** 59–69 (2009).

69. Parce, J. W. *et al.* Detection of cell-affecting agents with a silicon biosensor. *Science (80-.).* **246,** 243 LP-247 (1989).

70. Charnley, M., Textor, M., Khademhosseini, A. & Lutolf, M. P. Integration column: Microwell arrays for mammalian cell culture. *Integr. Biol.* **1,** 625–634 (2009).

71. Inoue, I., Wakamoto, Y., Moriguchi, H., Okano, K. & Yasuda, K. On-chip culture system for observation of isolated individual cells. *Lab Chip* **1,** 50–55 (2001).

72. Park, J., Morgan, M. & Sachs, A. Single cell trapping in larger microwells capable of supporting cell spreading and proliferation. *Microfluid. …* **8,** 263–268 (2010).

73. Roch, A. *et al.* Single-cell analyses identify bioengineered niches for enhanced maintenance of hematopoietic stem cells. *Nat. Commun.* **8,** 1–12 (2017).

74. Kobel, S. A. & Lutolf, M. P. in (eds. Navarro, M. & Planell, J. A.) 101–112 (Humana Press, 2012). doi:10.1007/978-1-61779-388-2_7

75. Napolitano, A. P. *et al.* Scaffold-free three-dimensional cell culture utilizing micromolded nonadhesive hydrogels. *Biotechniques* **43,** 494–500 (2007).

76. Lindström, S., Larsson, R. & Svahn, H. A. Towards high throughput single cell/clone cultivation and analysis. *Electrophoresis* **29,** 1219–1227 (2008).

77. Jang, Y.-H. *et al.* Deep wells integrated with microfluidic valves for stable docking and storage of cells. *Biotechnol. J.* **6,** 156–164 (2012).

78. Chen, H. *et al.* Microwell perfusion array for high-throughput, long-term imaging of clonal growth.

Biomicrofluidics **5,** 1–13 (2011).

79. Lecault, V. *et al.* High-throughput analysis of single hematopoietic stem cell proliferation in microfluidic cell culture arrays. *Nat. Methods* **8,** 581–6 (2011).

80. Di Carlo, D., Wu, L. Y. & Lee, L. P. Dynamic single cell culture array. *Lab Chip* **6,** 1445–9 (2006).

81. Tan, W. & Takeuchi, S. A trap-and-release integrated microfluidic system for dynamic microarray applications. *Proc. Natl. Acad. …* **104,** 4–6 (2007).

82. Kimmerling, R. J. *et al.* A microfluidic platform enabling single-cell RNA-seq of multigenerational lineages. *Nat. Commun.* **7,** 10220 (2016).

83. Rowat, A. C. Supporting Information. *Image (Rochester, N.Y.)* (2005).

84. Chung, J., Kim, Y. & Yoon, E. Highly-efficient single-cell capture in microfluidic array chips using differential hydrodynamic guiding structures. 12–14 (2011). doi:10.1063/1.3565236

85. Wlodkowic, D., Faley, S., Zagnoni, M., Wikswo, J. P. & Cooper, J. M. Microfluidic Single Cell Array Cytometry for the Analysis of Tumour Apoptosis. *Anal. Chem.* **81,** 5517–5523 (2009).

86. Iwai, K., Tan, W.-H., Ishihara, H. & Takeuchi, S. A resettable dynamic microarray device. *Biomed. Microdevices* **13,** 1089–94 (2011).

87. Chen, H., Sun, J., Wolvetang, E. & Cooper-White, J. High-throughput, deterministic single cell trapping and long-term clonal cell culture in microfluidic devices. *Lab Chip* **15,** 1072–1083 (2015).

88. Carlo, D. Di, Aghdam, N. & Lee, L. Single-cell enzyme concentrations, kinetics, and inhibition analysis using high-density hydrodynamic cell isolation arrays. *Anal. Chem.* **78,** 4925–4930 (2006).

89. Rowat, A. C., Bird, J. C., Agresti, J. J., Rando, O. J. & Weitz, D. a. Tracking lineages of single cells in lines using a microfluidic device. *Proc. Natl. Acad. Sci. U. S. A.* **106,** 18149–54 (2009).

90. Kobel, S., Valero, A., Latt, J., Renaud, P. & Lutolf, M. Optimization of microfluidic single cell trapping for long-term on-chip culture. *Lab Chip* **10,** 857–63 (2010).

91. White, A. K. *et al.* High-throughput microfluidic single-cell RT-qPCR. *Proc. Natl. Acad. Sci. U. S. A.* **108,** 13999–4004 (2011).

92. Streets, a. M. *et al.* Microfluidic single-cell whole-transcriptome sequencing. *Proc. Natl. Acad. Sci.* 1–6 (2014). doi:10.1073/pnas.1402030111

93. Yun, H., Kim, K. & Lee, W. G. Cell manipulation in microfluidics. *IOP Sci.* **022001,** (2013).

94. Bocchi, M. *et al.* Inverted open microwells for cell trapping, cell aggregate formation and parallel recovery of live cells. *Lab Chip* **12,** 3168 (2012).

95. Jang, L., Huang, P. & Lan, K. Single-cell trapping utilizing negative dielectrophoretic quadrupole and microwell electrodes. *Biosens. Bioelectron.* **24,** 3637–3644 (2009).

96. Johann, R. M. Cell trapping in microfluidic chips. *Anal. Bioanal. Chem.* **385,** 408–12 (2006).

97. Werner, M., Palankar, R., Arm, L., Hovius, R. & Vogel, H. Microfluidic Single-Cell Analysis with Affinity Beads. *Small* n/a-n/a (2015). doi:10.1002/smll.201402650

98. He, M. *et al.* Selective encapsulation of single cells and subcellular organelles into picoliter- and femtoliter-volume droplets. *Anal. Chem.* **77,** 1539–44 (2005).

99. Skylaki, S., Hilsenbeck, O. & Schroeder, T. Challenges in long-term imaging and quantification of single-cell dynamics. *Nat. Biotechnol.* **34,** 1137–1144 (2016).

100. Woodworth, M. B., Girskis, K. M. & Walsh, C. A. Building a lineage from single cells: Genetic techniques for cell lineage tracking. *Nat. Rev. Genet.* **18,** 230–244 (2017).

101. Kretzschmar, K. & Watt, F. M. Lineage tracing. *Cell* **148,** 33–45 (2012).

102. Eilken, H. *et al.* Continuous long-term detection of live cell surface markers by 'in culture' antibody staining. (2011).

103. Coutu, D. L. & Schroeder, T. Probing cellular processes by long-term live imaging--historic problems and current solutions. *J. Cell Sci.* **126,** 3805–15 (2013).

104. Kobel, S., Valero, A., Latt, J., Renaud, P. & Lutolf, M. Optimization of microfluidic single cell trapping for long-term on-chip culture. *Lab Chip* **10,** 857–63 (2010).

105. Moffitt, J. R., Lee, J. B. & Cluzel, P. The single-cell chemostat: an agarose-based, microfluidic device for high-throughput, single-cell studies of bacteria and bacterial communities. *Lab Chip* **12,** 1487 (2012).

106. Tabata, Y. In vitro modeling of complex microenvironmental regulation of stem cells. **7349,** (EPFL, 2017).

107. Kobel, S. Microtechnologies to Map the Fate of Single Stem Cells and their Progeny. **5322,** (EPFL, 2012).

108. Zhu, L. *et al.* Cell loss in integrated microfluidic device. *Biomed. Microdevices* **9,** 745–750 (2007).

109. Berthier, E., Young, E. & Beebe, D. Engineers are from PDMS-land, Biologists are from Polystyrenia. *Lab Chip* **12,** 1224–1237 (2012).

110. Lecault, V. *et al.* High-throughput analysis of single hematopoietic stem cell proliferation in microfluidic cell culture arrays. *Nat. Methods* **8,** 581–6 (2011).

111. Roch, A., Trachsel, V. & Lutolf, M. P. Brief Report: Single-Cell Analysis Reveals Cell Division-Independent Emergence of Megakaryocytes from Phenotypic Hematopoietic Stem Cells. *Stem Cells* **33,** 3152–3157 (2015).

112. Lindström, S. *et al.* High-density microwell chip for culture and analysis of stem cells. *PLoS One* **4,** 1–9 (2009).

113. Jo, B. H., Van Lerberghe, L. M., Motsegood, K. M. & Beebe, D. J. Three-dimensional micro-channel fabrication in polydimethylsiloxane (PDMS) elastomer. *J. Microelectromechanical Syst.* **9,** 76–81 (2000).

114. Bounds, C. O. *et al.* Fabrication and characterization of stable hydrophilic microfluidic devices prepared via the in situ tertiary-amine catalyzed Michael addition of multifunctional thiols to multifunctional acrylates. *ACS Appl. Mater. Interfaces* **5,** 1643–1655 (2013).

115. Saharil, F., Carlborg, C. F., Haraldsson, T. & Van Der Wijngaart, W. Biocompatible 'click' wafer bonding for microfluidic devices. *Lab Chip* **12,** 3032–3035 (2012).

116. Nair, D. P. *et al.* The Thiol-Michael addition click reaction: A powerful and widely used tool in materials chemistry. *Chem. Mater.* **26,** 724–744 (2014).

117. Lutolf, M. P. & Hubbell, J. A. Synthesis and physicochemical characterization of end-linked poly(ethylene glycol)-co-peptide hydrogels formed by Michael-type addition. *Biomacromolecules* **4,** 713–722 (2003).

118. Chatani, S., Nair, D. P. & Bowman, C. N. Relative reactivity and selectivity of vinyl sulfones and acrylates towards the thiol–Michael addition reaction and polymerization. *Polym. Chem.* **4,** 1048 (2013).

119. Blotny, G. Recent applications of 2,4,6-trichloro-1,3,5-triazine and its derivatives in organic synthesis. *Tetrahedron* **62,** 9507–9522 (2006).

120. Lutolf, M. P., Doyonnas, R., Havenstrite, K., Koleckar, K. & Blau, H. M. Perturbation of single hematopoietic stem cell fates in artificial niches. *Integr. Biol. (Camb).* **1,** 59–69 (2009).

121. Jo, Y. S. *et al.* Biomimetic PEG hydrogels crosslinked with minimal plasmin-sensitive tri-amino acid peptides. *J. Biomed. Mater. Res. - Part A* **93,** 870–877 (2010).

122. Tugulu, S. & Klok, H. A. Stability and nonfouling properties of poly(poly(ethylene glycol) methacrylate) Brushes under cell culture conditions. *Biomacromolecules* **9,** 906–912 (2008).

123. Nelson, C. M., Inman, J. L. & Bissell, M. J. Three-dimensional lithographically defined organotypic tissue arrays for quantitative analysis of morphogenesis and neoplastic progression. *Nat. Protoc.* 1–5 (2008). doi:10.1038/nprot.2008.35

124. Seita, J. & Weissman, I. L. Hematopoietic stem cell: self-renewal versus differentiation. *Wiley Interdiscip. Rev. Syst. Biol. Med.* **2,** 640–53 (2010).

125. Wilson, A. *et al.* Hematopoietic stem cells reversibly switch from dormancy to self-renewal during homeostasis and repair. *Cell* **135,** 1118–1129 (2008).

126. Wang, L. D. & Wagers, A. J. Dynamic niches in the origination and differentiation of haematopoietic stem cells. *Nat. Rev. Mol. Cell Biol.* **12,** 643–655 (2011).

127. Murke, F., Castro, S., Giebel, B. & Görgens, A. Concise Review: Asymmetric Cell Divisions in Stem Cell Biology. *Symmetry (Basel).* **7,** 2025–2037 (2015).

128. Ito, K. *et al.* A PML–PPAR-δ pathway for fatty acid oxidation regulates hematopoietic stem cell maintenance. *Nature Medicine* **18,** 1350–1358 (2012).

129. Vannini, N. *et al.* Identification of in vitro HSC fate regulators by differential lipid raft clustering. *Cell Cycle* **11,** 1535–43 (2012).

130. Stadler, T., Skylaki, S., D. Kokkaliaris, K. & Schroeder, T. On the statistical analysis of single cell lineage trees. *J. Theor. Biol.* **439,** 160–165 (2018).

131. Vannini, A. N. *et al.* Title : The NAD - booster nicotinamide riboside potently stimulates hematopoiesis through increased mitochondrial clearance.

132. Chalfoun, J. *et al.* Lineage mapper: A versatile cell and particle tracker. *Sci. Rep.* **6,** 1–9 (2016).

133. Tinevez, J. Y. *et al.* TrackMate: An open and extensible platform for single-particle tracking. *Methods* **115,** 80–90 (2017).

134. Meijering, E., Dzyubachyk, O. & Smal, I. *Methods for cell and particle tracking*. *Methods in Enzymology* **504,** (Elsevier Inc., 2012).

135. Al-Kofahi, O. *et al.* Automated cell lineage construction: A rapid method to analyze clonal development established with murine neural progenitor cells. *Cell Cycle* **5,** 327–335 (2006).

136. Kang Lia, Mei Chenb, Takeo Kanadea, Eric D. Millera, Lee E. Weissa, and P. G. C. & ACarnegie. *Cell Population Tracking and Lineage Construction with Spatiotemporal Context*. *October* **12,** (2008).

137. Meijering, E., Smal, I. & Danuser, G. Tracking in molecular bioimaging. *IEEE Signal Process. Mag.* **23,** 46–53 (2006).

138. Roccio, M. *et al.* Predicting stem cell fate changes by differential cell cycle progression patterns. *Development* **140,** 459–470 (2013).

139. Gilbert, P. M. *et al.* Substrate Elasticity Regulates Skeletal Muscle Stem Cell. *Science (80-.).* **1078,** 1078–1081 (2010).

140. Tonkin, J. A. *et al.* Automated cell identification and tracking using nanoparticle moving-light-displays. *PLoS One* **7,** 1–8 (2012).

141. Zartman, J. J. *et al.* Robust cell tracking in epithelial tissues\nthrough identification of maximum\ncommon subgraphs. *J. R. Stat. Soc. Interface* (2016).

142. Magidson, V. & Khodjakov, A. *Circumventing photodamage in live-cell microscopy*. *Methods in Cell Biology* **114,**

(Elsevier Inc., 2013).

143. Yen, J. C., Chang, F. J. & Chang, S. A New Criterion for Automatic Multilevel Thresholding. *IEEE Trans. Image Process.* **4,** 370–378 (1995).

144. Jonker, R. & Volgenant, T. Improving the Hungarian Assignment Algorithm. *Oper. Res. Lett.* **5,** 171–175 (1986).

145. Poirier, Y., Antonenkov, V. D., Glumoff, T. & Hiltunen, J. K. Peroxisomal β -oxidation — A metabolic pathway with multiple functions. *Biochim. Biophys. Acta* **1763,** 1413–1426 (2006).

146. Zeng, J. *et al.* Specific Inhibition of Acyl-CoA Oxidase-1 by an Acetylenic Acid Improves Hepatic Lipid and Reactive Oxygen Species (ROS) Metabolism in Rats Fed a High Fat Diet. *J. Biol. Chem.* **292,** 3800–3809 (2017).

147. Knobloch, M. *et al.* A Fatty Acid Oxidation-Dependent Metabolic Shift Regulates Adult Neural Stem Cell Activity. *Cell Rep.* **20,** 2144–2155 (2017).

148. Bian, F. *et al.* Peroxisomal and mitochondrial oxidation of fatty acids in the heart, assessed from the 13C labeling of malonyl-CoA and the acetyl moiety of citrate. *J. Biol. Chem.* **280,** 9265–9271 (2005).

149. Lutolf, M. P. & Blau, H. M. Artificial stem cell niches. *Adv. Mater.* **21,** 3255–68 (2009).

150. Dahlberg, A., Delaney, C. & Bernstein, I. D. Review article Ex vivo expansion of human hematopoietic stem and progenitor cells. *Blood* **117,** 6083–6090 (2011).

151. Hofmeister, C. C., Zhang, J., Knight, K. L., Le, P. & Stiff, P. J. Ex vivo expansion of umbilical cord blood stem cells for transplantation: Growing knowledge from the hematopoietic niche. *Bone Marrow Transplant.* **39,** 11–23 (2007).

152. Park, B., Yoo, K. H. & Kim, C. Hematopoietic stem cell expansion and generation : the ways to make a breakthrough. **50,** (2015).

153. Mishra, P. & Chan, D. C. Mitochondrial dynamics and inheritance during cell division, development and disease. *Nat. Rev. Mol. Cell Biol.* **15,** 634–46 (2014).

154. Rehman, J. Empowering self-renewal and differentiation: The role of mitochondria in stem cells. *J. Mol. Med.* **88,** 981–986 (2010).

155. Liang, R. & Ghaffari, S. Mitochondria and FOXO3 in stem cell homeostasis, a window into hematopoietic stem cell fate determination. *J. Bioenerg. Biomembr.* **49,** 343–346 (2017).

156. Simsek, T. *et al.* The distinct metabolic profile of hematopoietic stem cells reflects their location in a hypoxic niche. *Cell Stem Cell* **7,** 380–390 (2010).

157. de Almeida, M. J., Luchsinger, L. L., Corrigan, D. J., Williams, L. J. & Snoeck, H. W. Dye-Independent Methods Reveal Elevated Mitochondrial Mass in Hematopoietic Stem Cells. *Cell Stem Cell* **21,** 725–729.e4 (2017).

158. Yu, W. M. *et al.* Metabolic regulation by the mitochondrial phosphatase PTPMT1 is required for hematopoietic stem cell differentiation. *Cell Stem Cell* **12,** 62–74 (2013).

159. Woolthuis, C. M. & Park, C. Y. Hematopoietic stem/progenitor cell commitment to the megakaryocyte lineage. *Blood* **127,** 1242–1248 (2016).

160. Gvaramia, D. *et al.* Combined influence of biophysical and biochemical cues on maintenance and proliferation of hematopoietic stem cells. *Biomaterials* **138,** 108–117 (2017).

161. Diebold, L. P. & Chandel, N. S. HSC Fate Is Tethered to Mitochondria. *Cell Stem Cell* **18,** 303–304 (2016).

162. Kohli, L. & Passegué, E. Surviving change: The metabolic journey of hematopoietic stem cells. *Trends Cell Biol.* **24,** 479–487 (2014).

163. Knoblich, J. A. Mechanisms of Asymmetric Stem Cell Division. *Cell* **132,** 583–597 (2008).

164. Nygren, J. M., Bryder, D. & Jacobsen, S. E. W. Prolonged Cell Cycle Transit Is a Defining and Developmentally Conserved Hemopoietic Stem Cell Property. *J. Immunol.* **177,** 201 LP-208 (2006).

165. Orford, K. W. & Scadden, D. T. Deconstructing stem cell self-renewal: genetic insights into cell-cycle regulation. *Nat. Rev. Genet.* **9,** 115–28 (2008).

166. Wilson, A. *et al.* Hematopoietic stem cells reversibly switch from dormancy to self-renewal during homeostasis and repair. *Cell* **135,** 1118–29 (2008).

167. Staiber, W. Asymmetric distribution of mitochondria and of spindle microtubules in opposite directions in differential mitosis of germ line cells in Acricotopus. *Cell Tissue Res.* **329,** 197–203 (2007).

168. Katajisto, P. *et al.* Asymmetric apportioning of aged mitochondria between daughter cells is required for stemness. *Science* **348,** 340–343 (2015).

169. Suda, J., Suda, T. & Ogawa, M. Analysis of differentiation of mouse Hematopoeitic Stem Cells in culture by sequential replating of paired progenitors. *Blood* **64,** 393–399 (2017).

170. Morrison, S. J. & Kimble, J. Asymmetric and symmetric stem-cell divisions in development and cancer. *Nature* **441,** 1068–1074 (2006).

171. Giebel, B. *et al.* Primitive human hematopoietic cells give rise to differentially specified daughter cells upon their initial cell division. *Blood* **107,** 2146–2152 (2006).

172. Takano, H., Ema, H., Sudo, K. & Nakauchi, H. Asymmetric Division and Lineage Commitment at the Level of Hematopoietic Stem Cells. *J. Exp. Med.* **199,** 295–302 (2004).

173. Yamamoto, R. *et al.* Clonal analysis unveils self-renewing lineage-restricted progenitors generated directly from hematopoietic stem cells. *Cell* **154,** 1112–26 (2013).

174. Essers, M. A. G. *et al.* IFNα activates dormant haematopoietic stem cells in vivo. *Nature* **458,** 904–908 (2009).

175. Sarrazy, V. *et al.* Disruption of Glut1 in Hematopoietic Stem Cells Prevents Myelopoiesis and Enhanced Glucose Flux in Atheromatous Plaques of ApoE-/-Mice. *Circ. Res.* **118,** 1062–1077 (2016).

176. Forsberg, E. C. *et al.* Differential expression of novel potential regulators in hematopoietic stem cells. *PLoS Genet.* **1,** (2005).

177. Forsberg, E. C. *et al.* Molecular signatures of quiescent, mobilized and leukemia-initiating hematopoietic stem cells. *PLoS One* **5,** 1–11 (2010).

178. Umemoto, T. *et al.* p57Kip2is expressed in quiescent mouse bone marrow side population cells. *Biochem. Biophys. Res. Commun.* **337,** 14–21 (2005).

179. Cheng, T. *et al.* Hematopoietic Stem Cell Quiescence Maintained by p21cip1/waf1. *Science (80-.).* **1804,** 1804–1809 (2009).

180. Passegué, E., Wagers, A. J., Giuriato, S., Anderson, W. C. & Weissman, I. L. Global analysis of proliferation and cell cycle gene expression in the regulation of hematopoietic stem and progenitor cell fates. *J. Exp. Med.* **202,** 1599–1611 (2005).

181. Zou, P. *et al.* P57 Kip2 and p27 Kip1 cooperate to maintain hematopoietic stem cell quiescence through interactions with Hsc70. *Cell Stem Cell* **9,** 247–261 (2011).

182. Perry, J. M. *et al.* Cooperation between both Wnt / b -catenin and PTEN / PI3K / Akt signaling promotes primitive hematopoietic stem cell self-renewal and expansion. 1928–1942 (2011). doi:10.1101/gad.17421911.ated

183. Zhang, J. *et al.* PTEN maintains haematopoietic stem cells and acts in lineage choice and leukaemia prevention. *Nature* **441,** 518–522 (2006).

184. Ku, C. J., Hosoya, T., Maillard, I. & Engel, J. D. GATA-3 regulates hematopoietic stem cell maintenance and cell-cycle entry. *Blood* **119,** 2242–2251 (2012).

185. Krosl, J. *et al.* In vitro expansion of hematopoietic stem cells by recombinant TAT-HOXB4 protein. *Nat. Med.* **9,** 1428–1432 (2003).

186. Satoh, Y. *et al.* Roles for c-Myc in self-renewal of hematopoietic stem cells. *J. Biol. Chem.* **279,** 24986–24993 (2004).

187. Wilson, A., , Mark J. Murphy, Thordur Oskarsson, K. K., Michael D. Bettess, Gabriela M. Oser, Anne-Catherine Pasche, C. K. & H. Robson MacDonald, and A. T. c-Myc controls the balance between hematopoietic stem cell self-renewal and differentiation. *Genes Dev.* **18,** 2747–2763 (2004).

188. Takubo, K. *et al.* Regulation of glycolysis by Pdk functions as a metabolic checkpoint for cell cycle quiescence in hematopoietic stem cells. *Cell Stem Cell* **12,** 49–61 (2013).

189. Ito, K. *et al.* A PML–PPAR-δ pathway for fatty acid oxidation regulates hematopoietic stem cell maintenance. *Nat. Med.* **18,** 1350–1358 (2012).

190. Osawa, M., Hanada, K., Hamada, H. & Nakauchi, H. Long-term lymphohematopoietic reconstitution by a single CD34-low/negative hematopoietic stem cell. *Science* **273,** 242–245 (1996).

191. Arcangeli, M. *et al.* JAM-B regulates maintenance of hematopoietic stem cells in the bone marrow. **118,** 6–8 (2011).

192. Arcangeli, M. L. *et al.* Function of jam-B/Jam-C interaction in homing and mobilization of human and mouse hematopoietic stem and progenitor cells. *Stem Cells* **32,** 1043–1054 (2014).

193. Kiger, A. A., Jones, D. L., Schulz, C., Rogers, M. B. & Fuller, M. T. Stem cell self-renewal specified by JAK-STAT activation in response to a support cell cue. *Science (80-.).* **294,** 2542–2545 (2001).

194. Song, X. Bmp signals from niche cells directly repress transcription of a differentiation-promoting gene, bag of marbles, in germline stem cells in the Drosophila ovary. *Development* **131,** 1353–1364 (2004).

195. Tulina, N. Control of Stem Cell Self-Renewal in Drosophila Spermatogenesis by JAK-STAT Signaling. *Science (80-.).* **294,** 2546–2549 (2001).

196. Yamashita, Y. M. Signaling in stem cell niches: lessons from the Drosophila germline. *J. Cell Sci.* **118,** 665–672 (2005).

197. Arai, F. *et al.* Tie2/angiopoietin-1 signaling regulates hematopoietic stem cell quiescence in the bone marrow niche. *Cell* **118,** 149–161 (2004).

198. Mathupala, S. P., Rempel, A. & Pedersen, P. L. Glucose catabolism in cancer cells: Identification and characterization of a marked activation response of the type II hexokinase gene to hypoxic conditions. *J. Biol. Chem.* **276,** 43407–43412 (2001).

199. Signer, R. A. J., Magee, J. A., Salic, A. & Morrison, S. J. Haematopoietic stem cells require a highly regulated protein synthesis rate. *Nature* **508,** 49–54 (2014).

200. Gerlach, C. *et al.* One naive T cell, multiple fates in CD8 $^+$ T cell differentiation. *J. Exp. Med.* **207,** 1235–1246 (2010).

201. Williams, M. A. & Bevan, M. J. Effector and Memory CTL Differentiation. *Annu. Rev. Immunol.* **25,** 171–192 (2007).

202. Stemberger, C. *et al.* A Single Naive CD8+ T Cell Precursor Can Develop into Diverse Effector and Memory Subsets. *Immunity* **27,** 985–997 (2007).

203. Russell, S. How polarity shapes the destiny of T cells. *J. Cell Sci.* **121,** 131–136 (2008).

204. Kaech, S. M., Hemby, S., Kersh, E. & Ahmed, R. Molecular and functional profiling of memory CD8 T cell differentiation. *Cell* **111,** 837–851 (2002).

205. Arsenio, J., Metz, P. J. & Chang, J. T. Asymmetric Cell Division in T Lymphocyte Fate Diversification. *Trends Immunol.* **36,** 670–683 (2015).

206. Chang, J. T. *et al.* Asymmetric T Lymphocyte Adaptive Immune Responses. *Science (80-.).* **315,** 1687–1692 (2007).

207. King, C. G., Koehli, S., Hausmann, B., Schmaler, M. & Palmer, E. T Cell Affinity Regulates Asymmetric Division, Effector Cell Differentiation, and Tissue Pathology. *Immunity* **37,** 709–720 (2012).

208. Verbist, K. C. *et al.* Metabolic maintenance of cell asymmetry following division in activated T lymphocytes. *Nature* **532,** 389–393 (2016).

209. Chang, J. T. *et al.* Asymmetric T lymphocyte division in the initiation of adaptive immune responses. *Science (80- .).* **315,** 1687–1691 (2007).

210. Pennock, N. D. *et al.* T cell responses: naive to memory and everything in between. *AJP Adv. Physiol. Educ.* **37,** 273–283 (2013).

211. Oliaro, J. *et al.* Asymmetric Cell Division of T Cells upon Antigen Presentation Uses Multiple Conserved Mechanisms. *J. Immunol.* **185,** 367–375 (2010).

212. Dalyot-Herman, N., Bathe, O. F. & Malek, T. R. Reversal of CD8+ T Cell Ignorance and Induction of Anti-Tumor Immunity by Peptide-Pulsed APC. *J. Immunol.* **165,** 6731–6737 (2000).

213. Carbone, F. R., Sterry, S. J., Butler, J., Rodda, S. & Moore, M. W. T cell receptor a-chain pairing determines the specificity of residue 262 within the K b -restricted, ovalbumin 25 7-264 determinant. *Int. Immunol.* **4,** 861–867 (1992).

214. Ke, Y., Ma, H. & Kapp, J. A. Antigen Is Required for the Activation of Effector Activities, whereas Interleukin 2 Is Required for the Maintenance of Memory in Ovalbumin-specific, CD8 $^+$ Cytotoxic T Lymphocytes. *J. Exp. Med.* **187,** 49–57 (1998).

215. Ahlers, J. D. Review Article : Memories that last forever : strategies for optimizing vaccine T-cell mem ... Page 1 of 27 Memories that last forever : strategies for optimizing vaccine T-cell memory Review Article : Memories that last forever : strategies for optimizin. **115,** 1678–1689 (2012).

216. Pollizzi, K., Sun, I.-H. & Powel, J. Asymmetric inheritance of mTORC1 kinase activity during division dictates CD8 T cell differentiation. *Nat. Immunol.* **93,** 292–297 (2016).

217. Dustin, M. L. T-cell activation through immunological synapses and kinapses. *Immunol. Rev.* **221,** 77–89 (2008).

218. Böhmer, R. M., Bandala-Sanchez, E. & Harrison, L. C. Forward light scatter is a simple measure of T-cell activation

and proliferation but is not universally suited for doublet discrimination. *Cytom. Part A* **79A,** 646–652

219. Metz, P. J. *et al.* Regulation of Asymmetric Division by Atypical Protein Kinase C Influences Early Specification of CD8+ T Lymphocyte Fates. *Sci. Rep.* **6,** 19182 (2016).

220. Katajisto, P. *et al.* Asymmetric apportioning of aged mitochondria between daughter cells is required for stemness. *Science (80-.).* **348,** 340–343 (2015).

221. Chao, T., Wang, H. & Ho, P. C. Mitochondrial control and guidance of cellular activities of T cells. *Front. Immunol.* **8,** 1–7 (2017).

222. Huang, X., Zhu, B., Wang, X., Xiao, R. & Wang, C. Three-dimensional co-culture of mesenchymal stromal cells and differentiated osteoblasts on human bio-derived bone scaffolds supports active multi-lineage hematopoiesis in vitro: Functional implication of the biomimetic HSC niche. *Int. J. Mol. Med.* **38,** 1141–1151 (2016).

223. Salati, S. *et al.* Co-Culture of Hematopoietic Stem/Progenitor Cells with Human Osteblasts Favours Mono/Macrophage Differentiation at the Expense of the Erythroid Lineage. *PLoS One* **8,** (2013).

224. Jing, D. *et al.* Hematopoietic stem cells in co-culture with mesenchymal stromal cells -modeling the niche compartments in vitro. *Haematologica* **95,** 542–550 (2010).

225. Pietras, E. M., Warr, M. R. & Passegue, E. Cell cycle regulation in hematopoietic stem cells. *J. Cell Biol.* **195,** 709–720 (2011).

226. Baum, C. M., Weissman, I. L., Tsukamoto, A. S., Buckle, A. M. & Peault, B. Isolation of a candidate human hematopoietic stem-cell population. *Proc. Natl. Acad. Sci.* **89,** 2804–2808 (1992).

227. Muñoz, J. *et al.* The Lgr5 intestinal stem cell signature: Robust expression of proposed quiescent ' +4' cell markers. *EMBO J.* **31,** 3079–3091 (2012).

228. Pan, G. & Thomson, J. A. Nanog and transcriptional networks in embryonic stem cell pluripotency. *Cell Res.* **17,** 42–49 (2007).

229. Takahashi, K. *et al.* Induction of Pluripotent Stem Cells from Mouse Embryonic and Adult Fibroblast Cultures by Defined Factors. *Cell* **126,** 663–676 (2006).

230. Schmidt, R. & Plath, K. The roles of the reprogramming factors Oct4, Sox2 and Klf4 in resetting the somatic cell epigenome during induced pluripotent stem cell generation. *Genome Biol.* **13,** 251 (2012).

231. Gay, L., Baker, A. & Graham, T. A. Tumour Cell Heterogeneity. **5,** 1–14 (2016).

232. Navin, N. E. & Hicks, J. Tracing the tumor lineage. *Mol. Oncol.* **4,** 267–283 (2010).

233. Kobel, S. & Lutolf, M. P. High-throughput methods to define complex stem cell niches. *Biotechniques* **48,** (2010).

Curriculum Vitae

Vincent Trachsel
Rue des Fahys 221
2000 Neuchâtel
0794267407

30 years old

Married

Swiss

2014-2018 **PhD,** in Biotechnology and Bioengineering
Ecole polytechnique fédérale de Lausanne, EPFL, *Lausanne*
PhD thesis: "*In vitro* fate mapping of stem cell development at the single cell level"

2006-2013 **Master**, Ecole polytechnique fédérale de Lausanne, EPFL, *Lausanne*
Master of Science 'MSc en Bioingénierie, Mineur en technologie biomédicales

2012-2013 Master project at the Australian Institute of micro and nano-technologies, AIBN, Brisbane, Australie
2006-2010 **Bachelor,** in Life Sciences, Ecole polytechnique fédérale de Lausanne, EPFL, *Lausanne*

2003-2006 High School, Lycée Denis-de-Rougemont, *Neuchâtel.*
Biochemistry

Publications

(1) A. Roch, **V. Trachsel**, M.P. Lutolf. Brief Report: Single-Cell Analysis Reveals Cell Division-Independent Emergence of Megakaryocytes from Phenotypic Hematopoietic Stem Cells. *Stem Cells* **33,** 3152–3157 (2015).

(2) N. Vannini, V. Campos, M. Girotra, **V. Trachsel**, S. Rojas-Sutterlin,J. Tratwal, S. Ragusa, E. Stefanidis, D. Ryu, P.Y. Rainer, G. Nikitin, S. Giger,Y.L. Terytty, A. Semilietof, Y. Yersin, W.C. Cheng, L. Tauzin, E. Pirinen, J. Ratajczak,C. Canto, M. Ehrbar, F. Sizzano, A. Palini, T.V. Petrova, D. Vanhecke, A. Nahimana, M.A. Duchosal, P.C. Ho, B. Deplancke, G. Coukos, J. Auwerx, M. P. Lutolf and O.Naveiras. The NAD - booster nicotinamide riboside potently stimulates hematopoiesis through increased mitochondrial clearance. Cell Stem Cell (in revision)

(3) **V. Trachsel**, G. Nikitin, M.P. Lutolf Hydrogel-based groove array for lineage tracking of rare and fragile single cells (Submitted) (Chapter 2)

(4) **V. Trachsel**, G. Nikitin, M.P. Lutolf Monitoring of mitochondrial mass of HSCs in culture (In preparation) (Chapter 4)

(5) M. Girotra, **V. Trachsel**, A. Roch, S. Giger, M.P. Lutolf Analysis of asymmetric markers in the first generation of cells derived from murine HSCs (In preparation) (Chapter 5)

Poster and Oral presentations

(1) **V. Trachsel**, G. Nikitin, M.P. Lutolf In vitro fate mapping of stem cell development at the single cell level (junior session talk)
(2) **V. Trachsel**, G. Nikitin, M.P. Lutolf Hydrogel-based groove array for lineage tracking of rare and fragile single cells. Stem cell retreat (short talk and poster)
(3) **V. Trachsel**, M.P. Lutolf. Hydrogel-based platforms for single cell analysis. Summer School. Translational neuroscience & neuroengineering (Poster)